Fall 2021

From the Surface to the Reactor: Identifying the Active Sites for Propane Dehydrogenation on Platinum-Based Catalysts Through Density Functional Theory, Experimental Data, and Uncertainty Quantification

Charles Henry Fricke

FROM THE SURFACE TO THE REACTOR: IDENTIFYING THE ACTIVE SITES FOR PROPANE DEHYDROGENATION ON PLATINUM-BASED CATALYSTS THROUGH DENSITY FUNCTIONAL THEORY, EXPERIMENTAL DATA, AND UNCERTAINTY QUANTIFICATION

by

Charles Henry Fricke

Bachelor of Science
Virginia Commonwealth University, 2016

Submitted in Partial Fulfillment of the Requirements

For the Degree of Doctorate in Philosophy in

Chemical Engineering

College of Engineering and Computing

University of South Carolina

2022

Accepted by:

Andreas Heyden, Major Professor

Edward Gatzke, Committee Member

Brian Habing, Committee Member

John R. Monnier, Committee Member

Melissa A. Moss, Committee Member

Tracey L. Weldon, Interim Vice Provost and Dean of the Graduate School

DEDICATION

To my Opa, Dick Charles Vermeer.

A scientist, an engineer, and a loving grandfather.

ACKNOWLEDGEMENTS

The inception of novel science requires a brilliant scientist, and the completion of a great study requires a patient scientist. I am thankful that Dr. Heyden is both brilliant and patient, and mentors me with honesty, with understanding, and with zeal for good science.

I would like to thank my committee members, Dr. Gatzke, Dr. Habing, and Dr. Monnier, for their guidance, time, and help. In addition, much of this work would be impossible without the expertise and guidance of Dr. Salai Ammal, Dr. Gabriel Terejanu, and Dr. Eric Walker, and I am forever thankful for their help.

In addition, much would be amiss if I didn't thank my current and past groupmates, including Dr. Mohammed Saleheen, Dr. Wenqiang Yang, Dr. Osman Mamun, Dr. Kyung Eun You, Dr. Mehdi Zare, Dr. Yongjie Xi, Dr. Biplab Rajbanshi, Dr. Supriya Saha, Nicholas Szaro, Dia Sahsah, Olajide Bamidele, Mubarak Bello, Adam Yonge, Marie Burns, Subrata Kundu, Panuwat Watthaisong, Emmanuel Eluno, and Paratee Komen.

Finally, my family deserves much appreciation and thanks for their support, their patience, and their encouragement. Truly none of this would be possible without them.

ABSTRACT

Propane dehydrogenation is a critical process of producing propylene, an important feedstock for the chemical industrial. There are multiple key processes to produce propylene in this manner, but one of the largest processes involves non-oxidative dehydrogenation on a platinum-tin alloy based catalyst. In general, these reactions and catalytic particles are complex, with many dehydrogenation, cracking, and reforming reactions taking place during these processes on multiple surfaces. With this in mind, ab initio computational catalysis models are used to generate further insight into these catalytic processes. In this dissertation, there are three aims to be solved: identifying the most likely active surface on a catalytic platinum particle, modeling the catalyst particle itself, and understanding how alloying with platinum-tin impacts the selectivities of all surfaces studied.

For the first aim, three surfaces, Pt(100), Pt(111), and Pt(211) were used to model potential catalysts particle sites. Uncertainty quantification and Bayesian inference was applied to the developed models to understand the reported experimental quantities of interest like turnover frequencies, apparent activation energies, selectivities to propylene, and reaction orders. From this, it was found that the most likely active site was the Pt(211) model for certain simulations, and that the first dehydrogenation step of propane was rate limiting. To answer the next aim of this work, four platinum-tin surface skin models were developed to understand how tin doping affects the catalytic reaction. Four

models were chosen, Pt_3Sn/Pt(100), PtSn/Pt(100), Pt_3Sn/Pt(111), and Pt_2Sn/Pt(211). Using uncertainty analysis and Bayesian inference, it was found that the most supported model using the evidence of the calibration problem was Pt_2Sn/Pt(211), which has strong evidence for this to be the model when compared to the next highest evidence model, Pt_3Sn/Pt(111), which is in-line with the pure platinum model. In addition, the 1st dehydrogenation step is modeled to be the rate controlling step, however, on Pt_2Sn/Pt(211), often the 2nd dehydrogenation step is rate limiting as well.

TABLE OF CONTENTS

LIST OF TABLES

LIST OF FIGURES

CHAPTER 1

INTRODUCTION

To model catalytic particles and explain experimental results, ab initio computational models using density functional theory are often used to understand how reactions of interest take place on catalytic surfaces. There are inherent complexities in these models, including the choice of functional, which can generate a range of energies for reactants, products, and transitions states. These energies can range on the order of close to an eV, which when one can expect a rate change of ten times greater or less for every tenth of an eV decrease or increase in the activation barriers dependent on reaction temperatures, these errors have a large impact on the results given by modeling. There is a desire to model these functional errors and incorporate them into the microkinetic models that often predict whether a site or facet is active. This dissertation's focus is on incorporating these errors, and applying them to a key chemical reaction, direct dehydrogenation of propane to propylene. As this is a process of great industrial importance, published experimental data has been generate in terms of the kinetics of these reactions, with much focus on platinum particles. Through uncertainty quantification and Bayesian inference, the most likely dominant platinum surface can be identified. In addition, once the pure platinum catalyst has been well described, the improvements of tin-alloys, which is what most industrial processes use, can be studied to explain increases in selectivity to propylene.

This following work is written in manuscript style to answer the above aims. In Chapter 2, my first study, which has been published ACS Catalysis in October 2021, was to identify the most likely active site for propane dehydrogenation. Uncertainty quantification, Bayesian statistics, reported experimental literature, and density functional theory were analyzed to identify the most likely active site. Three different platinum surface models were use as models for active sites, these being Pt(100), Pt(111), and Pt(211). In addition, two different methodologies for generating uncertainty, using data from four DFT functionals and data from the BEEF-vdW ensemble were used and developed. Through using these three surface models using the Four Functional Model and BEEF-model with Ensembles, a total of six different computational models were generated and compared. Three experimental data sets, with varying numbers of reported observables, such as turnover frequencies, selectivity to propylene, apparent activation energy, and reaction orders, were calibrated and validated for these six surface models. Through this work, the study found no supportive evidence for Pt(100) as the dominant active facet, and finds that Pt(211) has evidence for being the most supported active site in some simulations, when compared to Pt(111). Through this work, we also find that there are differences in methodologies, in that the Four Functional Model did not model the experimental data as well as the BEEF-vdW Model with Ensembles. We also found that on both Pt(111) and Pt(211), the kinetically rate-controlling step is the first dehydrogenation step from propane to $C_3H_7^*$.

In Chapter 3, my second manuscript, we studied the effects of different platinum-tin alloy skin models on bulk platinum to evaluate the differences between the pure platinum models. This part of the work tests four different platinum-tin skins on bulk

surface models as potential catalytic sites, being Pt_3Sn/Pt(100), PtSn/Pt(100), Pt_3Sn/Pt(111), and Pt_2Sn/Pt(211), using an uncertainty analysis methodology that uses BEEF-vdW with its ensembles (BMwE) to generate the uncertainty for the energies of the intermediates and transition states. We calibrated against one experimental data set, with two experimental observations, being selectivity to propylene and turnover frequency of propylene, to evaluate the impact of the experimental data on informing the models. This study finds that the prior model for Pt_2Sn/Pt(211) is very selective towards propylene, while Pt_3Sn/Pt(111) is moderately selective towards propylene, and Pt_3Sn/Pt(100) and PtSn/Pt(100) are unselective towards propylene production. Pt_3Sn/Pt(111) shows greatly increased selectivity to propylene from the pure metal Pt(111) facet. Our work found that for Pt_3Sn/Pt(100), PtSn/Pt(100), and Pt_3Sn/Pt(111), the kinetically rate-controlling step is one of the two first dehydrogenation steps from adsorbed propane to a $C_3H_7^*$ intermediate, while for Pt_2Sn/Pt(211), the results are more inconclusive to whether the first or second dehydrogenation step is rate determining. In addition, all of the calibrated models of the surfaces were found to be selective towards propylene production, model the reported turnover frequency successfully, and that the rate determining steps are the 1st dehydrogenation step from propane to $C_3H_7^*$ for all of the surfaces, save some simulations showing that the 2nd dehydrogenation step from $C_3H_7^*$ to propylene being rate controlling. These results indicate that tin, in addition to affecting the binding strength of the adsorbed species, may prevent deeper dehydrogenation and cracking reaction steps through increasing activation barriers for unwanted side reactions, especially on Pt_3Sn/Pt(111). Finally, the most supported active

site is the Pt_2Sn/Pt(211) site with strong evidence when compared to the next highest evidence model, Pt_3Sn/Pt(111).

CHAPTER 2

PROPANE DEHYDROGENATION ON PLATINUM CATALYSTS: IDENTIFYING THE ACTIVE SITES THROUGH BAYESIAN ANALYSIS[1]

[1] Fricke, C.; Rajbanshi, B.; Walker, E.; Terejanu, G.; Heyden, A. *ACS Catalysis*, **2022**

Reprinted here with permission of publisher

2.1 Abstract

Uncertainty quantification, Bayesian statistics, the reported experimental literature, and density functional theory are synthesized to identify the active sites for the non-oxidative propane dehydrogenation on platinum catalysts. This study tests three different platinum surface models as active sites, Pt(100), Pt(111), and Pt(211), and two different methodologies for generating uncertainty, using data from four density functional theory functionals and data from the BEEF−vdW ensemble. By comparing these three surface facets using two uncertainty sources, a total of six different computational models were evaluated. Three experimental data sets, with varying numbers of reported observables, such as turnover frequencies, selectivity to propylene, apparent activation energy, and reaction orders, are calibrated and validated for these six models. This study finds no evidence for Pt(100) as the dominant active facet and finds that Pt(211) has some evidence for being the most relevant active site on the catalyst. In addition, all four functional models were excluded from final data analysis due to poor "goodness-of-fit". In contrast, the BEEF−vdW model with ensembles (BMwEs) was found to pass "goodness-of-fit" for most of the models tested. Finally, for both Pt(111) and Pt(211), this study finds that the majority of simulations found the kinetically rate-controlling step the first dehydrogenation step from propane to $C_3H_7^*$.

2.2 Introduction

Propane dehydrogenation to propylene research continues to attract significant scientific interest due to propylene's industrial importance and reaction complexity. Non-oxidative propane dehydrogenation (PDH) on platinum-based catalysts continues to be a significant pathway for producing propylene.[1] Understanding the reaction mechanism and

kinetics of surface catalyzed reactions and identifying the active sites for industrial catalysts can help design future catalysts for propane dehydrogenation. Many experimental studies have been done to measure kinetic data for non-oxidative propane dehydrogenation.[2-10] For example, in work by Biloen et al.,[2] platinum and platinum-gold catalysts were studied at 633 K, a partial pressure of hydrogen gas of 2 bar, and a partial pressure of propane of 0.04 bar. They found that the surface was covered by hydrogen at these reaction conditions and reported a turnover frequency (TOF) of propylene of 3.5×10^{-2} s^{-1}. They also calculated a reaction order of -1.1 for hydrogen gas, and 1 for propane gas, and measured an apparent activation energy of 121 kJ/mol. Finally, they proposed that the rate-determining step was the dehydrogenation step of a propyl radical, C_3H_7*, to propylene.

Others have found a similar TOF at higher temperatures with lower partial pressures of H_2. In work performed by Barias et al.[3] a propylene TOF of 0.2 s^{-1} was observed on platinum at 792 K, a partial pressure of propane of 0.29 bar, and a partial pressure of H_2 of 0.09 bar. In addition to reported TOF, they also reported a selectivity to propylene of 85%.

Experimental work on size-dependent platinum particles was performed by Zhu et al.[4] The group studied multiple sized particles to possibly identify the active site at temperatures from 723 K to 823 K, and pressures of H_2 and propane that vary from 1 kPa to 9 kPa. They found that particles 5 nm in diameter and larger had a higher selectivity, and lower TOF's for both propane and propylene than smaller particles. In addition, reaction orders for propane were approximately 1 for all sizes, but the reaction order for H_2 ranged from -0.07 to -0.51, with the reaction order decreasing for larger particles. The

apparent activation energy was found to range from 92 to 95 kJ/mol at steady-state conditions. Compared with Biloen et al.,[2] the propane reaction order is the same, but the H_2 reaction order is less inhibiting. The apparent activation order is slightly less. Both of these shifts are within reason given the different temperature and partial pressure conditions of propane and H_2. One would expect H_2 to exhibit a more negative reaction order at lower temperatures and higher H_2 partial pressures.

In work done by Yang et al.,[10] propane dehydrogenation was tested on two different particle shapes that they claimed to contain approximately only Pt(100) and Pt(111) sites. They then evaluated the selectivity to propylene and the TOF of propylene. They found that TOFs of propylene on both surfaces were relatively similar, 0.58 s^{-1} to 0.6 s^{-1}. However, the cubic particles had a selectivity to propylene of approximately 72%, while the selectivity towards propylene for the octahedral particles was approximately 93%. They believed that this difference in selectivity was due to the particular facets being more present on the cubic particles. They justified this claim by comparing theoretical results using density functional theory (DFT), where they theorized that the lower selectivity to propylene was due to a lower adsorption energy for intermediates involved in the propane dehydrogenation on Pt(100).

In similar work done by Zhu et al.,[4] experiments and DFT calculations were used to identify a dominant active site. Using a relatively small dehydrogenation network, they concluded that Pt(111) might be the most active site. Other theoretical work has been performed to identify the active site responsible for the activity of platinum catalysts for propane dehydrogenation, by either calculating the adsorption of propane and C3 species on platinum facets[11,12] or by generating microkinetic models on particular surfaces.[13,14]

Pt(211) has been studied as a model site representing edges and corners.[4,15,16] It was found that Pt(211) is active but may be unselective towards propane dehydrogenation, dependent on reaction conditions.[16] Numerous and competing theories of the active site for propane dehydrogenation persist.

In this work, we seek to identify the most likely dominant active site (assuming one facet dominants the reaction kinetics under experimental reaction conditions) by combining published experimental data with Bayesian statistics and our DFT calculations. This work compares three surface facets, Pt(100), Pt(111), and Pt(211), while using two different sources of generating uncertainty and its correlation structure. While modeling each facet, kinetic data such as TOFs for propylene, apparent activation energies, reaction orders, and selectivity to propylene are reported. Finally, this study also seeks to identify the mechanism and rate-controlling species for these potential active sites.

2.3 Methods

2.3.1 Computational Details

In this study, DFT calculations were performed using the Vienna Ab initio Simulation Package (VASP) version 5.4.4, which uses the projector augmented-wave (PAW) method.[17-21] A plane-wave energy cutoff of 400 eV was used, and together with a Monkhorst-Pack reciprocal space grid of $5 \times 5 \times 1$, converged energies were obtained for the reaction systems.[22,23] In addition, the Methfessel-Paxton method order 1 with a smearing width of 0.2 eV was used for calculating the electronic occupancies. The energy convergence criterion was 1×10^{-7} eV, and for geometry convergence, a force criterion of 0.03 eV/Å was used. Transition state searches were conducted using the nudged elastic

band method followed by further optimization with the dimer method.[24-28] In addition, it is known that the entropies calculated by a purely harmonic approach may be a poor approximation. Due to this, we apply a frequency correction to set all low frequencies below 50 cm^{-1} to 50cm^{-1}, as previously described by Haworth et al.[28]

Three surface models, Pt(100), Pt(111), and Pt(211), were chosen as model facets for this project. For Pt(100) and Pt(111), we used a (4×4) 4-layer, 64 atom surface, relaxing the first two layers. For Pt(211), an 80 atom, 10-layer surface model was used, and the first six layers were relaxed. The bulk fcc-platinum crystal was found to have an optimized lattice constant of 3.92 Å using the PBE-D3 functional,[29,30] and the optimized surfaces had cell parameters as indicated in Appendix A Table A.1 . A vacuum gap of 20 Å was included on each surface to avoid periodic interactions. Representations of these surfaces can be seen in Figure 2.1. In addition, 138 reactions were investigated, including cracking and deep dehydrogenation. Figure 2.2 displays the dehydrogenation reaction network for C_3 species studied in this system. The full reaction network is described tabularly in tables TA.2 – TA.13 in Appendix A.

We chose to first explore the system by using the Perdew-Burke-Ernzerhof functional with Grimme's van der Waals corrections (PBE-D3) for the optimization of the surfaces, adsorbed species, and transition states.[29,30] This functional was chosen for its generality, the computational communities extensive experience, and its inclusion of empirical van der Waals interactions. An additional three functionals were chosen, including the revised Perdew-Burke-Enzerhof functional (RPBE),[31] the Bayesian error estimate functional with van der Waals corrections (BEEF-vdW),[32] and the strongly constrained and appropriately normed functional with revised Vydrov and van Voorhis

nonlocal correlations (SCAN-rVV10),[33] to generate single point energies based off the PBE-D3 structures. Three generalized gradient approximation functionals, these being PBE-D3, RPBE, and BEEF-vdW, were specifically chosen due to the metallic nature of the surface model and their prominent use in the computational catalysis community, i.e., any of them could have been used for studying the propane dehydrogenation over Pt catalysts. In addition, we chose SCAN-rVV10, a meta-GGA that generally does not underpredict energy barriers as much as GGA functionals. Out of these four functionals, three include van der Waals interactions, which we believed to be critical for the adsorption processes of hydrocarbons, and one without van der Waals interactions that generally predicts lower adsorption energies (RPBE), but that is optimized for predicting adsorption energies of small molecules so that errors in adsorption energies would be more likely to be represented in the prior distribution. These functionals were also previously compared in other work, and it was thought that they might aid in identifying possible functional pairings that may better estimate the errors present.[34] Next, BEEF-vdW was used as it generates 2000 non-self-consistent ensemble energies based on the converged charge density. Finally, gas-phase thermodynamics were corrected to NIST data using a Dirichlet distribution as described in work done by Walker et al. in order to allow gas-phase uncertainties to be uniformly sampled among the three different gas-phase species.[35-38] The range for the gas-phase errors was allowed to range from ± 0.2 eV, assuming that propane, propylene, and H_2 are generally well described by DFT. All of the intermediate, gas-phase species, and transition state energies of these four functional calculations can be found in Tables A.2 – A.14 in Section A.2 of Appendix A.

2.3.2 Functional Latent Variable Model

To summarize the uncertainty present in our DFT calculations, factor analysis was applied to the four functionals used in this study in the same way as Walker et al.[37-39] This has been thought to be an encompassing methodology for calculating the uncertainties for the energies of the species involved. In general, the different functionals, stated in the in the previous paragraph, have been extensively used in the catalysis community, and these functionals have been thought of as relatively accurate in calculating emergent properties of catalytic surfaces, such as turnover frequencies (TOF). The uncertainty for the Four Functional Model (FFM) was generated by this method, with the covariance matrix calculated between the energies of the adsorbed species and transition state species, and the mean of the energies being the mean of the four functionals chosen in this study.

We also chose to generate a second model system using BEEF-vdW and its ensembles. For every species, including gas-phase, metal slab, adsorbed species, and transition state species, BEEF-vdW generates an ensemble of 2000 non-self-consistent energies. The adsorbed intermediate and transition state energies were referenced to propane, hydrogen, and the platinum slab, such that

$$v_{ref,i,j} = v_{i,j} - \left(N_{propane,i} v_{propane,j} + N_{H_2,i} v_{H_2,j} + v_{Platinum,slab,j}\right) \qquad (2.1)$$

where $v_{ref,i,j}$ is the referenced BEEF ensemble energy j for either adsorbed species or transition state i, $v_{i,j}$ is the BEEF ensemble energy output j for species i, $v_{H_2,j}$ and $v_{propane,j}$ are the gas phase values of the ensemble energies for propane and hydrogen gas, respectively, $v_{Platinum,slab,j}$ is the ensemble energy j of the specific slab the species is adsorbed on, and $N_{propane,i}$ and $N_{H_2,i}$ are the number of propane and hydrogen molecules

needed to correct the sum to the number of carbon and hydrogen atoms present in the species *i*, which can be fractional.

Next, the mean was taken of the referenced 2000 BEEF-vdW ensembles, $\mu_{ref,i}$, and subtracted from the referenced 2000 functional ensemble energy, $v_{ref,i,j}$, so that the mean of the ensembles would be zero, as described in equation 2.2.

$$v_{ref,i,j}{}^{*} = v_{ref,i,j} - \mu_i \tag{2.2}$$

where $v_{ref,i,j}{}^{*}$ are the 2000 BEEF ensemble energies for each species with a mean of zero. Finally, the BEEF-vdW referenced energy was added back into the ensemble by the following equation:

$$v_{ref,i,j}{}' = v_{ref,i,j}{}^{*} + G_{BEEF-vdw,ref,i} \tag{2.3}$$

where $G_{BEEF-vdw,ref,i}$ is the Gibbs free energy of species *i* computed from the mean of the BEEF-vdW functional (and referenced as before). Equation 3 ensures that the mean of the ensembles yields the BEEF-vdW Gibbs free energy for the intermediate or transition state *i*. After this, the BEEF-vdW ensemble energies were processed using a factor analysis model. It was found that the covariance matrix generated by the factor analysis and the covariance matrix generated without the factor analysis for BEEF-vdW were similar to each other. Still, this study used the factor analysis derived covariance matrix to keep the methodologies consistent. Using the BEEF-vdW data, this model is known as the BEEF-vdW Model with Ensembles (BMwE).

2.3.3 Likelihood Function and Model Discrepancy.

The likelihood function, p(D|θ,M), as defined in previous work,[37,38] provides the likelihood of finding experimental data, D, given the values of parameters, and the uncertainty of the model. This study compared our models against three datasets, each dataset of a different size. These three data sets are summarized in Table A.21 in Section A.3 of Appendix A. Dataset 1 (D1) contains the following quantities of interest,[2]

$$D_1 = \{TOF, \alpha_{propane,}\alpha_{H_2}, E_{apparent}\} \tag{2.4}$$

Dataset 2 (D2) contains five quantities of interest to calibrate on.[4]

$$D_2 = \{TOF, \alpha_{propane,}\alpha_{H_2}, E_{apparent}, Selectivity\} \tag{2.5}$$

Dataset 3 (D3) contains two quantities of interest to calibrate on.[3]

$$D_3 = \{TOF, Selectivity\} \tag{2.6}$$

The TOF is the turnover frequency, α_i is the reaction order of either propane or hydrogen gas for propane consumption, and $E_{apparent}$ is the apparent activation energy for propane consumption. Selectivity is defined to be the following:

$$Selectivity = \frac{TOF_{Propylene}}{TOF_{Propane}} \tag{2.7}$$

This study compares datasets of unequal size, remembering that likelihoods are multiplicative, and though incomplete datasets are less than ideal, they are unfortunately a reality of modeling and synthesizing already published experimental data. The measurements are assumed to be independent given our model, which can translate into the factorization of the likelihood function given the data such as D_1.

$$p(D_1|\theta, M) = p(TOF|\theta, M) * p\left(\alpha_{propane}\middle|\theta, M\right) * p\left(\alpha_{H_2}\middle|\theta, M\right) * p\left(E_{apparent}\middle|\theta, M\right) \quad (2.8)$$

For D_2, the equation is similar; however, it includes the additional selectivity term

$$p(D_2|\theta, M) = p(TOF|\theta, M) * p\left(\alpha_{propane}\middle|\theta, M\right) * p\left(\alpha_{H_2}\middle|\theta, M\right) * p\left(E_{apparent}\middle|\theta, M\right) * p(Selectivity\,|\theta, M) \quad (2.9)$$

D_3 only reports the TOF and selectivity, which reduces the likelihood function for this set to equation 2.10.

$$p(D_3|\theta, M) = p(TOF|\theta, M) * p(Selectivity\,|\theta, M) \quad (2.10)$$

Each individual likelihood function is defined by the difference between the simulations of our models and the experimental data. This discrepancy is due to unknown errors, both from the model and from the experiment.[36] We assume that the discrepancies are distributed with a mean of zero, and an unknown variance in each measurement of σ_i^2. Each of these variances is described using an inverse gamma distribution, which is reported in Table A.18 in Section A.2 of Appendix A, and an example is graphically described in Figure A.1. These discrepancies can be written such that the experimental values are equal to the model value plus an error term.

$$log_{10}TOF = log_{10}TOF^* + \epsilon_{TOF} \quad (2.11)$$

The likelihood function for the calibration of propane dehydrogenation for experimental D1 can be expanded, as shown in equation 2.12.

$$p(D_1|\theta,M) = \frac{1}{\sqrt{2\pi\sigma_{TOF}^2}}\exp\left(-\frac{1}{2}\frac{(log_{10}TOF - log_{10}TOF^*)^2}{\sigma_{TOF}^2}\right)$$

$$* \frac{1}{\sqrt{2\pi\sigma_{\alpha_{propane}}^2}}\exp\left(-\frac{1}{2}\frac{\left(\alpha_{propane} - \alpha_{propane}{}^*\right)^2}{\sigma_{\alpha_{propane}}^2}\right) *$$

$$\frac{1}{\sqrt{2\pi\sigma_{\alpha_{H_2}}^2}}\exp\left(-\frac{1}{2}\frac{\left(\alpha_{H_2} - \alpha_{H_2}{}^*\right)^2}{\sigma_{\alpha_{H_2}}^2}\right) *$$

$$\frac{1}{\sqrt{2\pi\sigma_{E_{apparent}}^2}}\exp\left(-\frac{1}{2}\frac{\left(E_{apparent} - E_{apparent}{}^*\right)^2}{\sigma_{E_{apparent}}^2}\right) \quad (2.12)$$

The derivations for the likelihood functions for datasets D2 and D3 are included in the Appendix A, Section A.2. The Quantification of Uncertainty for Estimation, Simulation and Optimization (QUESO) package is used to perform the statistical forward problem and calibration problem.[40] Using this, QUESO performed Metropolis-Hastings Markov Chain Monte Carlo simulations for calibrating our data sets and for simulating the experimental data through the use of the microkinetic model.[41,42]

A similar framework to previous work done by Walker et al. was used to proceed with the Bayesian analysis.[37,38] Bayesian inference was first performed for each surface. Then Bayes formula in equation 2.13 was used to generate a posterior distribution, $p(\theta|D,M)$ for each surface model, i.e., Pt(100), Pt(111), and Pt(211).

$$p(\theta|D,M) = \frac{p(D|\theta,M)p(\theta|M)}{p(D|M)} \quad (2.13)$$

The prior distribution, p(θ|M), contains all of the uncertainties present in the calculations, including the correlation between the molecules.

2.3.4 Microkinetic Modeling

To calculate the adsorption free energies, the following equations were used, with propane and hydrogen gas as references

$$\Delta G_{ads,i} = G_{slab,i} - G_{slab} - \left(N_{CH_3CH_2CH_3} * G_{CH_3CH_2CH_3}\right) - \left(N_{H_2} * G_{H_2}\right) \quad (2.14)$$

where $\Delta G_{ads,i}$ is the free energy of adsorption of intermediate i, $G_{slab,i}$ is the free energy of the slab and adsorbed intermediate i, G_{slab} is the free energy of the clean slab, $N_{CH_3CH_2CH_3}$ is the number of propane gas molecules involved in the reaction, $G_{CH_3CH_2CH_3}$ is the free energy of gas-phase propane, N_{H_2} is the number of correcting H_2 gas molecules present in the reaction, and G_{H_2} is the free energy of hydrogen gas.

The activation free energy is defined as the following and the forward rate constants using harmonic transition state theory (hTST).

$$\Delta G_j^{\ddagger} = G_j^{\ddagger} - \sum G_{ads,j}^{R} \quad (2.15)$$

$$k_{for,j} = \frac{k_B T}{h} e^{-\frac{\Delta G_j^{\ddagger}}{k_B T}} \quad (2.16)$$

Where $\Delta G_j^{\ddagger}$ is the activation free energy of reaction j, $G_{j,i}^{\ddagger}$ is the free energy of the transition state in reaction j, $G_{ads,j}^{R}$ is the reactant free energy of adsorption for reaction j, and $k_{for,j}$ is the forward rate constant.

Collision theory was used for calculating adsorption rate constants using the following equation

$$k_{ads} = \frac{1}{N_0\sqrt{2\pi m_A k_B T}} \tag{2.17}$$

where N_0 is the number of sites per surface area, and m_A is the molecular weight of species A. The sticking coefficient has been set to one.

A linear lateral interaction model was used to calculate the change in adsorption energies and transition state barriers as a result of the coverage of certain intermediates that dominate the surface, such as hydrogen on all three surfaces, CH_3C species on Pt(211) and Pt(111), acetylene and single atom carbon on Pt(100), and CH and CH_3CH_2C on Pt(111). It is assumed that errors in linear interaction parameters are small relative to the uncertainty in the low coverage species energy such that the linear lateral interaction parameters are only computed with PBE-D3 functional. This and additional details such as the site occupancy of each species are further described in Section A.4 of the Appendix A.

Reaction orders in H_2 and $CH_3CH_2CH_3$ were calculated using the following equation

$$\alpha_i = \frac{\partial \ln(TOF)}{\partial \ln(P_i)} \tag{2.18}$$

Where α_i is the reaction order of species i, ln(TOF) is the natural logarithm of the turnover frequency of propylene, and $\ln(P_i)$ is the natural logarithm of the partial pressure of species i. We also calculated the apparent activation energy using the following equation:

$$E_{app} = -R\left(\frac{\partial \ln(TOF)}{\partial(\frac{1}{T})}\right)_{P_i} \tag{2.19}$$

where E_{app} is the apparent activation energy.

Campbell's degrees of kinetic and thermodynamic rate control were calculated using the following equations.[43-45]

$$X_{KRC,i} = \left(\frac{\partial \ln(TOF)}{\partial \left(\frac{G_i^{\ddagger}}{-k_B T} \right)} \right)_{T,P_i,G_i^{ads},G_{j,j\neq i}^{\ddagger}} \tag{2.20}$$

$$X_{TRC,i} = \left(\frac{\partial \ln(TOF)}{\partial \left(\frac{G_i^{ads}}{-k_B T} \right)} \right)_{T,P_i,G_i^{\ddagger},G_{j,j\neq i}^{ads}} \tag{2.21}$$

where $X_{KRC,i}$ is the degree of kinetic rate control, and $X_{TRC,i}$ is the degree of thermodynamic rate control.

The reaction network studied includes coking (surface carbon atom formation) and other deep-dehydrogenation steps. All of the intermediates and transition states can be found in Section A.2 of the Appendix A.

2.3.5 Model Exclusion using Mahalanobis Distance

Because of the large number of models tested in this paper, a test was first conducted to see if the Pt(100), Pt(111), and Pt(211) surfaces did not fail to predict the quantities of interest for the calibration and validation data. Failure was checked using the squared Mahalanobis distance for each experimental data set and testing for goodness-of-fit using a chi-squared table.[46-48] The square of the Mahalanobis distance is the following

$$(d-\mu)'\Sigma^{-1}(d-\mu) \tag{2.22}$$

Where μ is a (n × 1) vector of the predicted mean values, n is the number of degrees of freedom present in the evaluated experiment, Σ is the n × n predicted covariance matrix, and d is the (n × 1) vector of reported data. The tested quantities can include turnover frequencies, selectivity, reaction orders in propane and hydrogen, and apparent activation energies.

If the distance statistic was outside of the probability of occurring at a 5% significance level, data was said that it failed to pass the goodness of fit, and those models would have to be removed from consideration. As shown in Table A.19 in Section A.2 of the Appendix A, each of our experiments has different degrees of freedom and thus different outlier exclusion values.

2.3.6 Bayesian Model Selection

A similar methodology to Walker et al.[38] was used to evaluate the model evidence, also referred to as p(D|M), to see how more probable a surface (and corresponding microkinetic model) is the active site compared to another surface. Each prior model was assumed to have an equal likelihood of being the active site. We note that it is assumed here that one "characteristic" surface model is able to describe all experimental kinetic data, i.e., the experimental observation is not a result of multiple, qualitatively different surface models. In other words, this study did not test combinations of surface facets and corresponding microkinetic models as the collective active site. This does not remove the possibility of a combination of surfaces being the active site, just that this work is only testing the surface models independently. The evidence that was generated is compared between models by using Jeffery's scale.[49] Jeffery's scale is a comparison tool for the

Bayes Factors to see if one model is more favored than another given the ratio of evidences between them. As described in Table A.20 of Section II of the Appendix A, Jeffery's scale can give a basic description of how much more likely, or how more well supported, a model might be when compared to another model based on evaluating the Bayes Factors.

2.4 Results and Discussion

For each catalyst model, a separate microkinetic model, uncertainty region, and gas-phase corrections were performed to generate the quantities of interest for each experimental result. Figures 2.3 and 2.4 illustrate the prior distribution of each model for both the BMwE and FFM models at D2 conditions. As visible in these figures, Pt(211) is the more selective of the surfaces, followed by Pt(111) and Pt(100). As reported in Table 2.1, after lateral interactions are included, we find that at D1 reaction conditions, Pt(211) and Pt(100) are dominated by H*, while Pt(111) has close to equal free and H* sites present on the surface. At higher temperatures, such as 793K and 792K for experiments D2 and D3, we find that Pt(100) is dominated by C* and CHCH* species, with minor contributions from CHC*,CH_3CCH*, and CH_2CCH*. At reaction conditions of D2 and D3, Pt(111) has a high free site coverage and a minor CH* coverage. Pt(211) has a high free site coverage, but CHC* and other minor coverage species, including CH_3CHCH_3*, CH_3CH_2C*, CH_2CHCH_2*,and CH_3CCH*, become more prevalent at these higher temperatures. Lateral interactions used and their methodology can be found in Section A.4 present in the Appendix A. Using the prior only, we find that Pt(211) has high selectivity to propylene for all reaction conditions, as seen in both Figure 2.3 and 2.4, and also displayed in Table A.27. Pt(100) has a relatively high selectivity to propylene at D1 conditions; however, it becomes unselective at D2 and D3 conditions, where dominant products include ethylene

and methane. Pt(111) is also selective to propylene at D1 conditions. At higher temperatures, Pt(111) becomes less selective towards propylene, with average selectivity to propylene falling from 77% and 84%, dependent on methodology, to approximately 50%. Methane and ethylene become important products at these temperatures, similar to what happens to Pt(100) at higher temperatures. These changes in selectivity can be explained through reviewing both the free energy of adsorption of propane and other key products, as described in Tables A.2-A.14, as well as in activation barriers around the propane to propylene dehydrogenation pathway, as described in Appendix A Tables A.15-A.17. Though the adsorption energies of propylene can partially explain the selectivity to propylene, selectivity to propylene may be better explained by the activation barriers for competitive dehydrogenation products for other C_3H_6 intermediates, deeper dehydrogenation of propylene, and cracking of propylene, which are all partially functions of the adsorption energy of propylene. For Pt(100), activation energies are lower for competitive dehydrogenation steps, such as $CH_3CH_2CH_2^* \rightarrow CH_3CH_2CH^* + H^*$, and $CH_3CHCH_3^*$ -> $CH_3CCH_3^* + H^*$, than for either $CH_3CH_2CH_2^*$ or $CH_3CHCH_3^*$ to produce propylene. At higher temperatures, cracking barriers of propylene and further propylene dehydrogenation are much more accessible, explaining the decrease in selectivity at the increasing temperatures of experimental datasets D2 and D3. For Pt(111), competitive dehydrogenation of the C_3H_7 intermediate species to other C_3H_6 species is relevant, as is similar to the case of Pt(100), but the barriers to further deep-dehydrogenation and cracking of propylene are higher, explaining the decrease in selectivity as temperature increases, but not to the extent of Pt(100). In addition, this may be most evident for the Pt(211) surface, where the dehydrogenation pathways from propane to propylene are more favorable than

competitive dehydrogenation reactions from the $CH_3CH_2CH_2^*$ and $CH_3CHCH_3^*$ intermediate species. The barriers for further dehydrogenation and cracking are much higher for Pt(211) than Pt(100), and similar to Pt(111), though much larger than the simple dehydrogenation pathways. These selectivity results change after calibration, and the selectivity to propylene becomes much higher for Pt(111) and Pt(211) for all models, which can be seen in Figures 5 and 6, as well as in the Appendix A, Figures A.14 through A.33.

After evaluating these prior models, we discuss model exclusion through the use of the squared Mahalanobis distance and chi-squared goodness of fit, and then through analyzing the model evidence to see if any one site can be called a characteristic active site describing the overall kinetics.

2.4.1 Model Exclusion

To check whether a catalyst model could be the active site, the goodness-of-fit of each model is checked to the data by using the squared Mahalanobis distance and comparing it to the chi-squared values as described in Table A.19 of Section A.2 in the Appendix A, after calibrating two experimental datasets to the surface microkinetic model, and then running at conditions of one of the three experimental data sets. If the squared Mahalanobis distance is smaller than the chi-squared value for the experiment given the number of degrees of freedom, the model is not excluded from further data analysis. However, suppose the squared Mahalanobis distance value is greater than the chi-squared value for a particular experimental condition given a calibration set; in that case, the catalyst model for the entirety of the calibration set is excluded, as its estimates and uncertainties of the quantities of interest are inconsistent with the published experimental

data.[2,3,4] As described in Table 2.2, we find that we can exclude from further analysis the Pt(100) surface as the potential only active site using both the FFM as well as the BMwE. In addition, similar results are found for Pt(111) and Pt(211) using the FFM, where the model fails to describe what is occurring in experiments D2 and D1, respectively.

Considering the squared Mahalanobis distance, the only models to check for Bayes Factors are Pt(111) and Pt(211) using the BEEF-vdW with ensembles model.

2.4.2 Model Evidence

After testing for goodness-of-fit using the squared Mahalanobis distance, the evidence generated is checked and compared for all non-excluded catalyst models. As described in Table 2.2, only the BMwE was able to pass the goodness-of-fit tests. This means that, in this particular case, the FFM fails to provide consistent predictions with the experimental data for the simulations and must not be considered as a potential model for any of the three catalyst surfaces. For BMwE, the evidence of the Pt(111) and Pt(211) catalyst models can be compared, as they have passed the goodness-of-fit test. Pt(100) is excluded from further analysis as the active site for both uncertainty generation models since the surface failed the goodness-of-fit in all calibration cases.

In generating the Bayes Factor between Pt(211) and Pt(111) for the BMwE, Table 2.3 describes that there is strong evidence for Pt(211) to be the active site for propane dehydrogenation when calibrating on D1 and D2. When calibrating models on D1 and D3, there is no evidence for or against either Pt(111) or Pt(211) to be the preferred active site. As described in Figure 2.5, Pt(211) and Pt(111) give similar results for the majority of the quantities of interest evaluated. Still, there are significant differences in the apparent

activation energy, where Pt(211) does a more successful job of capturing the experimental data point.

In addition, we analyzed the surfaces for the degree of kinetic rate control for propane consumption and propylene production. As shown in Figure 2.7, the Pt(211) and Pt(111) surfaces show that almost all of the rate-controlling steps are propane dehydrogenation to C_3H_7 species, in line with predictions from the rate-limiting step from the two experiments.[2,4] There is significant uncertainty with how rate-controlling these C_3H_7 species and these first dehydrogenation steps are, but in the kinetic degree of rate control for propane consumption, these two steps sum to one or close to 1 for the majority of simulations. Differences arise however when measuring the degree of kinetic rate control for propylene production. As the Pt(211) surface is highly selective, propane consumption and propylene production have the same values for the degree of kinetic rate control. However, for the less selective Pt(111) surface there are differences for the degree of kinetic rate control on propane consumption and propylene production. This difference is due to the competing mechanisms for different dehydrogenation and C-C cleavage products.

Next, the two propane to C_3H_7 dehydrogenation steps can best explain the reported kinetics, which is again supported by the reported reaction orders. When the rate-controlling step is the dehydrogenation of $CH_3CH_2CH_3^* + 1^* \rightarrow CH_3CH_2CH_2^* + H^*$, as described in Table A.2 in the Appendix A as Reaction 2,

$$CH_3CH_2CH_3^* + 1^* \rightarrow CH_3CH_2CH_2^* + H^* \quad (23)$$

Then, the rate equation is

$$r_2 = k_2 \theta_{CH_3CH_2CH_3} \theta_* \quad (24)$$

If one assumes the following adsorption reactions to be in equilibrium

$$CH_3CH_2CH_3(g) + 1^* \rightleftarrows CH_3CH_2CH_3^* \quad (25)$$

$$H_2(g) + 2^* \rightleftarrows 2\, H^* \quad (26)$$

then the surface coverage of the adsorbed species is found as

$$\theta_{CH_3CH_2CH_3} = K_{ads,CH_3CH_2CH_3} P_{CH_3CH_2CH_3} \theta_* \quad (27)$$

$$\theta_H = \sqrt{K_{ads,H_2} P_{H_2}}\, \theta_* \quad (28)$$

Inserting the above into the previous equation, it is found that

$$r_2 = k_2 K_{ads,CH_3CH_2CH_3} P_{CH_3CH_2CH_3} \theta_*^2 \quad (29)$$

If the majority of Pt sites is either free or covered by hydrogen, which is the case for Pt(211) sites and for Pt(111) sites at low temperature conditions, then the free site coverage can be written as

$$\theta_* = \frac{1}{1 + \sqrt{K_{ads,H_2} P_{H_2}}} \quad (30)$$

and we obtain for the observed reaction rate

$$r_2 = \frac{k_2 K_{ads,CH_3CH_2CH_3} P_{CH_3CH_2CH_3}}{\left(1 + \sqrt{K_{ads,H_2} P_{H_2}}\right)^2} \quad (31)$$

which can explain both the low temperature reaction orders found by Biloen[2] with a propane and hydrogen order of 1 and -1, respectively, and to some degree the higher temperature orders of 1 and -0.5 for propane and H_2, respectively, reported by Zhu et al.[4], that this model finds at somewhat covered surface.

2.4.3 Comparing FFM and BMwE models

In this study, three surfaces were modeled using two different methods of generating uncertainty, the BEEF-vdW with Ensembles Model (BMwE) and the Four Functional Model (FFM). We note that there are differences in the covariance matrix and Gibbs free energies between these models. Comparing these uncertainty-generating computational models, in addition to the three surfaces, will generate information about differences in the results from different uncertainty quantification methodologies and whether the FFM or BMwE is more successful at modeling the data. This can illuminate if the set of four functionals within the FFM were a good choice for this system and if BMwE, which is much less computationally involved, is more supported. There is strong evidence to support the BMwE models, as the FFM models all failed the "goodness-of-fit" tests. One can notice the differences in Figure 2.5 and Figure 2.6 between the calibrated datasets simulating the same conditions, as well as further graphically in the Appendix A. The differences between the models are due to the differences in the covariance matrixes from BMwE with ensembles models and the models using the FFM, as well as more positive Gibbs free energies of adsorption with BMwE. The differences for Pt(211) and Pt(111) in adsorption energies are depicted in Figure A.2 in Section II of the Appendix A. The BMwE 95% confidence intervals have a similar uncertainty for some intermediates to the FFM models, but for most intermediates, the BMwE confidence intervals are much larger. Though different, one model having greater uncertainty does not make the model better or worse than another model. Similar confidence intervals for the transition state energies are described in Figure S3. In this study, we find that BMwE can describe the catalysts' surfaces better, given the experimental data. Given that GGA functionals can generally

describe metal surfaces, we expect the BMwE methodology for quantifying uncertainties to be appropriate for most transition metal catalysis problems.

2.5 Conclusions

To identify the active site for the propane dehydrogenation to propylene over Pt catalysts, various elementary reactions for the propane dehydrogenation were studied from first principles over three surfaces: Pt(111), Pt(100), and Pt(211). To develop meaningful mean-field microkinetic models based on transition state theory for these individual surfaces, the lateral interactions between all surface species and transition states were calculated with all high surface coverage species. Given the uncertainties in the DFT energies, we developed two different methodologies for generating the correlation structure of the DFT functional energy uncertainty for each surface model. Next, we performed a Bayesian model selection to identify the most likely active site for propane dehydrogenation over Pt catalysts given reported experimental observables or quantities of interest such as turnover frequency, apparent activation barrier, reaction orders, and propylene selectivity in three different papers.[2,3,4] Here, we also studied whether using different methods of uncertainty quantification lead to different results or if one methodology is more favored for transition metal catalysis.

Using the FFM methodology for evaluating uncertainty, Pt(100), Pt(111), and Pt(211) were found to have failed the goodness-of-fit statistic as shown in the squared Mahalanobis distances, and as such were excluded from further data analysis. Using the BMwE model, Pt(100) was found to have no evidence due to its inability to fit the experimental data, and the Bayes Factor generated between evidence Pt(111) and Pt(211)

strongly supports, based on Jeffreys' scale,[49] Pt(211) as the active site at conditions D1 and D2. At conditions D1 and D3, there is no model evidence supporting one particular surface as the dominant active site.

There are noticeable differences between the BMwE and FFM model results, and the BMwE is the more supported model due to better fit for this specific system. Given that it is currently believed that GGA functionals can generally describe metal surfaces, we expect the BMwE methodology for quantifying uncertainties to be appropriate for most transition metal catalysis problems. Finally, the kinetically rate-controlling steps are some combination of the 1st dehydrogenation steps of adsorbed propane to adsorbed C_3H_7 intermediates.

Though this study focused on mainly quantifying and propagating the functional uncertainties present in the data, other uncertainties arise from different parts of these models. These include uncertainties present in the lateral interaction parameters, the site occupancies, and the entropy values for the intermediates and transition states. We hypothesize that much of the entropic uncertainty and that some of the uncertainty in lateral interactions can be viewed as potentially overwhelmed by the functional uncertainty, as the 95% confidence intervals within functionals, as described by Figures A.2 and A.3 in the Appendix A can span upwards of 1 eV. Uncertainty in the lateral interactions is, by necessity, not only a function of the uncertainty within the lateral interaction parameters themselves, but also by the functionals as well, as the thermodynamics and kinetics of the reaction can and does change, as can be seen by the site coverages reported in Table 1. Uncertainty within the site occupancies can affect results for the microkinetic models as well. Reported in Table A.26 in the , turnover frequencies of propylene change by a factor

of 10, while there are small, but significant, differences in selectivity and reaction orders. We theorize that the uncertainties in the lateral interactions and site occupancies become less relevant to general uncertainty quantification as the percentage of free sites increases on a surface, as the errors become less relevant to the general reaction mechanism, if the initial adsorbates, desired products, and intermediates have sites that can be well defined. Regardless, this is an important topic that should be explored further in future studies.

Although this study was comprehensive in determining whether one of the facets was the sole active site, this study did not test if combinations of surface facets formed together the active site that can describe the experimentally observed behavior at the various experimental reaction conditions. Almost all of the simulations yielded relatively high turnover frequencies for each surface, which may indicate that all are participating significantly in the reactions present on a catalyst particle. We plan on performing such a study in the future.

2.6 Acknowledgments

The National Science Foundation supported this work under grant number CBET-1534260 and additional partial support from grant number OIA-1632824. In addition, C.F. acknowledges partial support from the National Science Foundation IGERT program under grant number 1250052. Computer resources were used from the National Energy Research Scientific Computing Center (NERSC) Contract No. DE-AC02-05CH11231, Pacific Northwest National Laboratory (Ringgold ID 130367, Grant Proposals 51163 and 51711), and the University of South Carolina's High-Performance Computing Group.

2.7 Tables and Figures

Table 2.1: Average site coverages after including lateral interactions on Pt(100), Pt(111), and Pt(211) for D1, D2, and D3 conditions using the Four Functional Model (FFM) and BEEF Model with Ensembles (BMwE).

Average Coverage of Selected Species on Surface (%), after including lateral interactions, No Calibration									
	Four Functional Model (FFM)								
	D1 Conditions			D2 Conditions			D3 Conditions		
Species	Pt(100)	Pt(111)	Pt(211)	Pt(100)	Pt(111)	Pt(211)	Pt(100)	Pt(111)	Pt(211)
Free Site	3.71	33.6	13.1	8.11	65.9	86.0	14.0	64.7	86.2
H	96.1	66.1	86.4	0.00	0.45	1.22	0.97	0.96	1.36
CH_3C	0.00	0.00	0.00	0.00	0.22	0.00	0.00	0.45	0.00
CHCH	0.00	0.00	0.00	19.7	0.07	0.00	25.3	1.16	0.00
CHC	0.00	0.00	0.00	6.08	0.00	5.99	1.23	1.14	1.67
CH	0.00	0.00	0.00	1.44	28.3	0.21	2.75	30.6	0.04
C	0.00	0.00	0.00	40.1	2.82	0.12	45.1	0.66	0.00
Other Species	0.19	0.30	0.56	24.6	2.25	6.50	10.7	0.30	10.7
	BEEF Model with Ensembles (BMwE)								
	D1 Conditions			D2 Conditions			D3 Conditions		
Species	Pt(100)	Pt(111)	Pt(211)	Pt(100)	Pt(111)	Pt(211)	Pt(100)	Pt(111)	Pt(211)
Free Site	18.7	47.3	48.6	7.23	63.4	87.9	9.58	68.6	97.1
H	81.4	52.7	51.1	0.74	0.06	0.16	6.34	0.16	0.55
CH_3C	0.00	0.00	0.00	0.00	0.08	0.00	0.51	1.14	0.00
CHCH	0.00	0.00	0.00	0.16	0.00	0.00	4.16	0.00	0.00
CHC	0.00	0.00	0.00	0.07	0.00	10.4	3.58	0.00	1.44
CH	0.00	0.00	0.00	0.03	32.3	0.03	0.15	27.3	0.01
C	0.00	0.00	0.00	79.8	3.24	0.02	62.6	0.79	0.00
Other Species	0.00	0.00	0.34	11.9	0.92	1.48	13.1	2.00	0.95
Experiment	Reaction Conditions								
D1[2]	$PCH_3CH_2CH_3$ = 0.04 bar, PH_2 = 2 bar, T = 633K								
D2[4]	$PCH_3CH_2CH_3$ = 0.03 bar, PH_2 = 0.03 bar, T = 793K								
D3[3]	$PCH_3CH_2CH_3$ = 0.29 bar, PH_2 = 0.09 bar, T = 792K								

Table 2.2: Evaluated squared Mahalanobis distances for Pt(100), Pt(111), Pt(211) for experimental conditions for the three datasets and the models generated by the Four Functional Model (FFM) and the BEEF-vdW Model with Ensembles (BMwE).[a]

Squared Mahalanobis Distance									
	Four Functional Model (FFM)								
	Pt(100)			Pt(111)			Pt(211)		
Calibration	D3	D2	D1	D3	D2	D1	D3	D2	D1
D1 & D2	27.1	29.1	**3.41**	**0.82**	16.6	**2.05**	**0.50**	**1.18**	26.9
D1 & D3	**3.52**	21.7	**2.61**	**0.81**	16.0	**1.82**	**0.25**	**6.13**	24.0
D2 & D3	**5.01**	18.5	**2.72**	**0.34**	23.3	**9.21**	**0.62**	**0.40**	28.7
	BEEF-vdw Model with Ensembles (BMwE)								
	Pt(100)			Pt(111)			Pt(211)		
Calibration	D3	D2	D1	D3	D2	D1	D3	D2	D1
D1 & D2	**0.41**	**2.91**	11.5	**0.22**	**5.17**	**4.13**	**2.77**	**5.77**	**0.76**
D1 & D3	20.7	**8.49**	13.3	**0.25**	**4.39**	**2.91**	**0.70**	**3.63**	**0.96**
D2 & D3	**2.48**	13.8	26.9	**1.43**	**6.31**	18.4	**1.31**	**5.41**	**4.18**
Experiment	Reaction Conditions								
D1[2]	$PCH_3CH_2CH_3$ = 0.04 bar, PH_2 = 2 bar, T = 633K								
D2[4]	$PCH_3CH_2CH_3$ = 0.03 bar, PH_2 = 0.03 bar, T = 793K								
D3[3]	$PCH_3CH_2CH_3$ = 0.29 bar, PH_2 = 0.09 bar, T = 792K								

[a] Squared Mahalanobis distance numbers marked in bold font are the ones that pass the "goodness-of-fit" tests.

Table 2.3: Evidence of non-excluded models and their Bayes factor.[b]

Evidence			Bayes Factor
	BMwE		BMwE
Calibration Set	Pt(111)	Pt(211)	Pt(211)/Pt(111)
D1 & D2	2.48×10^{-7}	2.93×10^{-6}	11.8
D1 & D3	1.93×10^{-6}	4.34×10^{-6}	2.25
D2 & D3		1.05×10^{-5}	

[b]Data marked in black failed "goodness-of-fit" tests for the calibration and validation datasets and thus are excluded from evaluating evidence.

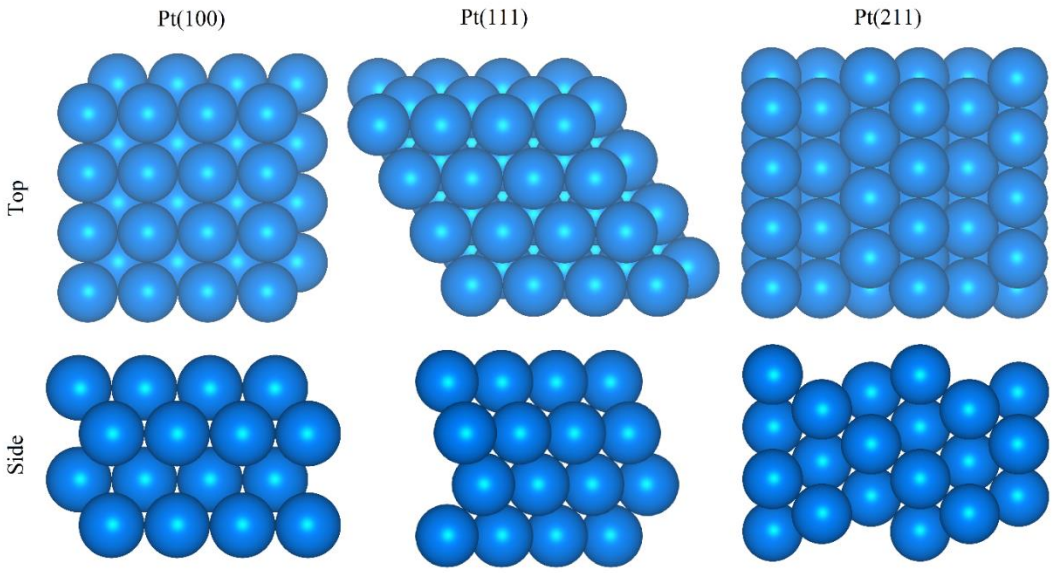

Figure 2.1: Schematics of all platinum facets used in this study.

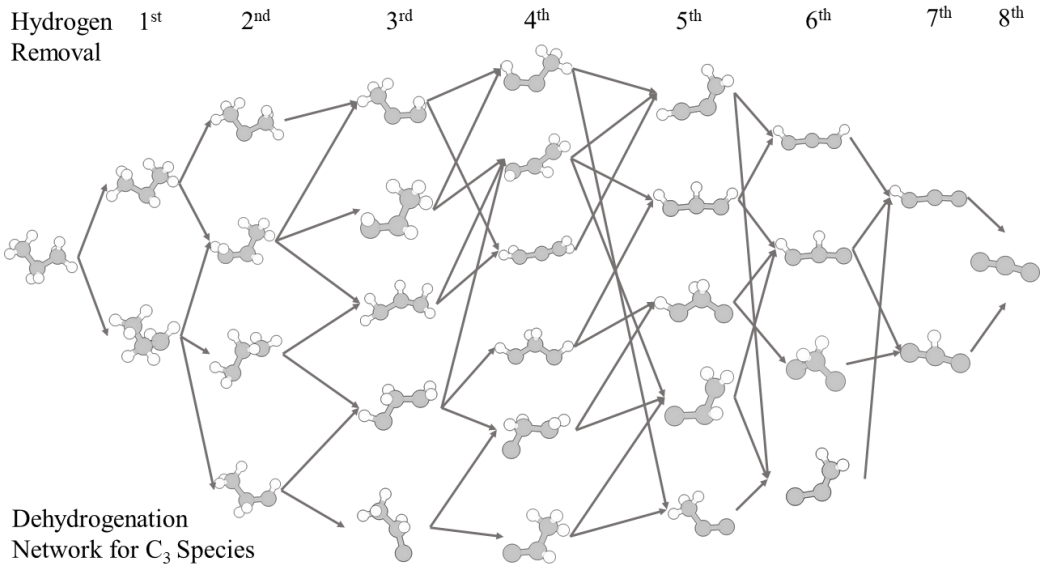

Figure 2.2: Dehydrogenation Reaction Network for C_3 species

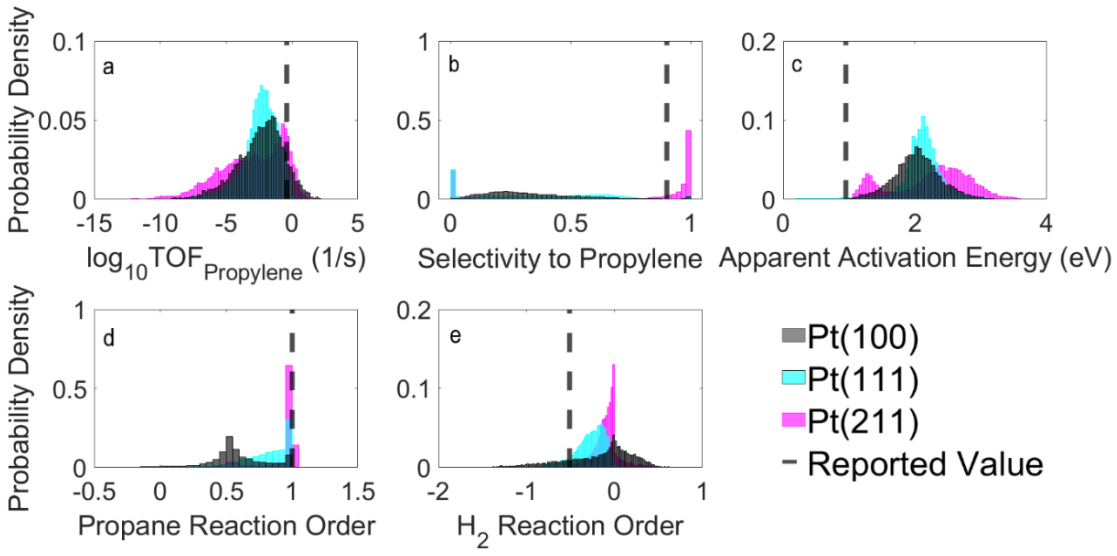

Figure 2.3: Probability densities of reported quantities of interest, including a) TOF (1/s), b) selectivity to propylene, c) apparent activation energy (eV), d) propane reaction order, and e) H_2 reaction order, modeling dataset D2 for Pt(100), Pt(111), and Pt(211) using the BEEF-vdW model with Ensembles (BMwE) for the forward-only model. Reported values are the experimental values reported in dataset D2.

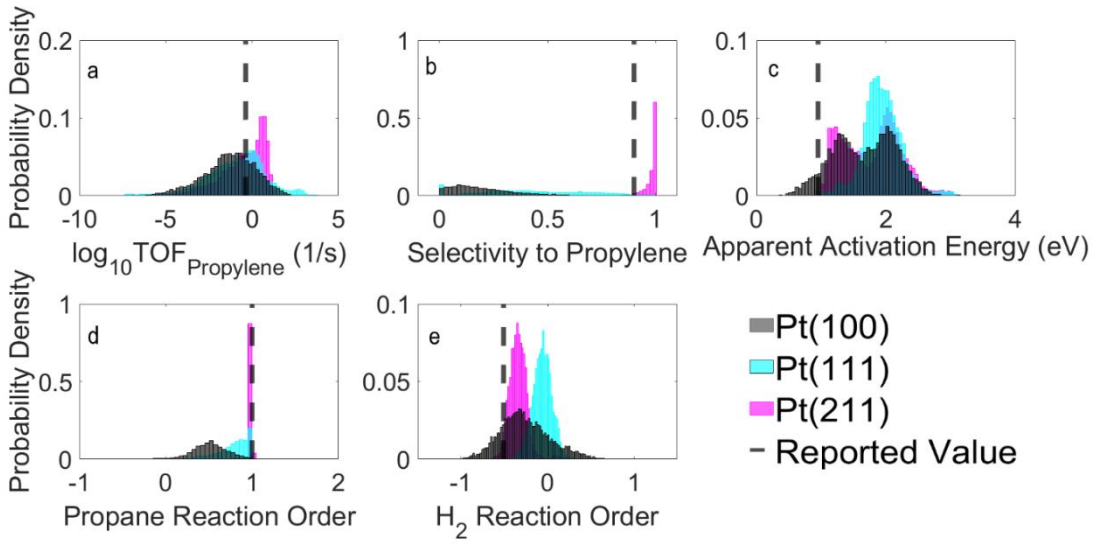

Figure 2.4: Probability densities of reported quantities of interest, including a) TOF (1/s), b) selectivity to propylene, c) apparent activation energy (eV), d) propane reaction order, and e) H_2 reaction order, modeling dataset D2 for Pt(100), Pt(111), and Pt(211) using the Four Functional model (FFM) for the forward-only model. Reported values are the experimental values reported in dataset D2.

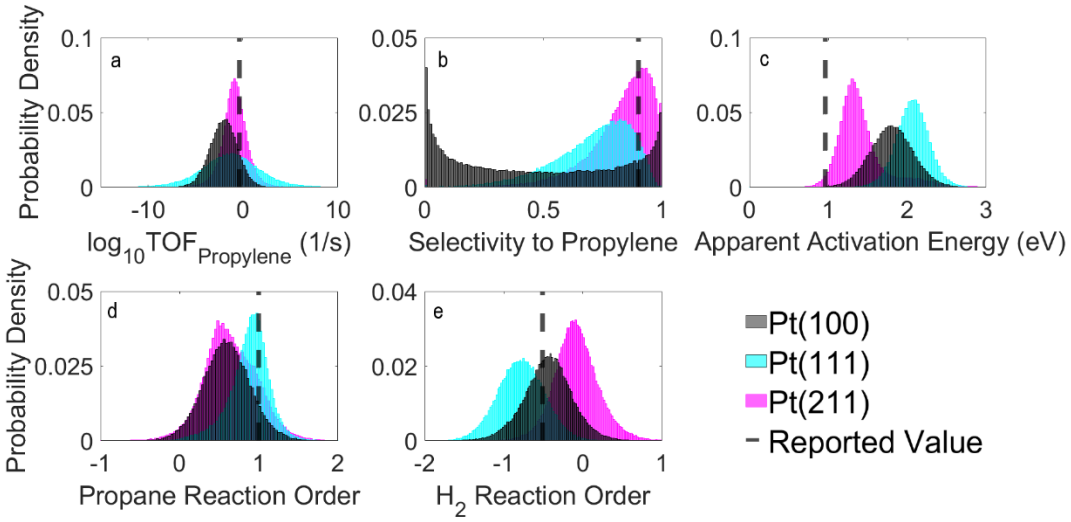

Figure 2.5: Probability densities of reported quantities of interest, including a) TOF (1/s), b) selectivity to propylene, c) apparent activation energy (eV), d) propane reaction order, and e) H_2 reaction order, calibrated with datasets D1 and D3 and validating using dataset D2 for Pt(100), Pt(111), and Pt(211) with the BEEF-vdW model with Ensembles (BMwE). Reported values are the experimental values reported in dataset D2.

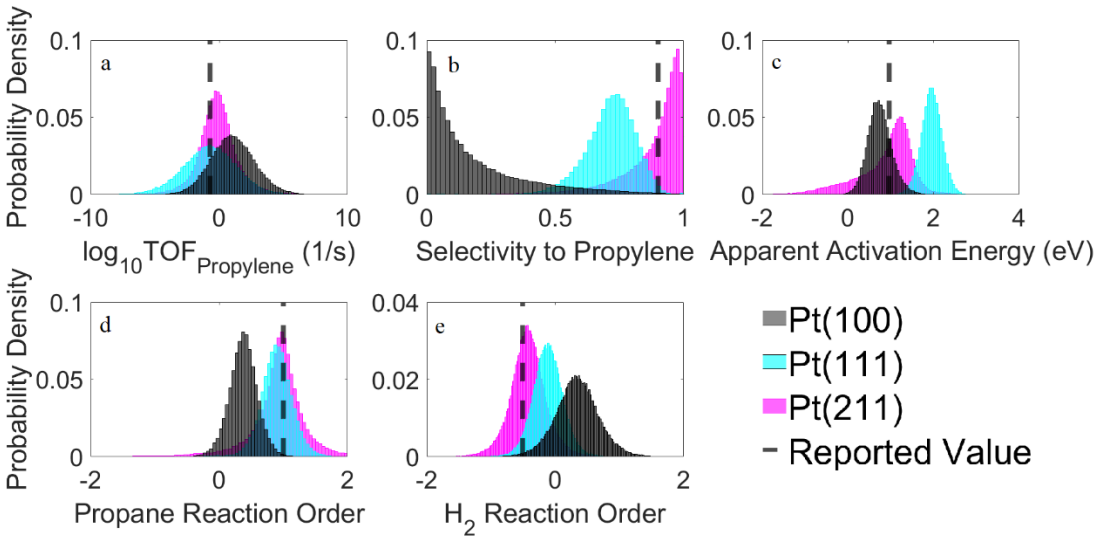

Figure 2.6: Quantities of interest including a) TOF (1/s), b) selectivity to propylene, c) apparent activation energy (eV), d) propane reaction order, e) H_2 reaction order, calibrated with datasets D1 and D3 and validating using dataset D2 for Pt(100), Pt(111), and Pt(211) with the FFM model. Reported values are the experimental values reported in dataset D2.

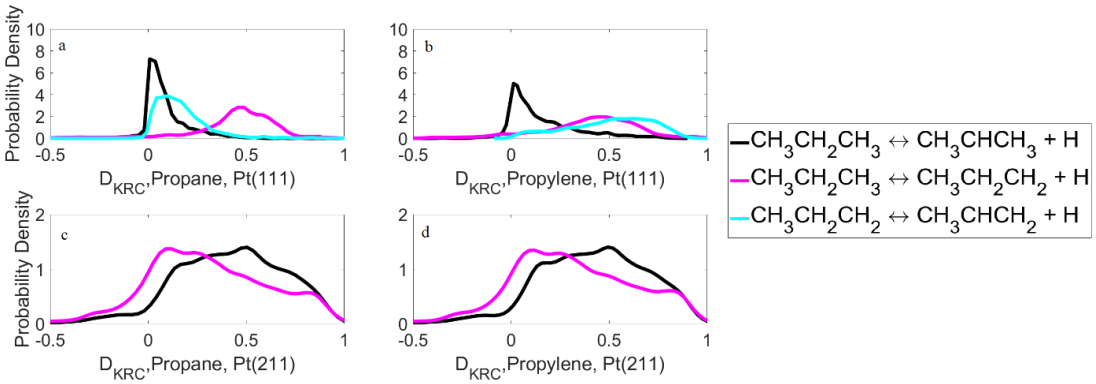

Figure 2.7: Degree of Kinetic Rate Control (D_{KRC}) for Propane Dehydrogenation to Propylene using the turnover frequencies of propane (a,c) and propylene (b,d) using the BMwE forward-only model at 793K for Pt(111) (a,b) and Pt(211) (c,d).

2.8 Bibliography

1. Sattler, J. J. H.; Ruiz-Martinez, J; Santillian-Jimenez, E.; Weckhuysen, B.M. Catalytic Dehydrogenation of Light Alkanes on Metals and Metal Oxides. *Chem. Rev.*, **2014**, *114*, 10613-10653

2. Biloen, P.; Dautzenberger, F. M.; Sachtler, W.M.H. Catalytic Dehydrogenation of Propane to Propene over Platinum and Platinum-Gold Alloys. *J. Catal.*, **1977**, *50* ,77-86

3. Barias, O. A.; Holmen, A.; Blekkan, E.A. Propane Dehydrogenation over Supported Pt and Pt–Sn Catalysts: Catalyst Preparation, Characterization, and Activity Measurements. *J. Catal.*, **1996**, *158*, 1–12

4. Zhu, J.; Yang, M.; Yu, Y.; Zhu, Y.; Sui, Z.; Zhou, X.; Holmen, A.; Chen, D. Size-Dependent Reaction Mechanism and Kinetics for Propane Dehydrogenation over Pt Catalysts, *ACS Catal*. **2015**, *5*, 6310−6319

5. Wang, Y.; Hu, P.; Yang, J.; Zhu, Y.; Chen, D.; C–H bond activation in light alkanes: a theoretical perspective, *Chem. Soc. Rev.*, **2021**, 50, 4299-4358

6. Wang, J.; Chang, X.; Chen, S.; Sun, G.; Zhou, X.; Vovk, E.; Yang, Y.; Deng, W; Zhao, Z; Mu, R.; Pei, C.; Gong, J.; On the Role of Sn Segregation of Pt-Sn Catalysts for Propane Dehydrogenation. *ACS Catal.* **2021** , 11 (8), 4401-4410

7. Xiong, H.; Lin, S.; Goetze, J.; Pletcher, P.; Guo, H.; Kovarik, L.; Artyushkova, K.; Weckhuysen, B. M; Datye, A. K.; Thermally Stable and Regenerable Platinum–Tin Clusters for Propane Dehydrogenation Prepared by Atom Trapping on Ceria, *Angew.Chem.Int. Ed*., **2017**, 56, 8986 –899

8. Motagamwala, A.H.; Almallahi, R.; Wortman, J.; Igenegbai, V. O.; Linic, S.; Stable and selective catalysts for propane dehydrogenation operating at thermodynamic limit, *Science* ,**2021**, 373 (6551), 217-222

9. Hannagan, R. T.; Giannakakis, G.; Reocreux, R.; Schumann, J.; Finzel, J.; Wang, Y.; Michaelides, A.; Deshlarhra, P.; Christopher, P.; Flytzani-Stephanopoulos, M.; Stamatakis, M.; Sykes, E. C. H.; First-principles design of a single-atom–alloy propane dehydrogenation catalyst, *Science* ,**2021**, 372 (6549), 1444-1447

10. Yang, M.W.; Zhu, J.; Zhu, Y.A; Sui, Z.J; Yu, Y.D.; Zhou, X.G.; Chen, D.; Tuning selectivity and stability in propane dehydrogenation by shaping Pt particles: A combined experimental and DFT study. *J. Mol. Catal. A: Chem.l*, **2014**, *395*, 329–336

11. Yang, M. L; Zhu, Y. Chen, F.; Sui, Z.; Chen, D.; Zhou, X. Density functional study of the chemisorption of C1, C2, and C3 intermediates in propane dissociation on Pt(111). *J. Mol. Catal. A: Chem.,* **2014,** *321*, 42-49

12. Nykanen, L.; Honkala, K. Density functional theory study on propane and propene adsorption on the Pt(111) and PtSn alloy surfaces. *J. Phys. Chem. C*, **2011**, *115*, 19, 9578–9586

13. Sun, G.; Zhao, Z.; Mu, R.; Zha, S.; Li. L.; Chen, S.; Zang, K.; Lou, J.; Li., Z.; Purdy, S.C; Kropf, A. J.; Miller, J. T.; Zeng, L.; Gong, J.. Breaking the scaling relationship via thermally stable Pt/Cu single atom alloys for catalytic dehydrogenation. *Nature Commun.,* **2018**, *9*, 4454

14. Saerens, S.; Sabbe, M.; Galvita V.; Redekop, E.; Reyneiers, M.l Marin, G. B. The positive role of hydrogen on the dehydrogenation of propane on Pt (111). *ACS Catal.* **2017**, *7* (11), 7495–7508

15. Yang, M.; Zhu, Y.; Fan, C.; Sui, Z.; Chen, D.; Zhou, X.; DFT study of propane dehydrogenation on Pt catalyst: effects of step sites, *Phys. Chem. Chem. Phys*., **2011**,13, 3257-3267.

16. Ling, X.; Shan, Y.; Sui, Z.; Chen, D.; Zhou, X.; Yuan, W.; Zhu, Y.; Beyond the Reverse Horiuti–Polanyi Mechanism in Propane Dehydrogenation over Pt Catalysts, *ACS Catal*. **2020**, 10, 24, 14887–14902

17. Kresse, G.; Furthmüller, J., Efficiency of ab-initio total energy calculations for metals and semiconductors using a plane-wave basis set. *Comput. Mat. Sci.,* **1996**, *6* (1), 15-50

18. Kresse, G.; Furthmüller, J. Efficient iterative schemes for ab initio total-energy calculations using a plane-wave basis set. *Phys. Rev. B,* **1996**, *54* (16), 11169

19. Kresse, G.; Hafner, J. Ab initio molecular dynamics for liquid metals. *Phys. Rev. B,* **1993**, *47* (1), 558

20. Blochl, P.E. "Projector augmented-wave method", *Phys. Rev. B,* 1994, 50,17953

21. Kresse, G.; Halfer, J. "Norm-conserving and ultrasoft pseudopotentials for first-row and transition elements" *J. Phys. Condens. Matter*, **1994**, *6*,8245

22. Monkhorst, H.; Pack, J. Special points for Brillouin-zone integrations. *Phys. Rev. B,* **1976**, *13*, 5188

23. Pack, J.; Monkhorst, H. Special points for Brillouin-zone integrations. *Phys. Rev. B*, **1977**, 16, 1748

24. Henkelman, G.; Jónsson, H. A climbing image nudged elastic band method for finding saddle points and minimum energy paths. *J. Chem. Phys*., **2000**, *113*, 9901-9904

25. Henkelman, G.; Jónsson, H. Improved tangent estimate in the nudged elastic band method for finding minimum energy paths and saddle points. *J. Chem. Phys*., **2000**, *113*, 9978-9985

26. Henkelman, G.; Jónsson, H. A dimer method for finding saddle points on high dimensional potential surfaces using only first derivatives. *J. Chem. Phys.*, **1999**, *111*, 7010

27. Heyden, A. ; Bell, A. T.; Keil, F. J. Efficient methods for finding transition states in chemical reactions: Comparison of improved dimer method and partitioned rational function optimization method. *J. Chem. Phys.*, **2005**, *123*, 224101

28. Haworth, N. L.; Wang, Q.; Coote, M. L., "Modeling Flexible Molecules in Solution: A pKa Case Study." *J. Phys. Chem. A.*, **2017**, *121* (27), 5217-5225.

29. Perdew, J. P.; Burke, K.; Ernzerhof, M. Generalized Gradient Approximation Made Simple. *Phys. Rev. Lett*., **1996**, *77*, 3865-3868

30. Grimme, S.; Antony, J.; Ehrlich, S.; Krieg, S. A consistent and accurate ab initio parametrization of density functional dispersion correction (DFT-D) for the 94 elements H-Pu. *J. Chem. Phys*., **2010**, *132*, 154104

31. Hammer, B.; Hansen, L. B.; Norskov, J. K. Improved Adsorption Energetics within Density- Functional Theory Using Revised Perdew-Burke-Ernzerhof Functionals. *Phys. Rev. B.*, **1999**, *59*, 7413-7421

32. Wellendorff, J; Lundgaard, K.T; Møgelhøj, A.; Petzold, V.; Landis, D.D.; Nørskov, J.K; Bligaard, T.; Jacobsen, K.W. Density functionals for surface science: Exchange-correlation model development with Bayesian error estimation. *Phys. Rev. B*, **2012**, *85*, 235149

33. Peng, H.; Yang, Z.H.; Sun, J.; Perdew, J.P. Versatile van der Waals Density Functional Based on a Meta-Generalized Gradient Approximation. *Phys. Rev. X*, **2016**, *6*, 041005

34. Sharada, M.S.; Karlsson, R.K.B.; Maimaiti, Y.; Voss, J.; Bligaard, T. Adsorption on transition metal surfaces: Transferability and accuracy of DFT using the ADS41 dataset. *Phys. Rev. B.,* **2019**, 100, 035439

35. Afeefy, H.; Liebman, J.; Stein, S. NIST Chemistry WebBook, NIST Standard Reference Database Number 69. (National Institute of Standards and Technology, Gaithersburg MD, USA 2010).

36. Plessis, S.; Carrasco, N.; Pernot, P. Knowledge-Based Probabilistic Representations of Branching Ratios in Chemical Networks: The Case of Dissociative Recombinations. *J.Chem. Phys*., **2010** ,*133*, 134110

37. Walker E. A.; Mitchell, D.; Terejanu, G. A.; Heyden, A. Identifying Active Sites of the Water−Gas Shift Reaction over Titania Supported Platinum Catalysts under Uncertainty" *ACS Catal.*, **2018**, 8, 3990-3998

38. Walker, E. A.; Ammal, S. C.; Terejanu, G. A.; Heyden, A. Uncertainty Quantification Framework Applied to the Water–Gas Shift Reaction over Pt-Based Catalysts. *J. Phys. Chem. C*., **2016**, *120*, 10328– 10339

39. Rencher, A. C. *Methods of Multivariate Analysis*; John Wiley and Sons, Inc.: Hoboken, NJ, 2007.

40. Prudencio, E.E.; Schulz. K.W. (2012) The Parallel C++ Statistical Library 'QUESO': Quantification of Uncertainty for Estimation, Simulation and Optimization. In: *Alexander M. et al. (eds) Euro-Par 2011: Parallel Processing Workshops. Euro-Par 2011. Lecture Notes in Computer Science*, Bordeaux, France, August 29 – September 2, 2011. Springer, Berlin, Heidelberg, 2011, vol 7155. pp 398-407

41. Horvatits, C.; Lee, J.; Kyriakidou, E.A.; Walker, E.A. Characterizing Adsorption Sites on Ag/SSZ-13 Zeolites: Experimental Observations and Bayesian Inference. *J. Phys. Chem. C,* **2020,** *124* (35), 19174-19186

42. Walker, E.A.; Ravisankar, K.; Savara, A. CheKiPEUQ Intro 2: Harnessing Uncertainties from Data Sets, Bayesian Design of Experiments in Chemical Kinetics. *ChemCatChem*., **2020**,12, 5401-5410.

43. Campbell, C. T. Future Directions and Industrial Perspectives Micro-and Macro-Kinetics: Their Relationship in Heterogeneous Catalysis. *Top. Catal.*, **1994**, *1*, 353–366

44. Campbell, C. T. The Degree of Rate Control: A Powerful Tool for Catalysis Research. *ACS Catal.* **2017**, *7*, 2770−2779

45. Campbell, C. T. Finding the Rate-Determining Step in a Mechanism: Comparing DeDonder Relations with the "Degree of Rate Control". *J. Catal.*, **2001**, *204*, 520–524

46. Mahalanobis, P.C. On the generalised distance in statistics. *Proceedings of the National Institute of Science of India*, **1936**, vol 12, pp. 49-55

47. Warren, R; Smith, R. E.; Cybenko, A. K. Use of Mahalanobis Distance for Detecting Outliers and Outlier Clusters in Markedly Non-Normal Data: a Vehicular Traffic Example. Wright-Patterson Air Force Base, 2011.

48. Brenton, R. G. The chi squared and multinormal distributions. *J. Chemometr*., **2015**; *29*, 9– 12.

49. Jeffreys, H. *The Theory of Probability*; Oxford University Press: Oxford, 1939; pp 356−357.

CHAPTER 3

MODELING THE EFFECT OF SURFACE PLATINUM-TIN ALLOYS ON PROPANE DEHYDROGENATION ON PLATINUM-TIN CATALYSTS[2]

[2] Fricke, C.; Bamidele, O.; Chowdhury, J.; Terejanu, G.; Heyden, A.; *To Be Submitted*

3.1 Abstract

Uncertainty analysis, reported experimental literature, and density functional theory were synthesized to model the effect of surface tin coverage on platinum-based catalysts for non-oxidative propane dehydrogenation to propylene. This study tests four different platinum-tin skins on bulk surface models as potential catalytic sites, these being Pt_3Sn/Pt(100), PtSn/Pt(100), Pt_3Sn/Pt(111), and Pt_2Sn/Pt(211), using an uncertainty analysis methodology that uses BEEF-vdW with its ensembles (BMwE) to generate the uncertainty for the energies of the intermediates and transition states. One experimental data set, with two experimental observations, selectivity to propylene and turnover frequency of propylene, was used as a calibration dataset to evaluate the impact of the experimental data on informing the models. This study finds that the prior model for Pt_2Sn/Pt(211) is very selective towards propylene, while Pt_3Sn/Pt(111) is moderately selective towards propylene. Next, this study finds that for Pt_3Sn/Pt(100) and Pt_3Sn/Pt(111), the kinetically rate-controlling step is one of the two first dehydrogenation steps from adsorbed propane to a $C_3H_7^*$ intermediate, while for Pt_2Sn/Pt(211) and PtSn/Pt(100), the results are more inconclusive to whether the first or second dehydrogenation step is rate determining. In addition, for all of the surfaces the calibrated models were found to be selective towards propylene production, model the reported turnover frequency successfully, and display as most rate determining steps the 1st dehydrogenation step. Nevertheless, Pt_2Sn/Pt(211) emerges as the active site with strong evidence based on Jeffreys' scale interpretation of Bayes factor. These results indicate that tin, in addition to affecting the binding strength of the adsorbed species, prevents

deeper dehydrogenation and cracking reactions through increasing activation barriers for unwanted side reactions, especially on Pt_3Sn/Pt(111).

3.2 Introduction

Propylene production from propane is a crucial reaction of importance, due to the industrial usage of propylene as a chemical feedstock, and the changing economics of propane to propylene dehydrogenation.[1] Non-oxidative propane dehydrogenation (PDH) on platinum-tin catalysts continues to be a significant industrial process of producing propylene, due to its high selectivity to propylene[2,3] Many experimental studies have been done to evaluate the effect of alloying platinum with tin on propane dehydrogenation. [4-22]

In Wang et al.,[4] work was performed to analyze the regeneration of Pt-Sn alloy catalyst particles, by measuring the depletion of tin and the following regeneration of the Pt-Sn surface by segregation processes that occur in the Pt-Sn alloy particle. They find that the particles, after undergoing etching of the original tin and then a regeneration treatment to drive tin from the bulk of the particle to the surface, maintains selectivity of 92% to propylene, with minimal effects on the catalytic properties of the particles. Similar results with Sn enriched surfaces for Pt-Sn catalysts for propane dehydrogenation were seen from Zhua et al.[5]

In Barias et al.,[6] Pt and Pt-Sn alloy nanoparticles were evaluated for propane dehydrogenation. It was found that the single metal platinum nanoparticles were less selective than the alloyed nanoparticles, with the pure metal particles having a selectivity toward propylene of 85% while the Pt-Sn particles had a selectivity close to 97%. In

addition, it was found that the turnover frequencies for propylene production were close to three times higher on Pt-Sn catalysts than on Pt catalysts, and that carbon deposition on the Pt-Sn catalysts was much less than on the Pt catalysts. Similar results were found by Kaylor and Davis,[7] where on silica supported catalysts, Pt-Sn exhibited a much higher selectivity to propylene than platinum-only catalysts. However, Kaylor found that dependent on the particle formed, the Pt-Sn catalysts may have lower turnover rates for propylene than the initial platinum catalysts.

In addition to the experimental literature, many density functional theory-based studies have been performed to analyze the impact of tin on platinum-tin catalysts for alkane dehydrogenation.[23-28] One such study by Nam and Celik was performed to analyze the differences between three surfaces Pt(111), Pt_3Sn(111), and a Pt_3Sn surface skin alloy on a bulk Pt (111) surface for ethane dehydrogenation.[23] They found that increasing Sn in the surface skin alloy may increase the selectivity, while forming a bulk alloy may not increase selectivity as significantly, as they find that the surface skin alloy has a higher selectivity to propylene relative to the bulk alloy. This surface skin alloy behavior may better replicate what is seen experimentally from Wang et al.[4] and Zhua et al.[5] However, disagreements do arise, as Yang et al. finds that the bulk Pt_3Sn alloy for Pt(111) may be the most active of the alloys.[24] The majority of density functional theory studies research Pt(111) and Pt(211) facets, in which they model either the facet to be composed of a bulk alloy, or the pure platinum facet with a surface Pt-Sn alloy skin.[25,26] Pt-Sn alloys cleaved in the (100) direction are not well studied, though it was found by Fricke et al. that Pt(100) has high turnover frequencies of propane consumption and low selectivity to propylene.[29]

In this work, we seek to identify how Sn doping modifies the kinetics of the surface facets of Pt particles for the non-oxidative dehydrogenation of propane to propylene. Specifically, we studied four model surfaces, Pt_3Sn/Pt(100), PtSn/Pt(100), Pt_3Sn/Pt(111), and Pt_2Sn/Pt(211) using density functional theory (DFT) calculations, uncertainty analysis using the BEEF-vdW with its ensembles (BMwE) model, and published experimental literature. While modeling each facet, kinetic data such as turnover frequencies (TOF) for propylene production and other product gases, apparent activation energies, reaction orders, and selectivities to different product gases are reported. Finally, this study also identifies the mechanism and rate-controlling species for these alloys, and explains how potential Pt-Sn alloyed catalysts are more selective and may have higher turnover frequencies to propylene than base platinum catalysts.

3.2 Methods

3.2.1 Computational Details

Calculations were run using the Vienna Ab initio Simulation Program (VASP) version 5.4.4.[30-32] BEEF-vdW was the functional chosen for this study.[33] It was found, in previous work, that BEEF-vdW with its ensembles (BMwE) was more successful in describing platinum surface behavior than an alternative method to describe the uncertainty in the functional choice.[29] A Methfessel-Paxton order of 1 with an electron smearing width of 0.2 eV was used to model the electronic occupancies.[34,35] In addition, an energy cutoff of 400 eV with a 5×5×1 reciprocal grid using Monkhorst-Pack was found to be well converged for the calculations.[36,37] The energy convergence criterium was 1×10^{-7} eV, and the force convergence criterium was 0.03 eV/Å. To correct for

errors in the entropy calculation within the harmonic approximation for small frequencies , frequencies less than 50 cm^{-1} were corrected to 50 cm^{-1}.[38] Transition states were first converged with nudged elastic band calculations, and then with dimer calculations using VTST to ensure that the transition states were well optimized.[39-42] In addition, for each transition state a frequency calculation was performed to verify that there was only one significant imaginary frequency, and that it corresponded to the desired bond cleavage. 46 intermediate species and 130 transition states were optimized for the system. Part of the reaction network is pictorially described in Figure 3.1. All reactions considered are tabulated in Appendix B.1.

Four surfaces were tested in this study, Pt_3Sn/Pt(100), PtSn/Pt(100), Pt_3Sn/Pt(111), and Pt_2Sn/Pt(211). They were chosen to evaluate how a substitutional replacement of platinum with tin would affect the bonding strength of intermediates and transition states. Two Pt(100) surface alloys were modeled, as there is currently little computational work done modeling these particular surfaces for propane dehydrogenation, and that previous computational work found low selectivity of the Pt(100) surface at temperatures of 793K and low partial pressures of hydrogen.[29] In addition, Pt_3Sn/Pt(111) was chosen, as previous work found that the adsorption of intermediates was most disturbed for the system, and that it was theorized that the segregation of the alloy may be occurring, which might be able to be explained by a platinum core/alloy skin model.[23,27] For all surfaces, multiple confirmations and Pt:Sn ratios between 3:1 and 1:1 were modeled, but only the lowest energy Pt:Sn ratio alloy composition was chosen to model the Pt(211) alloy. This is due to the complexity of the surface. Pt_3Sn/Pt(100), PtSn/Pt(100) and Pt3Sn/Pt(111) were chosen due to their ability to model specific sites, and reduce the

complexity of the surface, while Pt(211) has such high complexity, that only the lowest energy of formation (at zero Kelvin) for the alloy was chosen, as defined by the following equation:

$$\Delta E_{formation} = E_{Pt-Sn\ alloy} - E_{Pt,Surface} + n \times E_{Pt,bulk} - n \times E_{Sn,bulk} \qquad (3.1)$$

Where $\Delta E_{formation}$ is the formation energy of the alloy, $E_{Pt-Sn\ alloy}$ is the energy of the alloy, $E_{Pt,Surface}$ is the energy of the surface, n is the number of platinum atoms replaced by tin, and $E_{Pt,bulk}$ and $E_{Sn,bulk}$ are the bulk energies of platinum and β-tin, per atom.

The Pt_3Sn/Pt(100), PtSn/Pt(100), and Pt_3Sn/Pt(111) surfaces were modeled as 4×4×4 layer, 64 atom slabs, with a 15 Å vacuum gap added to prevent periodic interactions. The Pt_2Sn/Pt(211) is a 6 layer, 80 atom slab, with a 15 Å vacuum gap added to prevent periodic interactions. These surfaces are described pictorially in Figure 3.2, and their parameters, as well as their corresponding transition states and intermediates structures, may be found in the Supporting Information as two additional text files.

As mentioned in the previous section, BEEF-vdW with its ensembles (BMwE) was chosen to represent the uncertainty within the functional energy for the models.[29,43] Previous work found that this was a more supported model for describing platinum surface behavior when used for calibrating on experiments. The methodology for generating this model is the same as in Fricke et al., save that BEEF-vdW was used to optimize the entire system, instead of just as a single-point energy calculation.[29] We believe that these differences between the optimized versus single point energies are small in comparison to the total uncertainty in the functional errors, and this allows for data comparison between this study and the platinum-only study.

A common challenge present in computational heterogeneous catalysis is that few experimental data sets have been published on the reaction systems of interest that can be calibrated on, and as such, only differences will be evaluated between the prior model, without calibration, and the posterior model, with calibration, in this work. The experiment from Barias et al. is calibrated against,[6] which was performed at 792 K and at approximately 0.29 bar of propane and 0.1 bar H_2. The data is calibrated on turnover frequency of propane and selectivity to propylene. Selectivity to propylene is defined as the following.

$$Selectivity = \frac{TOF_{Propylene}}{TOF_{Propane}} \tag{3.2}$$

Where $TOF_{Propylene}$ is the turnover frequency of propylene, and $TOF_{Propane}$ is the turnover frequency of propane.

Given the experimental data, $D = \left[TOF_{propylene}, Selectivity\right]$, the likelihood function $p(D|\theta, M)$ assumes independence between experimental measurements and it is defined similarly with the previous work. [29,44,45]

$$p(D|\theta, M) = p\left(TOF_{propylene}\middle|\theta, M\right) * p(Selectivity\,|\theta, M) \tag{3.3}$$

A transformation was applied to the selectivity data using a logit function, as selectivity must be within the bounds of [0,1]. This transformation was done to change the function range to (-∞, ∞) which is necessary to properly include and analyze the errors. The logit function for selectivity is defined as the following.[46]

$$logit(Selectivity) = \ln\left(\frac{Selectivity}{1 - Selectivity}\right) \tag{3.4}$$

In addition, a similar rationale was determined for transforming the $TOF_{Propylene}$ data into the $\log_{10}$TOF data to evaluate the errors present in the model on the range from (-∞, ∞).

Combining the above equations, we find that the full description of the likelihood function is the following:

$$p(D|\theta, M) = \frac{1}{\sqrt{2\pi\sigma_{TOF}^2}} \exp\left(-\frac{1}{2}\frac{(log_{10}TOF - log_{10}TOF^*)^2}{\sigma_{TOF}^2}\right)$$

$$* \frac{1}{\sqrt{2\pi\sigma_{logit(Selectivity)}^2}} \exp\left(-\frac{1}{2}\frac{(logit(Selectivity) - logit(Selectivity)^*)^2}{\sigma_{logit(Selectivity)}^2}\right) \quad (3.5)$$

where σ_{TOF}^2 is the variance of the turnover frequency of propylene, $\sigma_{logit(Selectivity)}^2$ is the variance of the selectivity to propylene, $log_{10}TOF^*$ and $logit(Selectivity)^*$ are the model values of propylene turnover frequency and selectivity, and $log_{10}TOF$ and $logit(Selectivity)$ are the reported experimental values of the TOF and selectivity. Details for the distributions of the variances can be found in Appendix B, Section 2.

The Quantification of Uncertainty for Estimation, Simulation, and Optimization (QUESO) package was used to perform the statistical forward problem and calibration problem.[47] The multilevel Monte Carlo implementation in QUESO was used to calibrate the microkinetic model using experimental data.[48,49]

3.2.2 Microkinetic Modeling

To calculate the adsorption free energies, the following equations were used, with propane and hydrogen gas as references

$$\Delta G_{ads,i} = G_{slab,i} - G_{slab} - \left(N_{CH_3CH_2CH_3} * G_{CH_3CH_2CH_3}\right) - \left(N_{H_2} * G_{H_2}\right) \quad (3.6)$$

where $\Delta G_{ads,i}$ is the free energy of adsorption of intermediate i, $G_{slab,i}$ is the free energy of the slab and adsorbed intermediate i, G_{slab} is the free energy of the clean slab, $N_{CH_3CH_2CH_3}$ is the number of propane gas molecules involved in the reaction, $G_{CH_3CH_2CH_3}$ is the free energy of gas phase propane, N_{H_2} is the number of "balancing" H_2 gas molecules present in the reaction, and G_{H_2} is the free energy of hydrogen gas.

The activation free energy is defined as the following and the forward rate constants are computing using harmonic transition state theory (hTST).

$$\Delta G_j^{\ddagger} = G_j^{\ddagger} - \sum G_{ads,j}^{R} \tag{3.7}$$

$$k_{for,j} = \frac{k_B T}{h} e^{-\frac{\Delta G_j^{\ddagger}}{k_B T}} \tag{3.8}$$

Where $\Delta G_j^{\ddagger}$ is the activation free energy of reaction j, $G_{j,i}^{\ddagger}$ is the free energy of the transition state in reaction j, $G_{ads,j}^{R}$ is the reactant free energy of adsorption for reaction j, and $k_{for,j}$ is the forward rate constant.

Collision theory was used for calculating adsorption rate constants using the following equation:

$$k_{ads} = \frac{1}{N_0 \sqrt{2\pi m_A k_B T}} \tag{3.9}$$

where N_0 is the number of sites per surface area, and m_A is the molecular weight of species A.

A linear lateral interaction model was used to calculate the change in adsorption energies and transition state barriers as a result of the coverage of acetylene and single atomic carbon intermediates that occur on some simulations for the $Pt_3Sn/Pt(100)$ model. In the majority of all of the simulations of the other three surface models, the free sites made up more than 90% of the total sites present on each surface, and so lateral interactions were not warranted for further study. The lateral interaction parameters and methods are further described in Section B.3 in the Appendix.

Reaction orders in H_2 and $CH_3CH_2CH_3$ were calculated using the following equation

$$\alpha_i = \frac{\partial \ln(TOF)}{\partial \ln(P_i)} \tag{3.10}$$

Where α_i is the reaction order of species i, ln(TOF) is the natural logarithm of the turnover frequency of propylene, and $\ln(P_i)$ is the natural logarithm of the partial pressure of species i. We also calculated the apparent activation energy, using the following equation:

$$E_{app} = -R\left(\frac{\partial \ln(TOF)}{\partial(\frac{1}{T})}\right)_{P_i} \tag{3.11}$$

where E_{app} is the apparent activation energy.

Degrees of kinetic rate control using Campbell's degree of rate control theory were calculated using the following equations:

$$X_{KRC,i} = \frac{\partial \ln(TOF)}{\partial \left(\frac{\Delta G_i^{\ddagger}}{-k_B T}\right)} \tag{3.12}$$

where $X_{KRC,i}$ is the degree of kinetic rate control. [50-52]

The reaction network studied includes coking and deep-dehydrogenation steps. The intermediates and transition states can be found in Section B.1 of the appendix.

3.3 Results and Discussion

For each catalyst model, a separate microkinetic model, uncertainty quantification, and gas-phase corrections were performed to generate the quantities of interest for each experimental result. Figure 3.3 describes the distribution of the turnover frequencies for propylene and selectivity to propylene for each surface. All were ran at 792K, with partial pressures of propane and H_2 at 0.29 bar and 0.09 bar, respectively, to model Barias et al.[6] As visible in this figure, Pt_2Sn/Pt(211) is the most selective of the surfaces, followed by Pt_3Sn/Pt(111), Pt_3Sn/Pt(100), and then PtSn/Pt(100). In addition, the turnover frequency of propylene is highest for Pt_3Sn/Pt(100), then Pt_2Sn/Pt(211), Pt_3Sn/Pt(111), and finally PtSn/Pt(100). This selectivity and turnover frequency differences can be viewed as a function of multiple factors. One of these factors is the activation energy barriers of key steps surrounding the propane to propylene reaction barriers. As seen in Table 3.1, selectivity is highest when the barriers for further dehydrogenation or cracking of propylene is comparatively high, or activation energy barriers for alternative dehydrogenation of C_3H_7 species are higher than the dehydrogenation of C_3H_7 to propylene. This is especially evident for Pt_3Sn/Pt(100), where the reaction barrier for a competing product from a C_3H_7 intermediate is

approximately 50% lower than to dehydrogenation of propane, as seen in Table 3.1 as Reaction 7, when compared to the propylene dehydrogenation reaction, Reaction 3. Similar behavior can be seen for $Pt_3Sn/Pt(111)$ for the same mechanistic pathway. In addition, another competing C_3H_7 dehydrogenation mechanism exists for $Pt_3Sn/Pt(100)$ and $Pt_3Sn/Pt(111)$, which is Reaction 11 when compared to Reaction 4. Finally, the very low selectivity to propylene of $Pt_3Sn/Pt(100)$ can be further explained by the kinetics of further dehydrogenation and cracking of propylene. Reactions 20, 22, 23, and 24 are all considerably lower for $Pt_3Sn/Pt(100)$ than for the two very high selectivity surfaces, $Pt_3Sn/Pt(111)$ and $Pt_2Sn/Pt(211)$. $Pt_3Sn/Pt(111)$ has much higher barriers for carbon bond cleavages than $Pt_3Sn/Pt(100)$, partially explaining the much higher selectivity for $Pt_3Sn/Pt(111)$. The other factor is the adsorption strength of propylene. Propylene binds to $Pt_3Sn/Pt(100)$, which is the lowest energy of adsorption surface for propylene, with a 0.17 eV higher bond strength than to the next strongest binding surface, PtSn/Pt(100).

These factors can explain much of the selectivity differences observed between these surfaces. The interplay of these reactions is also described in other predicted behavior, such as in the apparent activation energies and reaction orders for propane and hydrogen gas, as reported in Figure 3.4. Through this figure, it is seen that the majority of surfaces have a reaction order of 1 for propane, and that reaction orders for hydrogen gas predominantly vary from -1 to 0 for PtSn/Pt(100), $Pt_3Sn/Pt(111)$, and $Pt_2Sn/Pt(211)$. $Pt_3Sn/Pt(100)$ has a predicted value of 0 for its hydrogen reaction order, with it varying from -0.5 to 0.5. All of these reaction orders indicate the changing nature of reaction mechanism dependent on the uncertainty within the adsorption and transition state energies.

In comparison with the pure metal, all of the tin-doped surfaces have approximately the same or higher selectivity than the bare platinum catalysts, which can be seen in Figure 3.5 and Figure 3.6, with the exception of Pt_2Sn/Pt(211). The Pt(211) alloy's behavior is due to the decreased barriers for further dehydrogenation and cracking. In addition, for Pt_3Sn/Pt(100), the most important side products are methane and ethylene, while for PtSn/Pt(100), they are methane and acetylene, as reported in the Appendix as Table B.16. PtSn/Pt(100) and Pt_3Sn/Pt(100) achieve an average selectivity to propylene of 31.3% and 36.3%, which is similar to the reported propylene selectivity of 33% on Pt(100) from Fricke et al.[29] It is noted that the selectivity distributions for both tin alloys have a heavier probability density in the higher selectivity region when compared to Pt(100).

These predicted values for propylene selectivity, and other observable data, are dependent on the rate determining steps. Figure 3.7 graphically describes the most important rate controlling steps. For Pt_3Sn/Pt(100) and Pt_3Sn/Pt(111), the first dehydrogenation step from propane to a $C_3H_7^*$ intermediate is rate controlling. On Pt_2Sn/Pt(211), the first dehydrogenation step is partially rate controlling, while the second dehydrogenation step is also partially rate controlling. These can be explained by the reaction pathways described in Table 3.1. PtSn/Pt(100) has multiple predicted rate determining steps for propane dehydrogenation. This complexity arises from the interplay of the rates, the coverages of different species, and the low barriers for an alternative dehydrogenation pathway to produce unwanted side products. These pathways are similarly rate determining when measuring the turnover frequency of propylene, as described in the Appendix B Figures B.3 and B.4. The reaction $CH_3CH_2CH_2 \rightarrow$

CH_3CH_2CH + H, has a lower barrier of 0.1 eV when compared to the propylene pathways of $CH_3CH_2CH_2 \rightarrow CH_3CHCH_2$ + H and $CH_3CHCH_3 \rightarrow CH_3CHCH_2$ + H. These variations in the figure of the degree of kinetically rate controlling species can be ascribed to the uncertainty within these barriers that changes the observed rate controlling step.

3.3.2 Calibration

In addition to the prior results discussed above, the models were also calibrated to the experimental selectivity and propylene turnover frequency, as previously discussed in the methods section. The experimental data can be viewed in the Appendix B Table B.4. Calibration informs the model by reducing the uncertainty in the prior uncertainty derived from BEEF-vdW such that the posterior simulations better explain the experimental data as compared with the prior simulations. This can be seen in Figures 8 and 9. The output of all of the turnover frequencies of the surfaces center around the reported turnover frequency. Selectivity to propylene for the calibrated models increases significantly, with all surfaces encapsulating the experimental data.

This calibration procedure not only affects the calibrated experimental quantities of interest, such as the TOF of propylene and selectivity to propylene, but also the reaction orders, apparent activation energies, and degree of rate control for each surface. As seen in Figures 3.8 and 3.9, the differences between the calibrated and prior apparent activation energies and reaction orders are significant. The peaks of the apparent activation energy distributions center at approximately 2 eV, and the reaction orders in hydrogen gas are between -1 and 0. Calibration affects the reactions that are kinetically

rate controlling, as seen in Figure 3.10. For Pt_3Sn/Pt(100) and Pt_3Sn/Pt(111), the main kinetically rate controlling step is $CH_3CH_2CH_3 \rightarrow CH_3CHCH_3 + H$. For PtSn/Pt(100), the dominant kinetically rate controlling step is $CH_3CH_2CH_3 \rightarrow CH_3CH_2CH_2 + H$, which is different than the previous uncalibrated data in Figure 3.7, where the reaction of $CH_3CH_2CH_2 \rightarrow CH_3CH_2CH + H$ is often rate controlling for propane consumption. Pt_2Sn/Pt(211) has multiple rate controlling steps, however, all of them are part of the direct propane to propylene dehydrogenation pathway. In addition, the degree of kinetic rate control using the turnover frequency of propylene, as reported in the Appendix B. As seen in Figure B.7 , the degree of kinetic rate control measuring propylene turnover frequency is nearly identical to the degree of kinetic rate control when measuring propane turnover frequency. This is due to the high selectivity to propylene for all surfaces.

Finally, the evidence of the surfaces to describe the experimental kinetic observations can be compared using Bayes factors, as shown in Table 3.2, and then evaluated using Jeffreys' scale, in Table 3.3.[53] We find that there is strong evidence to support Pt_2Sn/Pt(211) when referenced to Pt_3Sn/Pt(111), the next highest evidence model, as the active site for these catalysts. This observation agrees with the Pt-only models that also found the step sites to best describe the active sites in the experiments.

3.4 Conclusions

To identify the how platinum-tin alloys affect propane dehydrogenation to propylene over Pt-Sn catalysts, multiple elementary reactions for the propane dehydrogenation were studied from first principles over four surfaces: Pt_3Sn/Pt(100), PtSn/Pt(100), Pt_3Sn/Pt(111), and Pt_2Sn/Pt(211). Mean-field microkinetic models were

generated to give information that can directly be compared to experimental observation. Lateral interactions were included for high coverage species for Pt_3Sn/Pt(100). All other surface models displayed no high coverage species. Given the uncertainties in the DFT energies, we use the BEEF-vdW Model with Ensembles (BMwE) for generating the correlation structure of the DFT functional energy uncertainty for each surface model. In addition to testing at reported experimental conditions, we also calibrated our models to the reported experimental data.

The prior, uncalibrated models all show a high free site coverage, indicating the impact of tin on all of the platinum-tin surface alloys. In addition, the prior models for Pt_3Sn/Pt(111) show a greatly increased selectivity to propylene when compared to the pure platinum surface. Pt_3Sn/Pt(100) and PtSn/Pt(100) both show a wider distribution of selectivity values, however, their averages are similar to Pt(100), and Sn may not meaningfully increase the selectivity for this surface. Pt_2Sn/Pt(211) is highly selectivity to propylene production, which is similar to the pure Pt(211) facet. The rate controlling steps vary for propane consumption and propylene production for each facet, but most are the first dehydrogenation step of propane, with the exception of PtSn/Pt(100), where multiple second dehydrogenation steps could be rate controlling.

The calibrated model showed all surfaces were highly selective to propylene production, and all of the probability densities encapsulated the reported turnover frequencies. In addition, the first dehydrogenation step of propane was rate controlling over all surfaces, save Pt_2Sn/Pt(211), where the first and second dehydrogenation step were often rate controlling. Through Bayesian inference and Jeffreys' scale, Pt_2Sn/Pt(211) has strong evidence to be the active site.

Though this study was comprehensive in studying surface alloys of different platinum facets, there is much debated over what are the most representative models of Pt-Sn alloys. Though models may include bulk alloys, in actuality, there are many possibilities and we are still unsure how to describe the active site for these particular catalysts, especially when catalyst particle composition and distribution varies with catalyst synthesis, which may yield different alloys for catalyst particles, including the presence of pure metal surfaces as well. Finally, more kinetic experimental data, including additional TOFs, selectivities, reaction orders, apparent activation energies, and other reaction data is likely needed to further refine the calibration problem and perform fuller model analysis.

3.5 Acknowledgments

This work was supported by the Institute for Cooperative Upcycling of Plastics (iCOUP), an Energy Frontier Research Center funded by the U.S. Department of Energy (DOE), Office of Basic Energy Sciences under Contract DE-AC-02-07CH11358. In addition, partial support was provided by the National Science Foundation under grant number CBET-1534260. C.F. also acknowledges partial support from the National Science Foundation IGERT program under grant number 1250052. Computer resources were used from the National Energy Research Scientific Computing Center (NERSC) Contract No. DE-AC02-05CH11231, Pacific Northwest National Laboratory (Ringgold ID 130367, Grant Proposal 51711), and the University of South Carolina's High-Performance Computing Group.

3.6 Figures and Tables

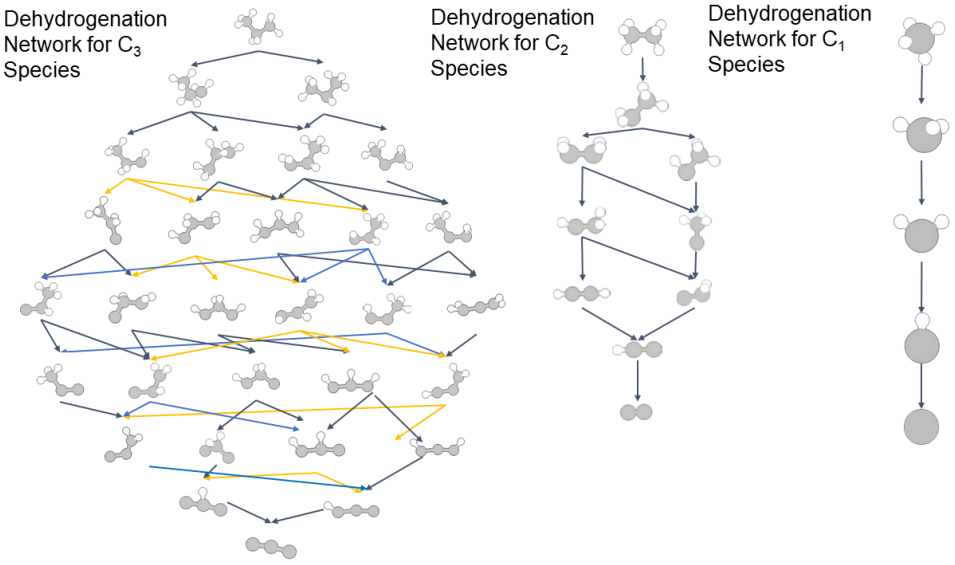

Figure 3.1: Dehydrogenation reaction network around $C_{1\text{-}3}$ species.

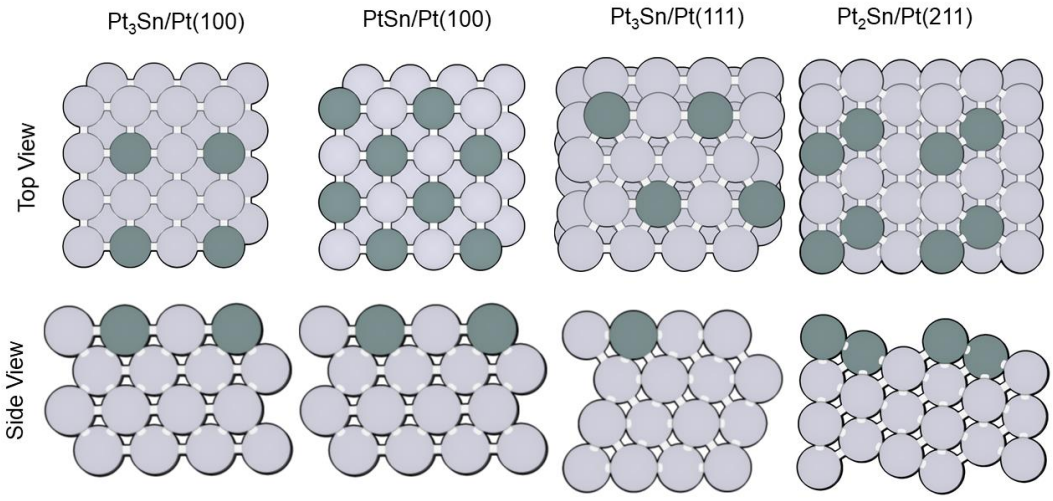

Figure 3.2: The four surfaces evaluated in this study.

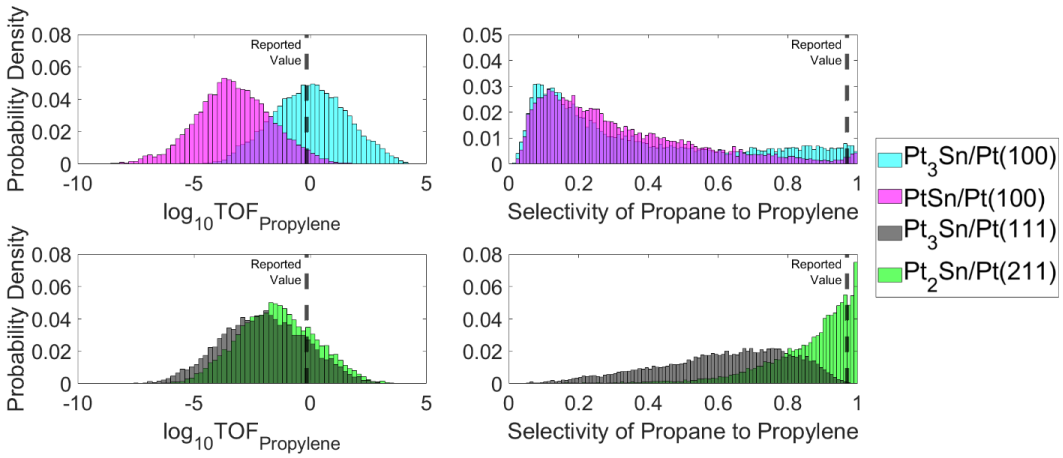

Figure 3.3: Histograms of the turnover frequency of propylene (TOF) and selectivity towards propylene on all four surfaces for the prior model, i.e., no calibration.

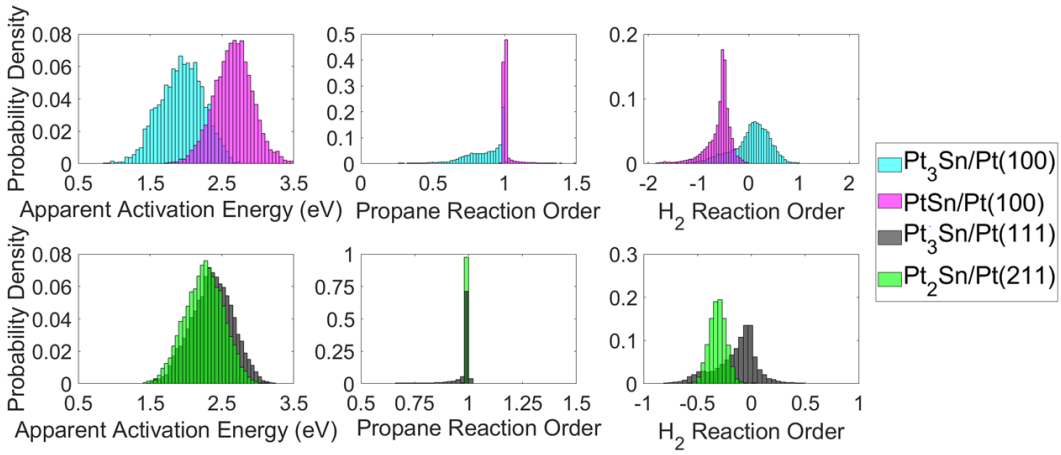

Figure 3.4: Apparent activation energy, reaction order of propane, and reaction order of H_2 for all four surfaces calculated using the TOF of propylene for the prior model, i.e., no calibration.

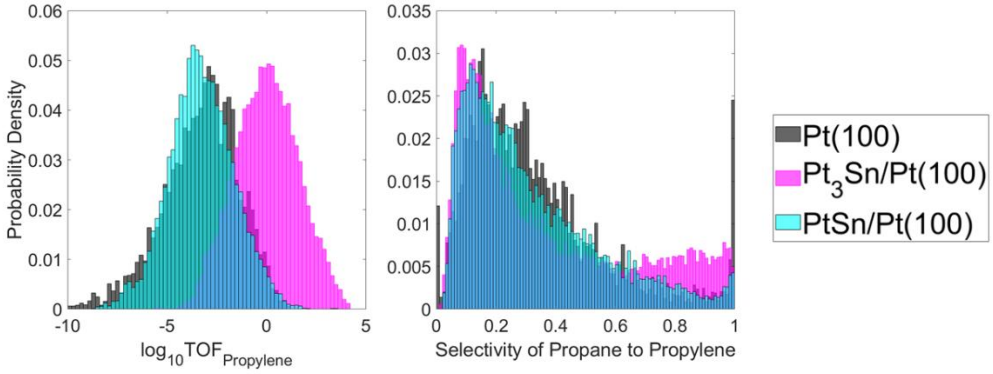

Figure 3.5: Comparison between pure Pt(100) surface as modeled in Fricke et al.[29] and its corresponding tin-doped surfaces studied in this work.

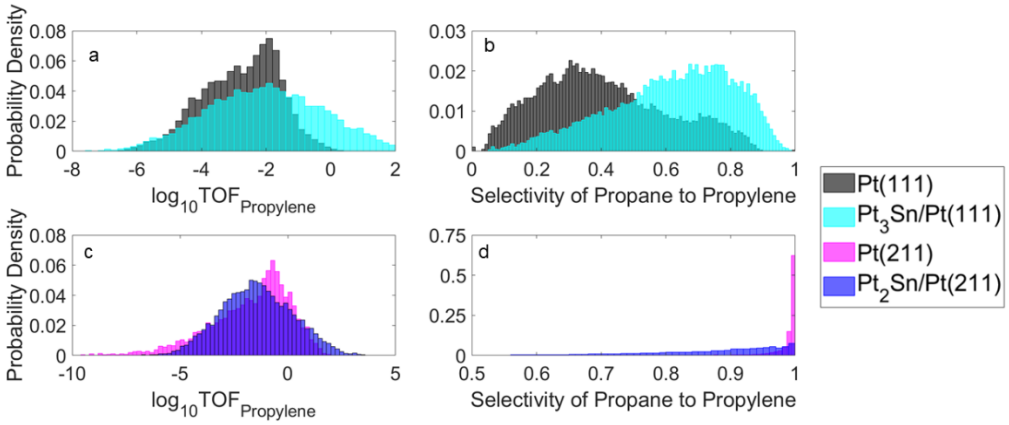

Figure 3.6: Comparison between pure Pt(111) and Pt(211) surfaces as modeled in Fricke et al.[29] versus their corresponding tin-doped surface studied in this work.

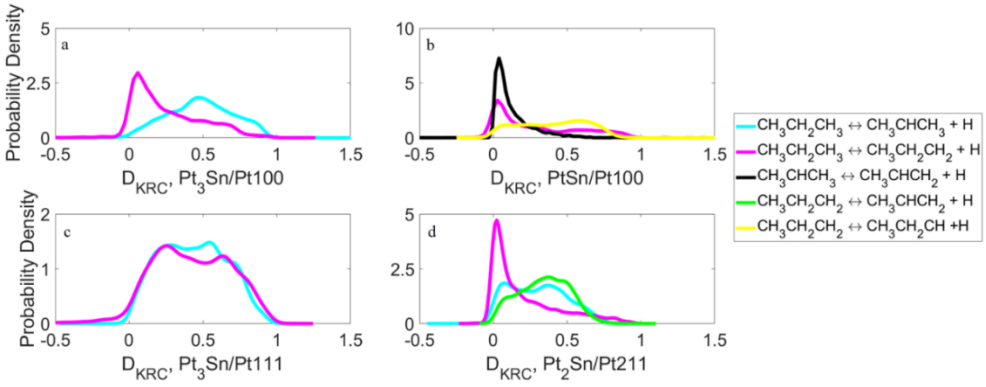

Figure 3.7: Degree of kinetic rate control (D_{KRC}) for the most important steps on all four Pt-Sn alloy surfaces calculated using the TOF of propane consumption. (a) $Pt_3Sn/Pt(100)$, (b) PtSn/Pt(100), (c) $Pt_3Sn/Pt(111)$, (d) $Pt_2Sn/Pt(211)$

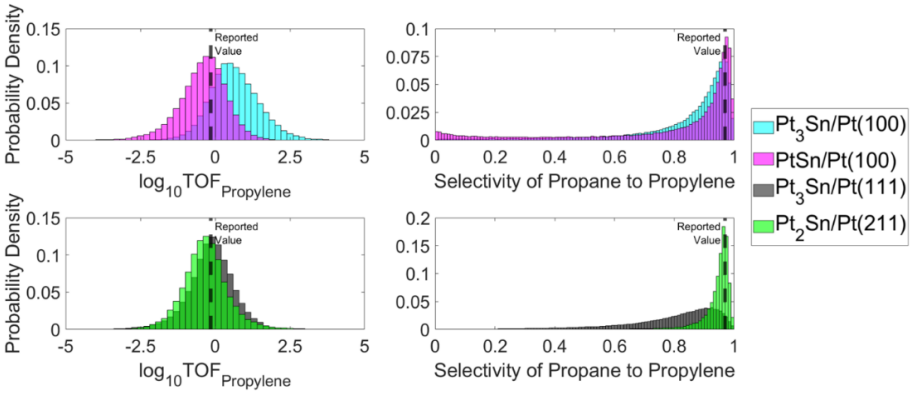

Figure 3.8: Calibrated models for TOFs of propylene production and selectivity towards propylene on all four Pt-Sn surface models.

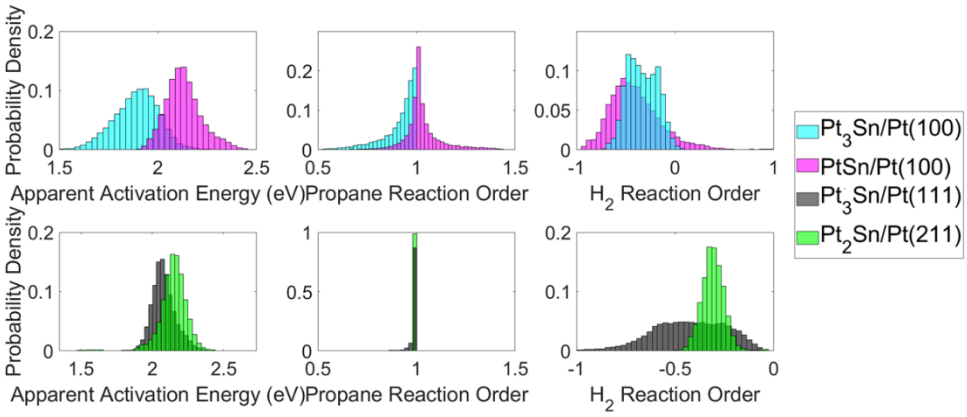

Figure 3.9: Calibrated models for apparent activation energies and reaction orders for propylene production for all four Pt-Sn alloy surface models.

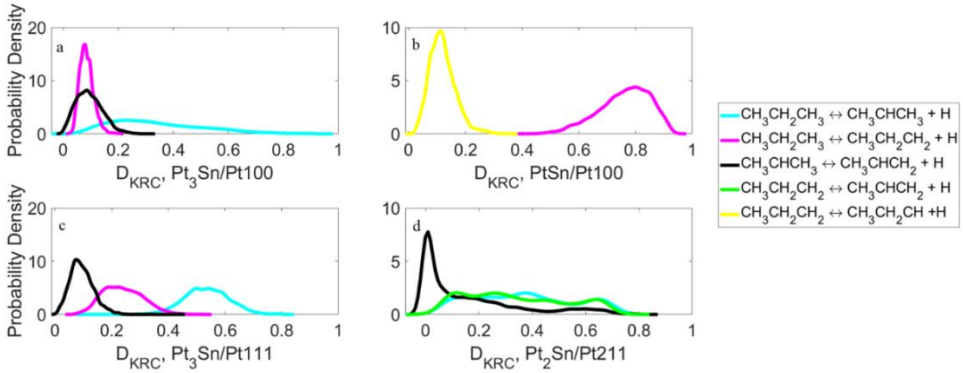

Figure 3.10: Degree of kinetic rate control (D_{KRC}) for the most important steps on all four Pt-Sn alloy surfaces calculated using the TOF of propane consumption calibrated to the experimental data[6].

Table 3.1: Activation barriers of select reactions that occur early in the dehydrogenation mechanism. Referenced to the reactant at 792K. All reactions occur on the surface.

		Activation Barrier (eV)			
Chemical Reaction	Reaction Number	Pt_3Sn/(100)	PtSn/Pt(100)	Pt_3Sn/(111)	Pt_2Sn/(211)
$CH_3CH_2CH_3 \rightarrow CH_3CHCH_3+H$	1	0.97	1.36	1.30	1.22
$CH_3CH_2CH_3 \rightarrow CH_3CH_2CH_2 +H$	2	1.05	1.33	1.30	1.05
$CH_3CHCH_3 \rightarrow CH_3CHCH_2+H$	3	0.82	1.48	1.01	0.92
$CH_3CH_2CH_2 \rightarrow CH_3CHCH_2+H$	4	0.76	1.49	1.03	1.09
$CH_3CH_2CH_3 \rightarrow CH_3+CH_2CH_3$	5	2.43	2.31	2.63	2.15
$CH_3CHCH_3 \rightarrow CH_3CH+CH_3$	6	1.86	2.46	2.04	2.22
$CH_3CHCH_3 \rightarrow CH_3CCH_3+H$	7	0.58	1.76	0.94	0.98
$CH_3CH_2CH_2 \rightarrow CH_3CH_2+CH_2$	8	1.63	2.39	1.97	2.08
$CH_3CH_2CH_2 \rightarrow CH_3+CH_2CH_2$	9	2.27	2.89	2.75	2.86
$CH_3CH_2CH_2 \rightarrow CH_2CH_2CH_2+H$	10	1.04	1.41	1.27	1.26
$CH_3CH_2CH_2 \rightarrow CH_3CH_2CH +H$	11	0.66	1.36	1.00	1.27
$CH_3CH_2CH \rightarrow CH_3CH_2C +H$	14	0.72	1.77	0.59	0.89
$CH_3CH_2CH \rightarrow CH_3CHCH+H$	15	0.86	0.58	0.90	0.68
$CH_3CH_2CH \rightarrow CH_2CH_2CH+H$	16	1.28	1.40	1.35	2.00
$CH_3CHCH_2 \rightarrow CH_3+CHCH_2$	20	1.49	3.17	2.01	1.90
$CH_3CHCH_2 \rightarrow CH_3CH+CH_2$	21	1.90	2.50	2.01	2.13
$CH_3CHCH_2 \rightarrow CH_3CCH_2+H$	22	0.91	1.74	0.99	1.42
$CH_3CHCH_2 \rightarrow CH_3CHCH+H$	23	0.78	1.33	1.01	1.54
$CH_3CHCH_2 \rightarrow CH_2CHCH_2+H$	24	0.93	0.93	1.05	0.94
$CH_3CHCH \rightarrow CH_3+CHCH$	39	1.45	2.47	1.67	1.60
$CH_3CHCH \rightarrow CH_3CH+CH$	40	1.82	2.53	1.77	2.88
$CH_3CHCH \rightarrow CH_3CHC+H$	41	1.01	0.80	0.53	0.59
$CH_3CHCH \rightarrow CH_3CCH+H$	42	1.37	1.77	0.92	0.57
$CH_3CHCH \rightarrow CH_2CHCH+H$	43	1.37	1.17	1.27	1.04
$CH_3CCH_2 \rightarrow CH_3+CH_2C$	44	1.70	2.42	1.46	1.37
$CH_3CCH_2 \rightarrow CH_3C+CH_2$	45	1.11	2.49	1.90	2.13
$CH_3CCH_2 \rightarrow CH_2CCH_2+H$	46	1.01	0.91	1.12	0.35
$CH_3CCH_2 \rightarrow CH_3CCH+H$	47	0.95	1.76	0.92	1.28

Table 3.2: Evidence and Bayes factor for each surface as compared to $Pt_3Sn/Pt(111)$

Surface	Evidence	Bayes Factor
$Pt_3Sn/Pt(100)$	3.67×10^{-4}	2.96×10^{-1}
PtSn/Pt(100)	3.60×10^{-4}	2.90×10^{-1}
$Pt_3Sn/Pt(111)$	1.24×10^{-3}	1.00
$Pt_2Sn/Pt(211)$	1.57×10^{-2}	12.6

Table 3.3: Jefferys' scale for Bayes factors, $B_{12} = p(D|M_1)/p(D|M_2)$[53]

B_{12}	Evidence for M_1
1 - 3.2	Not worth more than a bare mention
3.2 - 10	Positive
10 - 100	Strong
> 100	Very strong

3.7 References

1. Sattler, J. J. H.; Ruiz-Martinez, J; Santillian-Jimenez, E.; Weckhuysen, B.M. Catalytic Dehydrogenation of Light Alkanes on Metals and Metal Oxides. *Chem. Rev.*, **2014**, *114*, 10613-10653

2. Wang, Y.; Hu, P.; Yang, J.; Zhu, Y.; Chen, D.; C–H bond activation in light alkanes: a theoretical perspective, *Chem. Soc. Rev.*, **2021**, 50, 4299-4358

3. Zhao, Z.; Jiang, J.; Wang, F. An economic analysis of twenty light olefin production pathways. *Journal of Energy Chemistry*, **2021**, 56, 193-202

4. Wang, J.; Chang, X.; Chen, S.; Sun, G.; Zhou, X.; Vovk, E.; Yang, Y.; Deng, W; Zhao, Z; Mu, R.; Pei, C.; Gong, J.; On the Role of Sn Segregation of Pt-Sn Catalysts for Propane Dehydrogenation. *ACS Catal*., **2021** , 11 (8), 4401-4410

5. Zhua, H; Anjum, D. H;Wang, Q.; Abou-Hamad, E.; Emsley, L.; Dong , H.; Laveille, P.; Li, L.; Samal, A. K.; Basset, J.; Sn surface-enriched Pt–Sn bimetallic nanoparticles as a selective and stable catalyst for propane dehydrogenation, *J. Catal.*, **2014**, 320, 52-62

6. Bariås, O. A.; Holmen, A.; Blekkan, E. A. Propane Dehydrogenation over Supported Pt and Pt−Sn Catalysts: Catalyst Preparation, Characterization, and Activity Measurements. *J. Catal.*, **1996**, 158, 1−12.

7. Kaylor, N.; Davis, R. J.; Propane dehydrogenation over supported Pt-Sn nanoparticles, *J. Catal.*, **2018**, 367, 181-193

8. A. Iglesias-Juez, A. M. Beale, K. Maaijen, T. C. Weng, P. Glatzel, B. M. Weckhuysen, A combined in situ time-resolved UV-Vis, Raman and high-energy resolution X-ray absorption spectroscopy study on the deactivation behavior of Pt and PtSn propane dehydrogenation catalysts under industrial reaction conditions. *J. Catal.*, **2010**, 276, 268–279.

9. Xiong, H.; Lin, S.; Goetze, J.; Pletcher, P.; Guo, H.; Kovarik, L.; Artyushkova, K.; Weckhuysen, B. M; Datye, A. K.; Thermally Stable and Regenerable Platinum–Tin Clusters for Propane Dehydrogenation Prepared by Atom Trapping on Ceria, *Angew.Chem.Int. Ed*., **2017**, 56, 8986 –899

10. Motagamwala, A.H.; Almallahi, R.; Wortman, J.; Igenegbai, V. O.; Linic, S.; Stable and selective catalysts for propane dehydrogenation operating at thermodynamic limit, *Science* ,**2021**, 373 (6551), 217-222

11. Hannagan, R. T.; Giannakakis, G.; Reocreux, R.; Schumann, J.; Finzel, J.; Wang, Y.; Michaelides, A.; Deshlarhra, P.; Christopher, P.; Flytzani-Stephanopoulos, M.; Stamatakis, M.; Sykes, E. C. H.; First-principles design of a single-atom–alloy propane dehydrogenation catalyst, *Science* ,**2021**, 372 (6549), 1444-1447

12. Shi, L.; Deng, G. M.; Li, W. C.; Miao, S.; Wang, Q. N.; Zhang, W. P.; Lu, A. H. Al2O3 nanosheets rich in pentacoordinate Al3+ ions stabilize Pt-Sn clusters for propane dehydrogenation. *Angew. Chem., Int. Ed.,* **2015**, 54, 13994−13998.

13. Xu, Z.; Yue, X.; Bao, X.; Xie, Z.; Zhu, H. Propane Dehydrogenation over Pt Clusters Localized at the Sn Single-Site in Zeolite Framework, *ACS Catal*. **2020**, 10, 1, 818–828.

14. Iglesias-Juez, A.; Beale, A. M.; Maaijen, K.; Weng, T.C.;Glatzel, P.; Weckhuysen, B.M;A combined in situ time-resolved UV–Vis, Raman and high-energy resolution X-ray absorption spectroscopy study on the deactivation behavior of Pt and Pt single bond Sn propane dehydrogenation catalysts under industrial reaction conditions. *J. Catal.,* **2010**, 276 (2), 268-279

15. Pham, H. N.; Sattler, J. H. B; Weckhuysen, B. M.; Datye, A. K; *ACS Catal*., **2016**, 6, 4, 2257–2264

16. Deng, L; Shishido, T.; Teramura, K.; Tanaka,T. Effect of reduction method on the activity of Pt–Sn/SiO2 for dehydrogenation of propane. *Catalysis Today*, **2014**, 232, 33-39

17. Zhang, Y.; Zhou, Y.; Qiu, A.; Wang, Y.; Xu, Y. Wu, P. Propane dehydrogenation on PtSn/ZSM-5 catalyst: Effect of tin as a promoter. *Catal. Comm*., **2006**, 7 (11), 860-866

18. Duan, Y.; Zhou, Y.; Zhang, Y.; Sheng, X.; Xue, M. Effect of Sodium Addition to PtSn/AlSBA-15 on the Catalytic Properties in Propane Dehydrogenation, *Catalysis Letters*, **2011**, 141, 120-127.

19. Larsson, M.; Andersson, B.; Barias, O.A., Holmen, A.; The use of the H2-D2 equilibration reaction as a probe reaction to study the deactivation on Pt/Al2O3 and Pt-Sn/Al2O3 catalysts during propane dehydrogenation, *Studies in Surface Science and Catalysis*, **1994**, 88, 233-240

20. Wu, J.; Sharada, S. M.; Ho. C.; Hauser, A. W.; Head-Gordon, M. Ethane and propane dehydrogenation over PtIr/Mg(Al)O. *Appl. Catal. A*, **2015**, 506, 25-32

21. Barias, O.A.; Holmen, A.; Blekkan, E.A, Propane dehydrogenation over supported platinum catalysts: effect of tin as a promoter. *Catalysis Today*, **1995**, 24 (3), 361-364

22. Deng, L. Miura, K. Shishido, T.; Hosokawa, S.; Teramura, K.; Tanaka, T. Dehydrogenation of Propane over Silica-SupportedPlatinum–Tin Catalysts Prepared by Direct Reduction:Effects of Tin/Platinum Ratio and Reduction Temperature, *ChemCatChem*, **2014**, 6, 2680 – 2691

23. Nam, J.; Celik, F.; Effect of Tin in the Bulk of Platinum–Tin Alloys for Ethane Dehydrogenation. Topics in Catalysis, **2020**, 63, 700–713

24. Yang, M.; Zhu, Y.; Zhou, X.; Chen, D. First-Principles Calculations of Propane Dehydrogenation over PtSn Catalysts, *ACS Catal*. **2012**, 2, 6, 1247–1258

25. Nykanen, L.; Honkala, K. Density Functional Theory Study on¨Propane and Propene Adsorption on Pt(111) and PtSn Alloy Surfaces. *J. Phys. Chem. C* , **2011**, 115 (19), 9578−9586.

26. Honkala, Nykanen, Selectivity in Propene Dehydrogenation on Pt and Pt3Sn Surfaces from First Principles *ACS Catal.* **2013**, 3, 12, 3026–3030

27. Hook, A. Massa, J. D.; Celik, F. E. Effect of Tin Coverage on Selectivity for Ethane Dehydrogenation over Platinum-Tin Alloys. *J. Phys. Chem. C* 2016, 120, 48, 27307–27318

28. Wang, T.; Abild-Pedersen, F.; Identifying factors controlling the selective ethane dehydrogenation on Pt-based catalysts from DFT based micro-kinetic modeling. *Journal of Energy Chemistry*, **2021**, 37-40

29. Fricke, C; Rajbanshi, B.; Walker, E. A.; Terejanu, G.; Heyden, A.; Propane Dehydrogenation on Platinum Catalysts: Identifying the Active Sites through Bayesian Analysis, *ACS Catal.*, **2022**, 12, 2487-2498

30. Kresse, G.; Furthmüller, J., Efficiency of ab-initio total energy calculations for metals and semiconductors using a plane-wave basis set. *Comput. Mat. Sci.*, **1996**, 6 (1), 15-50

31. Kresse, G.; Furthmüller, J. Efficient iterative schemes for ab initio total-energy calculations using a plane-wave basis set. *Phys. Rev. B*, **1996**, 54 (16), 11169

32. Kresse, G.; Hafner, J. Ab initio molecular dynamics for liquid metals. *Phys. Rev. B*, **1993**, 47 (1), 558

33. Wellendorff, J; Lundgaard, K.T; Møgelhøj, A.; Petzold, V.; Landis, D.D.; Nørskov, J.K; Bligaard, T.; Jacobsen, K.W. Density functionals for surface science: Exchange-correlation model development with Bayesian error estimation. *Phys. Rev. B*, **2012**, 85, 235149

34. Blochl, P.E. "Projector augmented-wave method", Phys. Rev. B, 1994, 50,17953

35. Kresse, G.; Halfer, J. "Norm-conserving and ultrasoft pseudopotentials for first-row and transition elements*" J. Phys. Condens. Matter*, **1994**, 6,8245

36. Monkhorst, H.; Pack, J. Special points for Brillouin-zone integrations. *Phys. Rev. B*, **1976**, 13, 5188

37. Pack, J.; Monkhorst, H. Special points for Brillouin-zone integrations. *Phys. Rev. B*, **1977**, 16, 1748

38. Haworth, N. L.; Wang, Q.; Coote, M. L., "Modeling Flexible Molecules in Solution: A pKa Case Study*." J. Phys. Chem. A.,* **2017**, 121 (27), 5217-5225.

39. Henkelman, G.; Jónsson, H. A climbing image nudged elastic band method for finding saddle points and minimum energy paths. *J. Chem. Phys*., **2000**, 113, 9901-9904

40. Henkelman, G.; Jónsson, H. Improved tangent estimate in the nudged elastic band method for finding minimum energy paths and saddle points. *J. Chem. Phys*., **2000**, 113, 9978-9985

41. Henkelman, G.; Jónsson, H. A dimer method for finding saddle points on high dimensional potential surfaces using only first derivatives. *J. Chem. Phys.*, **1999**, 111, 7010

42. Heyden, A. ; Bell, A. T.; Keil, F. J. Efficient methods for finding transition states in chemical reactions: Comparison of improved dimer method and partitioned rational function optimization method. *J. Chem. Phys.*, **2005**, 123, 224101

43. Medford, A. J.; Wellendorf, J.; Vojvodic, A.; Studt, F.; Abild-Pedersen, F.; Jacobsen, K.; Bligaard, T.; Norskov, J.; Assessing the reliability of calculated catalytic ammonia synthesis rates. *Science*, **2014**, 345 (6193), 197-200

44. Walker E. A.,; Mitchell, D.; Terejanu, G. A.; Heyden, A. Identifying Active Sites of the Water−Gas Shift Reaction over Titania Supported Platinum Catalysts under Uncertainty" *ACS Catal.*, **2018**, 8, 3990-3998

45. Walker, E.; Ammal, S. C.; Terejanu, G. A.; Heyden, A. Uncertainty Quantification Framework Applied to the Water–Gas Shift Reaction over Pt-Based Catalysts. *J. Phys. Chem. C.*, **2016**, *120*, 10328– 10339

46. Cramer, J. S. *Logit Models from Economics and Other Fields*; Cambridge University Press: Cambridge, **2003**; pp 149–157.

47. Prudencio E.E., Schulz K.W. (2012) The Parallel C++ Statistical Library 'QUESO': Quantification of Uncertainty for Estimation, Simulation and Optimization. In: *Alexander M. et al. (eds) Euro-Par 2011: Parallel Processing Workshops. Euro-Par 2011. Lecture Notes in Computer Science,* Bordeaux, France, August 29 – September 2, 2011. Springer, Berlin, Heidelberg, **2011**, vol 7155. pp 398-407

48. Horvatits, C.; Lee, J.; Kyriakidou, E.A; Walker, E.A. Characterizing Adsorption Sites on Ag/SSZ-13 Zeolites: Experimental Observations and Bayesian Inference. *J. Phys. Chem. C,* **2020,** *124* (35), 19174-19186

49. Walker, E..A.; Ravisankar, K.; and Savara, A; CheKiPEUQ Intro 2: Harnessing Uncertainties from Data Sets, Bayesian Design of Experiments in Chemical Kinetics. *ChemCatChem*., **2020**,12, 5401-5410.

50. Campbell, C. T. Future Directions and Industrial Perspectives Micro-and Macro-Kinetics: Their Relationship in Heterogeneous Catalysis. *Top. Catal.*, **1994**, *1*, 353–366

51. Campbell, C. T. The Degree of Rate Control: A Powerful Tool for Catalysis Research. *ACS Catal.* **2017**, *7*, 2770−2779

52. Campbell, C. T. Finding the Rate-Determining Step in a Mechanism: Comparing DeDonder Relations with the "Degree of Rate Control". *J. Catal.*, **2001**, *204*, 520–524

53. Jeffreys, H., *The Theory of Probability*; Oxford University Press:Oxford, **1939**; pp 356−357.

APPENDIX A

SUPPORTING INFORMATION FOR PROPANE DEHYDROGENATION ON PLATINUM CATALYSTS: IDENTIFYING THE ACTIVE SITES THROUGH BAYESIAN ANALYSIS[3]

[3] Fricke, C.; Rajbanshi, B.; Walker, E.; Terejanu, G.; Heyden, A. *ACS Catalysis*, **2022**

A.1 Lattice Parameters for Surface Structures

The information in Appendix A Table A.1 describes the cell vectors for the proceeding calculations.

Table A.1: Cell parameter vectors for each of the slabs studied in this work.

Cell Parameter Vectors for Each Surface, in Å									
Vector	Pt(100)			Pt(111)			Pt(211)		
x	11.085	0.000	0.000	11.085	0.000	0.000	13.574	0.000	0.000
y	0.000	11.085	0.000	-5.542	9.600	0.000	0.000	11.083	0.000
z	0.000	0.000	25.878	0.000	0.000	26.788	0.000	0.000	27.199

A.2 Bayesian Statistics and Priors

A.2.1 Prior Construction for Intermediate and Transition States for the Four Functional Models

Previous work done by Walker et. al.[1,2] used four DFT functionals[3-7] to obtain a prior uncertainty. We chose four functionals in this study, as discussed in the main paper, to represent different possible ways functionals treat a hydrocarbon/metal systems on each of the different facets. Appendix A Tables A.2 – A.14 list the relative free energies of the adsorbed species, the gas species, as well as the free energies of the transition state species, in reference to gaseous propane and hydrogen gas (at reaction temperature and 1 bar), and the specific metal facet in which these calculations took place.

Table A.2: Free energies of adsorbed species on Pt(100) at 633 K, $P_{CH3CH2CH3}$ of 1 bar, and P_{H2} of 1 bar, referenced to gaseous propane, hydrogen, and platinum surface slab.

Pt(100)		Free Energy of Adsorption, $\Delta G_{ads,i}$ (eV)			
Adsorbed Species	Adsorption Number (ADS #)	PBE-D3	BEEF-vdW	RPBE	SCAN-rVV10
$CH_3CH_2CH_3$	1	0.36	0.89	1.15	0.91
CH_3CHCH_3	2	0.16	0.73	1.08	0.53
$CH_3CH_2CH_2$	3	0.32	0.78	1.02	0.67
CH_3CHCH_2	4	0.00	0.49	0.82	0.36
CH_3CH_2CH	5	-0.00	0.46	0.92	0.29
$CH_2CH_2CH_2$	6	0.10	0.69	1.20	0.36
CH_3CCH_3	7	-0.14	0.41	0.95	0.19

CH_3CH_2C	8	-0.25	0.15	0.61	0.23
CH_2CH_2CH	9	0.54	1.08	1.55	0.73
CH_2CHCH_2	10	-0.31	0.21	0.73	-0.04
CH_3CHCH	11	-0.06	0.42	0.88	0.10
CH_3CCH_2	12	0.06	0.53	0.96	0.25
CH_3CHC	13	0.31	0.74	1.14	0.57
CH_2CH_2C	14	0.05	0.45	0.88	0.36
$CHCH_2CH$	15	-0.38	0.15	0.59	-0.26
CH_2CHCH	16	-0.32	0.20	0.67	-0.13
CH_2CCH_2	17	-0.14	0.37	0.83	0.01
CH_3CCH	18	-0.84	-0.41	0.04	-0.62
CH_3CC	19	-0.41	-0.12	0.30	-0.16
CH_2CHC	20	0.01	0.39	0.85	0.22
CHCHCH	21	1.17	1.64	2.03	1.27
$CHCH_2C$	22	-0.05	0.40	0.81	0.03
CH_2CCH	23	-0.26	0.24	0.65	-0.11
CH_2CC	24	-0.16	0.15	0.57	-0.03
CHCHC	25	-0.08	0.28	0.70	0.01
CCH_2C	26	1.24	1.62	1.97	1.34
CHCCH	27	-0.07	0.34	0.75	0.19
CCHC	28	1.52	1.69	2.07	2.17
CHCC	29	0.59	0.88	1.30	0.84
CCC	30	1.73	1.78	2.16	2.32
CH_3CH_3	31	0.15	0.46	0.76	0.57
CH_3CH_2	32	0.07	0.40	0.74	0.33
CH_3CH	33	-0.14	0.21	0.53	0.05
CH_3C	34	-0.40	-0.16	0.13	-0.03
CH_2CH_2	35	-0.16	0.21	0.54	0.06
CH_2CH	36	-0.12	0.22	0.52	0.01
CH_2C	37	-0.01	0.16	0.45	0.14
CHCH	38	-0.80	-0.53	-0.26	-0.66
CHC	39	-0.31	-0.16	0.10	-0.16
CC	40	0.50	0.54	0.81	0.70
CH_4	41	-0.16	-0.07	0.10	0.12
CH_3	42	-0.08	0.09	0.27	0.06
CH_2	43	-0.09	0.07	0.23	-0.02
CH	44	-0.31	-0.24	-0.13	-0.02
C	45	-0.14	-0.23	-0.10	0.24
H	46	-0.30	-0.17	-0.22	-0.22

Table A.3. Free energies of transition state species on Pt(100) at 633 K, $P_{CH3CH2CH3}$ of 1 bar, and P_{H2} of 1 bar, referenced to gaseous propane, hydrogen, and platinum surface slab.

Pt(100)		Free Energy of the Transition State, $\Delta G_j^{\ddagger}$ (eV)			
Chemical Reaction	Reaction Number	PBE-D3	BEEF-vdW	RPBE	SCAN-rVV10
$CH_3CH_2CH_3 \rightarrow CH_3CHCH_3+H$	1	0.72	1.41	1.85	1.01
$CH_3CH_2CH_3 \rightarrow CH_3CH_2CH_2 +H$	2	0.79	1.54	1.87	1.16
$CH_3CHCH_3 \rightarrow CH_3CHCH_2+H$	3	0.48	1.31	1.73	0.97
$CH_3CH_2CH_2 \rightarrow CH_3CHCH_2+H$	4	0.59	1.32	1.69	0.98
$CH_3CH_2CH_3 \rightarrow CH_3+CH_2CH_3$	5	2.54	3.47	3.86	2.93
$CH_3CHCH_3 \rightarrow CH_3CH+CH_3$	6	1.45	2.21	2.71	1.85
$CH_3CHCH_3 \rightarrow CH_3CCH_3+H$	7	0.47	1.23	1.67	0.66
$CH_3CH_2CH_2 \rightarrow CH_3CH_2+CH_2$	8	1.50	2.21	2.63	1.87
$CH_3CH_2CH_2 \rightarrow CH_3+CH_2CH_2$	9	2.53	3.46	3.83	2.82
$CH_3CH_2CH_2 \rightarrow CH_2CH_2CH_2+H$	10	0.68	1.55	1.97	0.97
$CH_3CH_2CH_2 \rightarrow CH_3CH_2CH +H$	11	0.56	1.31	1.65	0.80
$CH_3CH_2CH \rightarrow CH_3CH_2+CH$	12	1.42	2.11	2.52	1.66
$CH_3CH_2CH \rightarrow CH_3+CH_2CH$	13	1.73	2.49	2.96	2.07
$CH_3CH_2CH \rightarrow CH_3CH_2C +H$	14	0.52	0.92	1.27	0.69
$CH_3CH_2CH \rightarrow CH_3CHCH+H$	15	0.32	1.33	1.70	0.85
$CH_3CH_2CH \rightarrow CH_2CH_2CH+H$	16	0.68	1.53	1.91	0.93
$CH_2CH_2CH_2 \rightarrow CH_2+CH_2CH_2$	17	1.44	2.11	2.59	1.71
$CH_2CH_2CH_2 \rightarrow CH_2CH_2CH+H$	18	0.52	1.37	1.77	0.66
$CH_2CH_2CH_2 \rightarrow CH_2CHCH_2+H$	19	0.67	1.46	1.93	0.95
$CH_3CHCH_2 \rightarrow CH_3+CHCH_2$	20	1.16	1.86	2.34	1.45
$CH_3CHCH_2 \rightarrow CH_3CH+CH_2$	21	1.16	1.97	2.41	1.48
$CH_3CHCH_2 \rightarrow CH_3CCH_2+H$	22	0.37	1.15	1.58	0.57
$CH_3CHCH_2 \rightarrow CH_3CHCH+H$	23	0.34	1.09	1.48	0.57
$CH_3CHCH_2 \rightarrow CH_2CHCH_2+H$	24	0.38	1.18	1.62	0.69
$CH_3CCH_3 \rightarrow CH_3+CH_3C$	25	1.31	2.02	2.48	1.54
$CH_3CCH_3 \rightarrow CH_3CCH_2+H$	26	0.75	1.55	1.89	1.00
$CH_3CH_2C \rightarrow CH_3+CH_2C$	27	1.66	2.20	2.64	2.11
$CH_3CH_2C \rightarrow CH_3CH_2+C$	28	1.23	1.71	2.14	1.78
$CH_3CH_2C \rightarrow CH_2CH_2C+H$	29	0.62	1.28	1.62	0.89
$CH_3CH_2C \rightarrow CH_3CHC+H$	30	0.52	1.07	1.42	0.77
$CH_2CH_2CH \rightarrow CH_2+CH_2CH$	31	1.48	2.14	2.61	1.71
$CH_2CH_2CH \rightarrow CH_2CH_2+CH$	32	1.75	2.35	2.80	1.98
$CH_2CH_2CH \rightarrow CH_2CH2C+H$	33	0.90	1.57	1.91	1.23
$CH_2CH_2CH \rightarrow CH_2CHCH+H$	34	1.34	2.20	2.57	1.50
$CH_2CH_2CH \rightarrow CHCH_2CH+H$	35	0.60	1.43	1.79	0.72

$CH_2CHCH_2 \rightarrow CH_2+CH_2CH$	36	1.10	1.83	2.28	1.34
$CH_2CHCH_2 \rightarrow CH_2CHCH+H$	37	0.63	1.42	1.84	0.86
$CH_2CHCH_2 \rightarrow CH_2CCH_2+H$	38	0.30	1.05	1.46	0.43
$CH_3CHCH \rightarrow CH_3+CHCH$	39	0.81	1.51	1.92	1.08
$CH_3CHCH \rightarrow CH_3CH+CH$	40	1.41	1.99	2.38	1.72
$CH_3CHCH \rightarrow CH_3CHC+H$	41	0.63	1.26	1.60	0.92
$CH_3CHCH \rightarrow CH_3CCH+H$	42	0.06	0.81	1.17	0.25
$CH_3CHCH \rightarrow CH_2CHCH+H$	43	0.36	1.19	1.56	0.51
$CH_3CCH_2 \rightarrow CH_3+CH_2C$	44	0.71	1.40	1.79	0.82
$CH_3CCH_2 \rightarrow CH_3C+CH_2$	45	1.11	1.85	2.20	1.32
$CH_3CCH_2 \rightarrow CH_2CCH_2+H$	46	1.15	1.87	2.27	1.55
$CH_3CCH_2 \rightarrow CH_3CCH+H$	47	0.37	1.02	1.37	0.68
$CH_3CHC \rightarrow CH_3+CHC$	48	1.30	1.85	2.26	1.59
$CH_3CHC \rightarrow CH_3CH+C$	49	1.37	1.68	2.07	1.66
$CH_3CHC \rightarrow CH_3CC+H$	50	0.83	1.41	1.72	1.12
$CH_3CHC \rightarrow CH_2CHC+H$	51	1.29	1.88	2.28	1.71
$CH_2CH_2C \rightarrow CH_2CH_2+C$	52	1.12	1.50	1.92	1.56
$CH_2CH_2C \rightarrow CH_2+CH_2C$	53	1.47	2.01	2.45	1.93
$CH_2CH_2C \rightarrow CH_2CHC+H$	54	0.57	1.22	1.57	0.67
$CH_2CH_2C \rightarrow CHCH_2C+H$	55	1.38	1.98	2.33	1.71
$CHCH_2CH \rightarrow CH_2CH+CH$	56	1.38	1.97	2.39	1.48
$CHCH_2CH \rightarrow CHCH_2C+H$	57	2.73	3.24	3.57	3.07
$CHCH_2CH \rightarrow CHCHCH+H$	58	2.02	2.54	2.92	2.32
$CH_2CHCH \rightarrow CH_2+CHCH$	59	0.99	1.60	2.03	1.16
$CH_2CHCH \rightarrow CH_2CH+CH$	60	1.49	2.15	2.56	1.67
$CH_2CHCH \rightarrow CH_2CHC+H$	61	0.53	1.19	1.58	0.69
$CH_2CHCH \rightarrow CH_2CCH+H$	62	-0.18	0.55	0.91	-0.07
$CH_2CHCH \rightarrow CHCHCH+H$	63	0.80	1.55	1.90	0.96
$CH_2CCH_2 \rightarrow CH_2C+CH_2$	64	1.62	2.02	2.47	1.73
$CH_2CCH_2 \rightarrow CH_2CCH+H$	65	0.76	1.40	1.77	1.11
$CH_3CCH \rightarrow CH_3C+CH$	66	0.50	1.02	1.41	0.70
$CH_3CCH \rightarrow CH_3+CHC$	67	0.62	1.16	1.56	0.78
$CH_3CCH \rightarrow CH_3CC+H$	68	0.10	0.66	1.00	0.27
$CH_3CCH \rightarrow CH_2CCH+H$	69	-0.13	0.58	0.94	0.02
$CH_3CC \rightarrow CH_3+CC$	70	1.38	1.81	2.20	1.56
$CH_3CC \rightarrow CH_3C+C$	71	0.96	1.32	1.70	1.14
$CH_3CC \rightarrow CH_2CC+H$	72	0.46	1.03	1.37	0.55
$CH_2CHC \rightarrow CH_2+CHC$	73	1.69	2.25	2.67	1.93
$CH_2CHC \rightarrow CH_2CH+C$	74	1.85	2.21	2.61	2.11
$CH_2CHC \rightarrow CH_2CC+H$	75	1.54	2.10	2.48	1.72
$CH_2CHC \rightarrow CHCHC+H$	76	1.43	2.00	2.33	1.64
$CHCH_2C \rightarrow CH+CH_2C$	77	1.69	2.75	3.15	2.68
$CHCH_2C \rightarrow CH_2CH+C$	78	1.74	2.09	2.48	1.87

$CHCH_2C \rightarrow CHCHC+H$	79	1.74	2.31	2.62	2.08
$CHCH_2C \rightarrow CCH_2C+H$	80	0.84	1.49	1.78	0.94
CHCHCH → CH+CHCH	81	1.54	2.08	2.42	1.50
CHCHCH → CHCHC+H	82	2.27	2.88	3.24	2.62
CHCHCH → CHCCH+H	83	1.35	1.99	2.32	1.46
$CH_2CCH \rightarrow CH_2+CHC$	84	1.62	2.15	2.51	1.86
$CH_2CCH \rightarrow CH_2C+CH$	85	1.57	2.06	2.46	1.77
$CH_2CCH \rightarrow CH_2CC+H$	86	1.88	2.38	2.78	2.21
$CH_2CCH \rightarrow CHCCH+H$	87	1.63	2.20	2.58	2.15
$CH_2CC \rightarrow CH_2+CC$	88	1.36	1.74	2.15	1.68
$CH_2CC \rightarrow CHC+C$	89	2.62	2.85	3.19	2.84
$CH_2CC \rightarrow CHCC+H$	90	1.20	1.75	2.08	1.49
CHCHC→ CH+CHC	91	2.38	2.75	3.16	2.68
CHCHC→ CHCH+C	92	2.26	2.46	2.87	2.75
CHCHC→ CHCC+H	93	1.45	1.96	2.32	1.56
CHCHC→ CCHC+H	94	2.65	3.02	3.35	3.00
$CCH_2C \rightarrow C+CH_2C$	95	2.27	2.45	2.84	2.68
$CCH_2C \rightarrow CCHC+H$	96	2.64	3.06	3.38	2.98
CHCCH → CH+CCH	97	1.32	1.77	2.10	1.64
CHCCH → CHCC+H	98	2.43	2.80	3.20	2.85
CCHC → CHC+C	99	1.93	2.27	2.61	2.39
CCHC → CCC+H	100	2.98	3.38	3.73	3.36
CHCC → CH+CC	101	1.96	2.28	2.65	2.38
CHCC → CHC+C	102	1.85	2.13	2.46	2.35
CHCC → CCC+H	103	1.97	2.36	2.72	2.25
CCC → C+CC	104	2.67	2.82	3.20	2.99
$CH_4 \rightarrow CH_3+H$	105	0.36	0.81	0.89	0.53
$CH_3 \rightarrow CH_2+H$	106	0.24	0.70	0.77	0.24
$CH_2 \rightarrow CH+H$	107	0.38	0.73	0.77	0.52
CH → C+H	108	0.58	0.77	0.81	0.88
$CH_3CH_3 \rightarrow CH_3+CH_3$	109	2.03	2.67	2.98	2.39
$CH_3CH_3 \rightarrow CH_3CH_2+H$	110	0.52	1.17	1.41	0.81
$CH_3CH_2 \rightarrow CH_3+CH_2$	111	1.26	1.85	2.14	1.54
$CH_3CH_2 \rightarrow CH_3CH+H$	112	0.36	0.98	1.22	0.50
$CH_3CH_2 \rightarrow CH_2CH_2+H$	113	0.49	1.04	1.32	0.77
$CH_3CH \rightarrow CH_3+CH$	114	1.50	2.06	2.30	1.69
$CH_3CH \rightarrow CH_3C+H$	115	0.22	0.70	0.91	0.44
$CH_3CH \rightarrow CH_2CH+H$	116	0.48	1.14	1.35	0.62
$CH_3C \rightarrow CH_3+C$	117	1.09	1.38	1.63	1.51
$CH_3C \rightarrow CH_2C+H$	118	0.49	0.92	1.12	0.73
$CH_2CH_2 \rightarrow CH_2+CH_2$	119	1.46	1.97	2.28	1.67
$CH_2CH_2 \rightarrow CH_2CH+H$	120	0.31	0.92	1.15	0.40
$CH_2CH \rightarrow CH_2+CH$	121	0.92	1.45	1.67	0.92

$CH_2CH \rightarrow CH_2C+H$	122	0.65	0.60	1.31	0.83
$CH_2CH \rightarrow CHCH+H$	123	0.11	1.10	0.90	0.20
$CH_2C \rightarrow CH_2+C$	124	1.41	1.64	1.86	1.57
$CH_2C \rightarrow CHC+H$	125	0.24	0.69	0.86	0.30
$CHCH \rightarrow CH+CH$	126	0.70	1.09	1.30	0.77
$CHCH \rightarrow CHC+H$	127	0.18	0.60	0.78	0.24
$CHC \rightarrow CH+C$	128	2.01	2.31	2.52	2.08
$CHC \rightarrow CC + H$	129	0.88	1.20	1.39	0.98
$CC \rightarrow C+C$	130	1.87	1.97	2.20	2.02

Table A.4: Free energies of Adsorbed Species on Pt(111) at 633 K, $P_{CH3CH2CH3}$ of 1 bar, and P_{H2} of 1 bar, referenced to gaseous propane, hydrogen, and platinum surface slab.

Pt(111)		Free Energy of Adsorption, $\Delta G_{ads,i}$ (eV)			
Adsorbed Species	Adsorption Number (ADS #)	PBE-D3	BEEF-vdW	RPBE	SCAN-rVV10
$CH_3CH_2CH_3$	1	0.26	0.76	1.22	0.65
CH_3CHCH_3	2	0.24	0.87	1.44	0.47
$CH_3CH_2CH_2$	3	0.38	0.92	1.37	0.57
CH_3CHCH_2	4	0.08	0.72	1.27	0.21
CH_3CH_2CH	5	0.42	0.93	1.41	0.57
$CH_2CH_2CH_2$	6	0.26	0.94	1.50	0.32
CH_3CCH_3	7	0.12	0.73	1.28	0.26
CH_3CH_2C	8	-0.33	0.11	0.56	-0.18
CH_2CH_2CH	9	0.54	1.14	1.66	0.55
CH_2CHCH_2	10	0.28	0.90	1.46	0.36
CH_3CHCH	11	0.23	0.79	1.30	0.30
CH_3CCH_2	12	0.10	0.66	1.19	0.13
CH_3CHC	13	0.12	0.60	1.06	0.21
CH_2CH_2C	14	0.37	0.89	1.34	0.42
$CHCH_2CH$	15	0.37	0.96	1.48	0.38
CH_2CHCH	16	1.20	1.80	2.27	0.88
CH_2CCH_2	17	0.38	0.92	1.42	0.39
CH_3CCH	18	0.18	0.67	1.13	0.26
CH_3CC	19	0.80	1.20	1.60	0.92
CH_2CHC	20	0.74	1.23	1.71	0.76
$CHCHCH$	21	0.46	1.00	1.47	0.34
$CHCH_2C$	22	1.73	2.14	2.60	1.79
CH_2CCH	23	0.35	0.87	1.34	0.27
CH_2CC	24	0.93	1.43	1.88	0.85
$CHCHC$	25	1.05	1.37	1.82	1.17
CCH_2C	26	1.35	1.66	2.09	1.45
$CHCCH$	27	0.74	1.23	1.68	0.67
$CCHC$	28	1.34	1.68	2.10	1.28
$CHCC$	29	1.72	2.02	2.46	1.75
CCC	30	2.47	2.68	3.14	2.59
CH_3CH_3	31	0.10	0.46	0.76	0.38
CH_3CH_2	32	0.13	0.55	0.90	0.26
CH_3CH	33	0.26	0.64	0.98	0.29
CH_3C	34	-0.38	-0.11	0.18	-0.31
CH_2CH_2	35	0.03	0.48	0.84	0.05
CH_2CH	36	0.17	0.56	0.89	0.09
CH_2C	37	0.00	0.35	0.64	-0.16

CHCH	38	0.22	0.58	0.88	0.10
CHC	39	1.02	1.26	1.54	0.97
CC	40	1.76	1.98	2.24	1.68
CH_4	41	-0.24	-0.09	0.05	-0.09
CH_3	42	0.07	0.32	0.51	0.05
CH_2	43	0.32	0.53	0.69	0.23
CH	44	-0.22	-0.09	0.03	-0.33
C	45	0.51	0.60	0.73	0.46
H	46	-0.18	-0.03	-0.10	-0.17

Table A.5: Free energies of transition state species on Pt(111) at 633 K, $P_{CH3CH2CH3}$ of 1 bar, and P_{H2} of 1 bar, referenced to gaseous propane, hydrogen, and platinum surface slab.

Pt(111)		Free Energy of the Transition State, $\Delta G_{ads,j}^{\ddagger}$ (eV)			
Chemical Reaction	Reaction Number	PBE-D3	BEEF-vdW	RPBE	SCAN-rVV10
$CH_3CH_2CH_3 \rightarrow CH_3CHCH_3+H$	1	1.01	1.92	2.39	1.29
$CH_3CH_2CH_3 \rightarrow CH_3CH_2CH_2 +H$	2	0.99	1.78	2.12	1.20
$CH_3CHCH_3 \rightarrow CH_3CHCH_2+H$	3	0.85	1.76	2.22	0.99
$CH_3CH_2CH_2 \rightarrow CH_3CHCH_2+H$	4	0.91	1.79	2.21	1.00
$CH_3CH_2CH_3 \rightarrow CH_3+CH_2CH_3$	5	2.71	3.50	3.93	2.97
$CH_3CHCH_3 \rightarrow CH_3CH+CH_3$	6	2.06	2.87	3.41	2.32
$CH_3CHCH_3 \rightarrow CH_3CCH_3+H$	7	0.85	1.71	2.19	0.92
$CH_3CH_2CH_2 \rightarrow CH_3CH_2+CH_2$	8	2.23	2.93	3.38	2.43
$CH_3CH_2CH_2 \rightarrow CH_3+CH_2CH_2$	9	2.55	3.46	3.98	2.76
$CH_3CH_2CH_2 \rightarrow CH_2CH_2CH_2+H$	10	0.97	1.96	2.41	1.05
$CH_3CH_2CH_2 \rightarrow CH_3CH_2CH +H$	11	1.02	1.79	2.16	1.08
$CH_3CH_2CH \rightarrow CH_3CH_2+CH$	12	2.68	3.53	4.02	2.88
$CH_3CH_2CH \rightarrow CH_3+CH_2CH$	13	2.56	3.35	3.84	2.74
$CH_3CH_2CH \rightarrow CH_3CH_2C +H$	14	0.79	1.51	1.91	0.94
$CH_3CH_2CH \rightarrow CH_3CHCH+H$	15	0.93	1.77	2.20	0.98
$CH_3CH_2CH \rightarrow CH_2CH_2CH+H$	16	1.13	2.05	2.47	1.18
$CH_2CH_2CH_2 \rightarrow CH_2+CH_2CH_2$	17	1.61	2.46	2.98	1.72
$CH_2CH_2CH_2 \rightarrow CH_2CH_2CH+H$	18	1.05	1.94	2.39	0.98
$CH_2CH_2CH_2 \rightarrow CH_2CHCH_2+H$	19	0.71	1.61	2.10	0.73
$CH_3CHCH_2 \rightarrow CH_3+CHCH_2$	20	1.79	2.62	3.13	1.95
$CH_3CHCH_2 \rightarrow CH_3CH+CH_2$	21	1.98	2.76	3.26	2.18
$CH_3CHCH_2 \rightarrow CH_3CCH_2+H$	22	0.81	1.70	2.14	0.82
$CH_3CHCH_2 \rightarrow CH_3CHCH+H$	23	0.80	1.64	2.10	0.79
$CH_3CHCH_2 \rightarrow CH_2CHCH_2+H$	24	0.79	1.65	2.15	0.92
$CH_3CCH_3 \rightarrow CH_3+CH_3C$	25	1.64	2.41	2.92	1.77
$CH_3CCH_3 \rightarrow CH_3CCH_2+H$	26	1.02	1.79	2.23	1.23
$CH_3CH_2C \rightarrow CH_3+CH_2C$	27	1.91	2.55	3.02	1.91
$CH_3CH_2C \rightarrow CH_3CH_2+C$	28	1.56	2.28	2.72	1.52
$CH_3CH_2C \rightarrow CH_2CH_2C+H$	29	1.02	1.82	2.21	1.11
$CH_3CH_2C \rightarrow CH_3CHC+H$	30	1.04	1.89	2.25	1.06
$CH_2CH_2CH \rightarrow CH_2+CH_2CH$	31	2.01	2.77	3.27	2.09
$CH_2CH_2CH \rightarrow CH_2CH_2+CH$	32	1.76	2.50	2.98	1.88
$CH_2CH_2CH \rightarrow CH_2CH2C+H$	33	1.07	1.87	2.28	1.06
$CH_2CH_2CH \rightarrow CH_2CHCH+H$	34	1.23	2.10	2.54	1.19
$CH_2CH_2CH \rightarrow CHCH_2CH+H$	35	1.69	2.51	2.93	1.71

$CH_2CHCH_2 \rightarrow CH_2+CH_2CH$	36	1.96	2.72	3.23	2.13
$CH_2CHCH_2 \rightarrow CH_2CHCH+H$	37	0.86	1.73	2.17	0.75
$CH_2CHCH_2 \rightarrow CH_2CCH_2+H$	38	1.22	2.05	2.49	1.17
$CH_3CHCH \rightarrow CH_3+CHCH$	39	2.01	2.81	3.28	2.05
$CH_3CHCH \rightarrow CH_3CH+CH$	40	1.67	2.28	2.74	1.72
$CH_3CHCH \rightarrow CH_3CHC+H$	41	0.76	1.53	1.93	0.83
$CH_3CHCH \rightarrow CH_3CCH+H$	42	0.87	1.65	2.06	0.92
$CH_3CHCH \rightarrow CH_2CHCH+H$	43	1.04	1.92	2.34	1.01
$CH_3CCH_2 \rightarrow CH_3+CH_2C$	44	1.87	2.60	3.08	1.89
$CH_3CCH_2 \rightarrow CH_3C+CH_2$	45	1.64	2.30	2.77	1.73
$CH_3CCH_2 \rightarrow CH_2CCH_2+H$	46	0.97	1.57	1.98	0.71
$CH_3CCH_2 \rightarrow CH_3CCH+H$	47	0.81	1.90	2.35	0.99
$CH_3CHC \rightarrow CH_3+CHC$	48	2.49	3.20	3.65	2.55
$CH_3CHC \rightarrow CH_3CH+C$	49	2.03	2.48	2.93	2.11
$CH_3CHC \rightarrow CH_3CC+H$	50	1.29	1.93	2.29	1.38
$CH_3CHC \rightarrow CH_2CHC+H$	51	1.13	1.95	2.32	1.13
$CH_2CH_2C \rightarrow CH_2CH_2+C$	52	1.89	2.37	2.85	1.86
$CH_2CH_2C \rightarrow CH_2+CH_2C$	53	1.76	2.43	2.84	1.86
$CH_2CH_2C \rightarrow CH_2CHC+H$	54	1.84	2.62	2.99	1.84
$CH_2CH_2C \rightarrow CHCH_2C+H$	55	2.03	2.79	3.16	2.05
$CHCH_2CH \rightarrow CH_2CH+CH$	56	2.04	2.65	3.11	2.04
$CHCH_2CH \rightarrow CHCH_2C+H$	57	2.16	2.91	3.30	2.14
$CHCH_2CH \rightarrow CHCHCH+H$	58	1.54	2.40	2.76	1.40
$CH_2CHCH \rightarrow CH_2+CHCH$	59	1.93	2.55	3.04	2.06
$CH_2CHCH \rightarrow CH_2CH+CH$	60	2.02	2.68	3.15	2.16
$CH_2CHCH \rightarrow CH_2CHC+H$	61	1.64	2.35	2.78	1.62
$CH_2CHCH \rightarrow CH_2CCH+H$	62	1.09	1.89	2.31	0.97
$CH_2CHCH \rightarrow CHCHCH+H$	63	1.20	2.03	2.43	1.01
$CH_2CCH_2 \rightarrow CH_2C+CH_2$	64	2.16	2.79	3.28	2.23
$CH_2CCH_2 \rightarrow CH_2CCH+H$	65	1.99	2.64	3.05	2.23
$CH_3CCH \rightarrow CH_3C+CH$	66	1.70	2.34	2.78	1.66
$CH_3CCH \rightarrow CH_3+CHC$	67	2.05	2.68	3.12	2.10
$CH_3CCH \rightarrow CH_3CC+H$	68	1.52	2.15	2.51	1.65
$CH_3CCH \rightarrow CH_2CCH+H$	69	1.04	1.84	2.24	0.94
$CH_3CC \rightarrow CH_3+CC$	70	3.33	3.88	4.33	3.24
$CH_3CC \rightarrow CH_3C+C$	71	1.74	2.23	2.61	1.72
$CH_3CC \rightarrow CH_2CC+H$	72	1.51	2.11	2.49	1.63
$CH_2CHC \rightarrow CH_2+CHC$	73	2.47	3.05	3.51	2.57
$CH_2CHC \rightarrow CH_2CH+C$	74	2.08	2.50	2.96	2.26
$CH_2CHC \rightarrow CH_2CC+H$	75	1.89	2.61	3.01	1.72
$CH_2CHC \rightarrow CHCHC+H$	76	1.57	2.17	2.55	1.66
$CHCH_2C \rightarrow CH+CH_2C$	77	2.04	2.49	2.95	2.14
$CHCH_2C \rightarrow CH_2CH+C$	78	2.42	2.96	3.42	2.45

$CHCH_2C \rightarrow CHCHC+H$	79	2.49	3.10	3.49	2.51
$CHCH_2C \rightarrow CCH_2C+H$	80	2.39	2.89	3.27	2.42
CHCHCH → CH+CHCH	81	1.49	2.08	2.51	1.51
CHCHCH → CHCHC+H	82	1.11	1.92	2.27	1.00
CHCHCH → CHCCH+H	83	2.13	2.89	3.27	2.01
$CH_2CCH \rightarrow CH_2+CHC$	84	2.69	3.26	3.72	2.77
$CH_2CCH \rightarrow CH_2C+CH$	85	1.79	2.40	2.81	1.69
$CH_2CCH \rightarrow CH_2CC+H$	86	1.80	2.53	2.93	1.61
$CH_2CCH \rightarrow CHCCH+H$	87	1.84	2.57	2.93	1.61
$CH_2CC \rightarrow CH_2+CC$	88	3.32	3.76	4.25	3.25
$CH_2CC \rightarrow CHC+C$	89	2.43	2.83	3.26	2.43
$CH_2CC \rightarrow CHCC+H$	90	2.36	2.97	3.38	2.40
CHCHC→ CH+CHC	91	1.89	2.47	2.87	1.77
CHCHC→ CHCH+C	92	3.11	3.47	3.91	3.26
CHCHC→ CHCC+H	93	2.80	3.24	3.63	3.03
CHCHC→ CCHC+H	94	2.54	3.09	3.50	2.65
$CCH_2C \rightarrow C+CH_2C$	95	2.03	2.46	2.89	2.12
$CCH_2C \rightarrow CCHC+H$	96	2.76	3.24	3.58	2.89
CHCCH → CH+CCH	97	2.35	2.90	3.30	2.36
CHCCH → CHCC+H	98	2.13	2.69	3.08	2.10
CCHC → CHC+C	99	2.62	3.03	3.46	2.71
CCHC → CCC+H	100	3.39	3.87	4.24	3.40
CHCC → CH+CC	101	3.14	3.50	3.89	3.08
CHCC → CHC+C	102	3.07	3.47	3.87	3.16
CHCC → CCC+H	103	3.33	3.78	4.15	3.48
CCC → C+CC	104	3.79	4.06	4.48	3.84
$CH_4 \rightarrow CH_3+H$	105	0.67	1.24	1.33	0.69
$CH_3 \rightarrow CH_2+H$	106	0.81	1.31	1.39	0.64
$CH_2 \rightarrow CH+H$	107	0.45	0.92	0.96	0.23
CH → C+H	108	0.98	1.42	1.45	0.68
$CH_3CH_3 \rightarrow CH_3+CH_3$	109	2.90	3.81	4.07	3.12
$CH_3CH_3 \rightarrow CH_3CH_2+H$	110	0.82	1.59	1.85	0.96
$CH_3CH_2 \rightarrow CH_3+CH_2$	111	1.81	2.45	2.78	1.94
$CH_3CH_2 \rightarrow CH_3CH+H$	112	0.88	1.56	1.83	0.84
$CH_3CH_2 \rightarrow CH_2CH_2+H$	113	0.94	1.59	1.87	1.10
$CH_3CH \rightarrow CH_3+CH$	114	1.60	2.17	2.46	1.71
$CH_3CH \rightarrow CH_3C+H$	115	0.62	1.16	1.39	0.65
$CH_3CH \rightarrow CH_2CH+H$	116	0.85	1.52	1.75	0.76
$CH_3C \rightarrow CH_3+C$	117	1.64	2.13	2.40	1.63
$CH_3C \rightarrow CH_2C+H$	118	0.88	1.46	1.68	0.76
$CH_2CH_2 \rightarrow CH_2+CH_2$	119	2.00	2.59	2.91	2.08
$CH_2CH_2 \rightarrow CH_2CH+H$	120	0.81	1.51	1.76	0.68
$CH_2CH \rightarrow CH_2+CH$	121	1.85	2.41	2.68	1.67

$CH_2CH \rightarrow CH_2C+H$	122	0.61	1.27	1.49	0.38
$CH_2CH \rightarrow CHCH+H$	123	0.89	1.56	1.78	0.73
$CH_2C \rightarrow CH_2+C$	124	2.04	2.44	2.70	1.93
$CH_2C \rightarrow CHC+H$	125	1.30	1.85	2.07	1.15
$CHCH \rightarrow CH+CH$	126	1.64	2.14	2.36	1.38
$CHCH \rightarrow CHC+H$	127	1.52	2.04	2.27	1.40
$CHC \rightarrow CH+C$	128	2.14	2.48	2.71	1.99
$CHC \rightarrow CC + H$	129	2.57	2.15	3.16	2.60
$CC \rightarrow C+C$	130	3.03	3.22	3.47	2.98

Table A.6: Free energies of adsorbed species on Pt(211) at 633 K, $P_{CH3CH2CH3}$ of 1 bar, and P_{H2} of 1 bar, referenced to gaseous propane, hydrogen, and platinum surface slab.

Pt(211)		Free Energy of Adsorption, $\Delta G_{ads,i}$ (eV)			
Adsorbed Species	Adsorption Number (ADS #)	PBE-D3	BEEF-vdW	RPBE	SCAN-rVV10
$CH_3CH_2CH_3$	1	0.20	0.98	1.54	0.60
CH_3CHCH_3	2	0.18	1.01	1.62	0.35
$CH_3CH_2CH_2$	3	0.34	1.04	1.48	0.42
CH_3CHCH_2	4	-0.19	0.55	1.02	0.05
CH_3CH_2CH	5	0.18	0.77	1.14	0.38
$CH_2CH_2CH_2$	6	0.21	0.97	1.37	0.34
CH_3CCH_3	7	-0.15	0.70	1.17	-0.02
CH_3CH_2C	8	-0.24	0.41	0.87	-0.13
CH_2CH_2CH	9	0.41	1.13	1.52	0.56
CH_2CHCH_2	10	-0.34	0.39	0.81	-0.25
CH_3CHCH	11	0.20	0.96	1.48	0.21
CH_3CCH_2	12	0.04	0.80	1.30	0.03
CH_3CHC	13	0.05	0.67	1.12	0.24
CH_2CH_2C	14	0.21	0.89	1.32	0.29
$CHCH_2CH$	15	-0.25	0.48	0.91	-0.26
CH_2CHCH	16	0.36	1.04	1.47	0.34
CH_2CCH_2	17	-0.03	0.65	1.09	-0.04
CH_3CCH	18	-0.24	0.61	1.16	-0.12
CH_3CC	19	-0.35	0.19	0.64	-0.13
CH_2CHC	20	-0.03	0.66	1.13	0.13
$CHCHCH$	21	-0.26	0.48	0.93	-0.23
$CHCH_2C$	22	0.01	0.83	1.37	0.09
CH_2CCH	23	0.06	0.78	1.31	0.21
CH_2CC	24	-0.05	0.45	0.89	0.19
$CHCHC$	25	-0.34	0.27	0.71	-0.23
CCH_2C	26	1.32	1.83	2.17	1.51
$CHCCH$	27	0.98	1.64	2.11	1.15
$CCHC$	28	1.35	1.88	2.26	1.38
$CHCC$	29	0.63	1.11	1.53	0.94
CCC	30	1.43	1.87	2.37	1.68
CH_3CH_3	31	0.14	0.70	0.93	0.24
CH_3CH_2	32	0.06	0.58	0.85	0.13
CH_3CH	33	-0.19	0.30	0.57	-0.07
CH_3C	34	-0.39	0.02	0.25	-0.31
CH_2CH_2	35	-0.25	0.30	0.54	-0.19
CH_2CH	36	0.17	0.73	1.02	0.05
CH_2C	37	0.07	0.49	0.77	0.06

CHCH	38	-0.06	0.56	0.90	-0.02
CHC	39	-0.25	0.15	0.43	-0.10
CC	40	0.50	0.81	1.11	0.71
CH_4	41	-0.12	0.18	0.27	-0.12
CH_3	42	-0.13	0.23	0.34	-0.19
CH_2	43	-0.11	0.22	0.32	-0.13
CH	44	-0.13	0.25	0.35	-0.24
C	45	0.50	0.71	0.88	0.44
H	46	-0.28	0.00	-0.08	-0.35

Table A.7: Free energies of transition state species on Pt(211) at 633 K, $P_{CH3CH2CH3}$ of 1 bar, and P_{H2} of 1 bar, referenced to gaseous propane, hydrogen, and platinum surface slab.

Pt(211)		Free Energy of the Transition State, $\Delta G^{\ddagger}_{ads,j}$ (eV)			
Chemical Reaction	Reaction Number	PBE-D3	BEEF-vdW	RPBE	SCAN-rVV10
$CH_3CH_2CH_3 \rightarrow CH_3CHCH_3+H$	1	0.77	1.80	2.13	0.87
$CH_3CH_2CH_3 \rightarrow CH_3CH_2CH_2 +H$	2	0.92	1.80	2.01	1.07
$CH_3CHCH_3 \rightarrow CH_3CHCH_2+H$	3	0.49	1.52	1.83	0.61
$CH_3CH_2CH_2 \rightarrow CH_3CHCH_2+H$	4	0.54	1.49	1.76	0.65
$CH_3CH_2CH_3 \rightarrow CH_3+CH_2CH_3$	5	2.65	3.75	4.28	3.05
$CH_3CHCH_3 \rightarrow CH_3CH+CH_3$	6	1.99	3.01	3.57	2.17
$CH_3CHCH_3 \rightarrow CH_3CCH_3+H$	7	0.89	1.93	2.40	0.92
$CH_3CH_2CH_2 \rightarrow CH_3CH_2+CH_2$	8	2.03	2.93	3.39	2.21
$CH_3CH_2CH_2 \rightarrow CH_3+CH_2CH_2$	9	2.12	3.09	3.71	2.27
$CH_3CH_2CH_2 \rightarrow CH_2CH_2CH_2+H$	10	0.71	1.83	2.22	1.17
$CH_3CH_2CH_2 \rightarrow CH_3CH_2CH +H$	11	1.07	2.06	2.43	0.60
$CH_3CH_2CH \rightarrow CH_3CH_2+CH$	12	1.52	2.75	3.15	2.02
$CH_3CH_2CH \rightarrow CH_3+CH_2CH$	13	1.82	2.31	2.63	1.68
$CH_3CH_2CH \rightarrow CH_3CH_2C +H$	14	0.66	1.42	1.70	0.79
$CH_3CH_2CH \rightarrow CH_3CHCH+H$	15	0.74	1.72	2.08	0.82
$CH_3CH_2CH \rightarrow CH_2CH_2CH+H$	16	0.70	1.77	2.13	0.83
$CH_2CH_2CH_2 \rightarrow CH_2+CH_2CH_2$	17	1.32	2.23	2.60	1.55
$CH_2CH_2CH_2 \rightarrow CH_2CH_2CH+H$	18	1.32	2.30	2.60	1.50
$CH_2CH_2CH_2 \rightarrow CH_2CHCH_2+H$	19	0.57	1.67	2.14	0.47
$CH_3CHCH_2 \rightarrow CH_3+CHCH_2$	20	1.63	2.62	3.12	1.73
$CH_3CHCH_2 \rightarrow CH_3CH+CH_2$	21	1.66	2.73	3.23	1.72
$CH_3CHCH_2 \rightarrow CH_3CCH_2+H$	22	0.71	1.79	2.22	0.63
$CH_3CHCH_2 \rightarrow CH_3CHCH+H$	23	0.71	1.77	2.21	0.63
$CH_3CHCH_2 \rightarrow CH_2CHCH_2+H$	24	0.81	1.90	2.29	0.89
$CH_3CCH_3 \rightarrow CH_3+CH_3C$	25	1.34	2.24	2.70	1.43
$CH_3CCH_3 \rightarrow CH_3CCH_2+H$	26	1.52	2.45	2.71	1.68
$CH_3CH_2C \rightarrow CH_3+CH_2C$	27	1.40	2.18	3.18	2.06
$CH_3CH_2C \rightarrow CH_3CH_2+C$	28	1.64	2.43	2.90	1.72
$CH_3CH_2C \rightarrow CH_2CH_2C+H$	29	0.75	1.68	2.05	0.71
$CH_3CH_2C \rightarrow CH_3CHC+H$	30	1.67	2.73	3.13	1.79
$CH_2CH_2CH \rightarrow CH_2+CH_2CH$	31	1.29	2.12	2.50	1.50
$CH_2CH_2CH \rightarrow CH_2CH_2+CH$	32	1.51	2.40	2.79	1.54
$CH_2CH_2CH \rightarrow CH_2CH2C+H$	33	1.25	2.25	2.49	1.40
$CH_2CH_2CH \rightarrow CH_2CHCH+H$	34	1.45	2.42	2.75	1.54
$CH_2CH_2CH \rightarrow CHCH_2CH+H$	35	1.39	2.38	2.70	1.40

$CH_2CHCH_2 \rightarrow CH_2+CH_2CH$	36	1.50	2.38	2.77	1.55
$CH_2CHCH_2 \rightarrow CH_2CHCH+H$	37	0.64	1.64	1.97	0.68
$CH_2CHCH_2 \rightarrow CH_2CCH_2+H$	38	0.56	1.59	2.05	0.50
$CH_3CHCH \rightarrow CH_3+CHCH$	39	1.76	2.67	3.14	1.87
$CH_3CHCH \rightarrow CH_3CH+CH$	40	1.62	2.48	2.95	1.76
$CH_3CHCH \rightarrow CH_3CHC+H$	41	0.61	1.63	2.07	0.59
$CH_3CHCH \rightarrow CH_3CCH+H$	42	0.83	1.85	2.28	0.88
$CH_3CHCH \rightarrow CH_2CHCH+H$	43	1.14	2.19	2.58	1.18
$CH_3CCH_2 \rightarrow CH_3+CH_2C$	44	1.47	2.41	2.89	1.51
$CH_3CCH_2 \rightarrow CH_3C+CH_2$	45	1.46	2.26	2.74	1.47
$CH_3CCH_2 \rightarrow CH_2CCH_2+H$	46	0.58	1.54	1.96	0.61
$CH_3CCH_2 \rightarrow CH_3CCH+H$	47	1.02	2.03	2.39	1.07
$CH_3CHC \rightarrow CH_3+CHC$	48	2.22	3.11	3.56	2.38
$CH_3CHC \rightarrow CH_3CH+C$	49	1.82	2.47	2.89	1.96
$CH_3CHC \rightarrow CH_3CC+H$	50	1.10	1.90	2.27	1.27
$CH_3CHC \rightarrow CH_2CHC+H$	51	1.24	2.14	2.58	1.63
$CH_2CH_2C \rightarrow CH_2CH_2+C$	52	1.78	2.47	3.11	2.11
$CH_2CH_2C \rightarrow CH_2+CH_2C$	53	1.83	2.62	3.10	2.09
$CH_2CH_2C \rightarrow CH_2CHC+H$	54	1.43	2.40	2.73	1.41
$CH_2CH_2C \rightarrow CHCH_2C+H$	55	1.95	2.97	3.33	2.18
$CHCH_2CH \rightarrow CH_2CH+CH$	56	1.88	2.82	3.26	1.98
$CHCH_2CH \rightarrow CHCH_2C+H$	57	1.22	2.17	2.49	1.15
$CHCH_2CH \rightarrow CHCHCH+H$	58	1.44	2.35	2.71	1.46
$CH_2CHCH \rightarrow CH_2+CHCH$	59	1.69	2.47	2.84	1.82
$CH_2CHCH \rightarrow CH_2CH+CH$	60	1.79	2.66	3.06	1.83
$CH_2CHCH \rightarrow CH_2CHC+H$	61	1.33	2.43	2.89	1.22
$CH_2CHCH \rightarrow CH_2CCH+H$	62	1.00	1.95	2.29	1.01
$CH_2CHCH \rightarrow CHCHCH+H$	63	0.53	1.52	1.85	0.37
$CH_2CCH_2 \rightarrow CH_2C+CH_2$	64	1.88	2.67	3.07	1.95
$CH_2CCH_2 \rightarrow CH_2CCH+H$	65	0.79	1.77	2.06	0.84
$CH_3CCH \rightarrow CH_3C+CH$	66	1.45	2.23	2.57	1.52
$CH_3CCH \rightarrow CH_3+CHC$	67	1.43	2.23	2.69	1.49
$CH_3CCH \rightarrow CH_3CC+H$	68	0.77	1.64	2.10	0.87
$CH_3CCH \rightarrow CH_2CCH+H$	69	0.48	1.47	1.91	0.51
$CH_3CC \rightarrow CH_3+CC$	70	1.46	2.15	2.55	1.67
$CH_3CC \rightarrow CH_3C+C$	71	1.73	2.31	2.68	1.87
$CH_3CC \rightarrow CH_2CC+H$	72	0.41	1.19	1.54	0.56
$CH_2CHC \rightarrow CH_2+CHC$	73	2.52	3.28	3.71	2.78
$CH_2CHC \rightarrow CH_2CH+C$	74	1.95	2.70	3.16	2.08
$CH_2CHC \rightarrow CH_2CC+H$	75	0.45	1.26	1.62	0.67
$CH_2CHC \rightarrow CHCHC+H$	76	0.10	1.03	1.38	0.21
$CHCH_2C \rightarrow CH+CH_2C$	77	1.89	2.71	3.20	1.93
$CHCH_2C \rightarrow CH_2CH+C$	78	2.17	2.95	3.35	2.30

$CHCH_2C \rightarrow CHCHC+H$	79	1.05	1.98	2.27	0.89
$CHCH_2C \rightarrow CCH_2C+H$	80	0.76	1.76	2.12	0.73
$CHCHCH \rightarrow CH+CHCH$	81	1.79	2.58	2.96	1.90
$CHCHCH \rightarrow CHCHC+H$	82	1.15	2.07	2.39	1.10
$CHCHCH \rightarrow CHCCH+H$	83	1.21	2.12	2.43	1.10
$CH_2CCH \rightarrow CH_2+CHC$	84	2.36	3.13	3.53	2.36
$CH_2CCH \rightarrow CH_2C+CH$	85	1.72	2.29	2.70	1.99
$CH_2CCH \rightarrow CH_2CC+H$	86	1.15	1.94	2.38	1.20
$CH_2CCH \rightarrow CHCCH+H$	87	1.30	2.11	2.45	1.34
$CH_2CC \rightarrow CH_2+CC$	88	2.32	2.91	3.30	2.53
$CH_2CC \rightarrow CHC+C$	89	1.61	2.27	2.65	1.79
$CH_2CC \rightarrow CHCC+H$	90	1.85	2.82	3.15	1.96
$CHCHC\rightarrow CH+CHC$	91	1.35	2.12	2.53	1.29
$CHCHC\rightarrow CHCH+C$	92	1.75	2.39	2.82	1.87
$CHCHC\rightarrow CHCC+H$	93	2.41	3.11	3.45	2.56
$CHCHC\rightarrow CCHC+H$	94	1.06	1.94	2.57	1.11
$CCH_2C \rightarrow C+CH_2C$	95	1.84	2.44	2.40	2.06
$CCH_2C \rightarrow CCHC+H$	96	2.10	2.84	3.14	2.29
$CHCCH \rightarrow CH+CCH$	97	2.15	2.80	3.19	2.98
$CHCCH \rightarrow CHCC+H$	98	2.34	3.21	3.59	2.57
$CCHC \rightarrow CHC+C$	99	2.32	2.85	3.33	2.47
$CCHC \rightarrow CCC+H$	100	2.12	2.88	3.30	2.29
$CHCC \rightarrow CH+CC$	101	1.92	2.51	2.86	2.16
$CHCC \rightarrow CHC+C$	102	3.08	3.73	4.17	3.09
$CHCC \rightarrow CCC+H$	103	1.90	2.62	3.03	2.10
$CCC \rightarrow C+CC$	104	3.31	3.68	4.14	3.42
$CH_4 \rightarrow CH_3+H$	105	0.35	1.03	1.04	0.33
$CH_3 \rightarrow CH_2+H$	106	0.21	0.88	0.88	0.11
$CH_2\rightarrow CH+H$	107	0.41	1.02	1.01	0.28
$CH \rightarrow C+H$	108	0.91	1.35	1.44	0.81
$CH_3CH_3 \rightarrow CH_3+CH_3$	109	1.63	2.45	2.73	1.83
$CH_3CH_3 \rightarrow CH_3CH_2+H$	110	0.70	1.52	1.69	0.81
$CH_3CH_2 \rightarrow CH_3+CH_2$	111	1.21	1.97	2.18	1.31
$CH_3CH_2 \rightarrow CH_3CH+H$	112	0.85	1.70	1.97	0.72
$CH_3CH_2 \rightarrow CH_2CH_2+H$	113	0.37	1.21	1.35	0.44
$CH_3CH \rightarrow CH_3+CH$	114	1.21	1.94	2.12	1.28
$CH_3CH \rightarrow CH_3C+H$	115	0.50	1.14	1.29	0.54
$CH_3CH \rightarrow CH_2CH+H$	116	0.60	1.41	1.62	0.49
$CH_3C \rightarrow CH_3+C$	117	1.44	2.06	2.32	1.56
$CH_3C \rightarrow CH_2C+H$	118	0.76	1.48	1.67	0.73
$CH_2CH_2 \rightarrow CH_2+CH_2$	119	1.33	2.02	2.23	1.41
$CH_2CH_2 \rightarrow CH_2CH+H$	120	0.31	1.06	1.23	0.24
$CH_2CH \rightarrow CH_2+CH$	121	1.30	2.00	2.20	1.24

$CH_2CH \rightarrow CH_2C+H$	122	0.63	1.39	1.60	0.50
$CH_2CH \rightarrow CHCH+H$	123	0.74	1.49	1.72	0.64
$CH_2C \rightarrow CH_2+C$	124	1.73	2.29	2.50	1.65
$CH_2C \rightarrow CHC+H$	125	1.37	2.07	2.27	1.34
$CHCH \rightarrow CH+CH$	126	1.62	2.35	1.92	0.96
$CHCH \rightarrow CHC+H$	127	1.02	1.69	1.93	1.01
$CHC \rightarrow CH+C$	128	1.31	1.83	2.08	1.37
$CHC \rightarrow CC + H$	129	0.91	1.47	1.69	1.08
$CC \rightarrow C+C$	130	2.11	2.50	2.70	2.05

Table A.8: Free energies of adsorbed species on Pt(100) at 793 K, $P_{CH3CH2CH3}$ of 1 bar, and P_{H2} of 1 bar. Referenced to gaseous propane, hydrogen, and platinum surface.

Pt(100)		Free Energy of Adsorption, $\Delta G_{ads,i}$ (eV)			
Adsorbed Species	Adsorption Number (ADS #)	PBE-D3	BEEF-vdW	RPBE	SCAN-rVV10
$CH_3CH_2CH_3$	1	0.56	0.92	1.60	1.18
CH_3CHCH_3	2	0.31	0.69	1.36	0.61
$CH_3CH_2CH_2$	3	0.47	0.73	1.29	0.75
CH_3CHCH_2	4	0.06	0.34	0.88	0.20
CH_3CH_2CH	5	0.06	0.28	0.76	0.14
$CH_2CH_2CH_2$	6	0.17	0.52	1.06	0.21
CH_3CCH_3	7	-0.12	0.19	0.75	-0.01
CH_3CH_2C	8	-0.31	-0.28	0.20	-0.18
CH_2CH_2CH	9	0.53	0.70	1.18	0.37
CH_2CHCH_2	10	-0.33	-0.19	0.35	-0.42
CH_3CHCH	11	-0.09	0.02	0.50	-0.27
CH_3CCH_2	12	-0.02	0.08	0.53	-0.18
CH_3CHC	13	0.15	0.07	0.49	-0.08
CH_2CH_2C	14	-0.08	-0.19	0.26	-0.26
$CHCH_2CH$	15	-0.48	-0.46	0.00	-0.85
CH_2CHCH	16	-0.46	-0.45	0.04	-0.75
CH_2CCH_2	17	-0.26	-0.27	0.21	-0.61
CH_3CCH	18	-0.97	-1.05	-0.59	-1.24
CH_3CC	19	-0.67	-1.02	-0.59	-1.05
CH_2CHC	20	-0.23	-0.48	-0.01	-0.65
$CHCHCH$	21	0.95	0.78	1.18	0.42
$CHCH_2C$	22	-0.27	-0.46	-0.04	-0.81
CH_2CCH	23	-0.50	-0.64	-0.22	-0.98
CH_2CC	24	-0.50	-0.97	-0.55	-1.14
$CHCHC$	25	-0.42	-0.83	-0.41	-1.10
CCH_2C	26	0.90	0.51	0.86	0.23
$CHCCH$	27	-0.42	-0.78	-0.38	-0.94
$CCHC$	28	1.03	0.30	0.68	0.78
$CHCC$	29	0.12	-0.49	-0.09	-0.54
CCC	30	1.13	0.15	0.52	0.67
CH_3CH_3	31	0.30	0.72	1.05	0.86
CH_3CH_2	32	0.19	0.49	0.85	0.45
CH_3CH	33	-0.10	0.08	0.42	-0.05
CH_3C	34	-0.49	-0.55	-0.24	-0.40
CH_2CH_2	35	-0.10	0.10	0.46	-0.03
CH_2CH	36	-0.17	-0.13	0.19	-0.32
CH_2C	37	-0.18	-0.43	-0.14	-0.45

CHCH	38	-0.94	-1.10	-0.83	-1.23
CHC	39	-0.57	-0.99	-0.73	-0.99
CC	40	0.12	-0.54	-0.27	-0.38
CH_4	41	-0.06	0.22	0.41	0.43
CH_3	42	0.00	0.22	0.42	0.21
CH_2	43	-0.06	0.02	0.18	-0.06
CH	44	-0.40	-0.54	-0.43	-0.32
C	45	-0.34	-0.77	-0.64	-0.30
H	46	-0.20	0.05	0.01	-0.11

Table A.9: Free energies of the transition state species on Pt(100) at 793 K, $P_{CH3CH2CH3}$ of 1 bar, and P_{H2} of 1 bar. Referenced to gaseous propane, hydrogen, and platinum surface.

Pt(100)		Free Energy of the Transition State, $\Delta G^{\ddagger}_{ads,j}$ (eV)			
Chemical Reaction	Reaction Number	PBE-D3	BEEF-vdW	RPBE	SCAN-rVV10
$CH_3CH_2CH_3 \rightarrow CH_3CHCH_3+H$	1	0.99	1.70	2.18	1.33
$CH_3CH_2CH_3 \rightarrow CH_3CH_2CH_2+H$	2	1.05	1.81	2.18	1.48
$CH_3CHCH_3 \rightarrow CH_3CHCH_2+H$	3	0.67	1.39	1.84	1.08
$CH_3CH_2CH_2 \rightarrow CH_3CHCH_2+H$	4	0.77	1.39	1.80	1.08
$CH_3CH_2CH_3 \rightarrow CH_3+CH_2CH_3$	5	2.78	3.74	4.17	3.24
$CH_3CHCH_3 \rightarrow CH_3CH+CH_3$	6	1.62	2.26	2.80	1.94
$CH_3CHCH_3 \rightarrow CH_3CCH_3+H$	7	0.62	1.27	1.74	0.73
$CH_3CH_2CH_2 \rightarrow CH_3CH_2+CH_2$	8	1.68	2.28	2.74	1.98
$CH_3CH_2CH_2 \rightarrow CH_3+CH_2CH_2$	9	2.73	3.54	3.95	2.94
$CH_3CH_2CH_2 \rightarrow CH_2CH_2CH_2+H$	10	0.89	1.66	2.11	1.11
$CH_3CH_2CH_2 \rightarrow CH_3CH_2CH+H$	11	0.74	1.37	1.75	0.90
$CH_3CH_2CH \rightarrow CH_3CH_2+CH$	12	1.50	1.95	2.38	1.52
$CH_3CH_2CH \rightarrow CH_3+CH_2CH$	13	1.80	2.31	2.81	1.92
$CH_3CH_2CH \rightarrow CH_3CH_2C+H$	14	0.59	0.74	1.12	0.54
$CH_3CH_2CH \rightarrow CH_3CHCH+H$	15	0.39	1.16	1.56	0.70
$CH_3CH_2CH \rightarrow CH_2CH_2CH+H$	16	0.81	1.41	1.82	0.83
$CH_2CH_2CH_2 \rightarrow CH_2+CH_2CH_2$	17	1.53	1.97	2.47	1.59
$CH_2CH_2CH_2 \rightarrow CH_2CH_2CH+H$	18	0.63	1.24	1.66	0.55
$CH_2CH_2CH_2 \rightarrow CH_2CHCH_2+H$	19	0.77	1.32	1.81	0.83
$CH_3CHCH_2 \rightarrow CH_3+CHCH_2$	20	1.24	1.71	2.21	1.33
$CH_3CHCH_2 \rightarrow CH_3CH+CH_2$	21	1.23	1.80	2.27	1.34
$CH_3CHCH_2 \rightarrow CH_3CCH_2+H$	22	0.47	1.01	1.46	0.45
$CH_3CHCH_2 \rightarrow CH_3CHCH+H$	23	0.41	0.92	1.34	0.43
$CH_3CHCH_2 \rightarrow CH_2CHCH_2+H$	24	0.48	1.04	1.50	0.58
$CH_3CCH_3 \rightarrow CH_3+CH_3C$	25	1.39	1.85	2.34	1.41
$CH_3CCH_3 \rightarrow CH_3CCH_2+H$	26	0.81	1.37	1.74	0.84
$CH_3CH_2C \rightarrow CH_3+CH_2C$	27	1.63	1.79	2.25	1.73
$CH_3CH_2C \rightarrow CH_3CH_2+C$	28	1.19	1.30	1.74	1.38
$CH_3CH_2C \rightarrow CH_2CH_2C+H$	29	0.61	0.90	1.26	0.53
$CH_3CH_2C \rightarrow CH_3CHC+H$	30	0.48	0.65	1.02	0.38

$CH_2CH_2CH \rightarrow CH_2+CH_2CH$	31	1.47	1.77	2.26	1.35
$CH_2CH_2CH \rightarrow CH_2CH_2+CH$	32	1.73	1.95	2.42	1.61
$CH_2CH_2CH \rightarrow CH_2CH2C+H$	33	0.90	1.19	1.56	0.87
$CH_2CH_2CH \rightarrow CH_2CHCH+H$	34	1.34	1.83	2.21	1.15
$CH_2CH_2CH \rightarrow CHCH_2CH+H$	35	0.61	1.07	1.45	0.37
$CH_2CHCH_2 \rightarrow CH_2+CH_2CH$	36	1.09	1.45	1.92	0.98
$CH_2CHCH_2 \rightarrow CH_2CHCH+H$	37	0.63	1.05	1.49	0.51
$CH_2CHCH_2 \rightarrow CH_2CCH_2+H$	38	0.28	0.66	1.09	0.06
$CH_3CHCH \rightarrow CH_3+CHCH$	39	0.80	1.13	1.56	0.72
$CH_3CHCH \rightarrow CH_3CH+CH$	40	1.36	1.57	1.98	1.32
$CH_3CHCH \rightarrow CH_3CHC+H$	41	0.61	0.86	1.22	0.54
$CH_3CHCH \rightarrow CH_3CCH+H$	42	0.05	0.43	0.81	-0.12
$CH_3CHCH \rightarrow CH_2CHCH+H$	43	0.36	0.81	1.20	0.15
$CH_3CCH_2 \rightarrow CH_3+CH_2C$	44	0.70	1.01	1.42	0.45
$CH_3CCH_2 \rightarrow CH_3C+CH_2$	45	1.08	1.46	1.83	0.94
$CH_3CCH_2 \rightarrow CH_2CCH_2+H$	46	1.11	1.46	1.88	1.16
$CH_3CCH_2 \rightarrow CH_3CCH+H$	47	0.31	0.59	0.96	0.27
$CH_3CHC \rightarrow CH_3+CHC$	48	1.18	1.22	1.64	0.97
$CH_3CHC \rightarrow CH_3CH+C$	49	1.23	1.03	1.44	1.02
$CH_3CHC \rightarrow CH_3CC+H$	50	0.66	0.73	1.06	0.46
$CH_3CHC \rightarrow CH_2CHC+H$	51	1.13	1.22	1.64	1.06
$CH_2CH_2C \rightarrow CH_2CH_2+C$	52	0.97	0.84	1.28	0.92
$CH_2CH_2C \rightarrow CH_2+CH_2C$	53	1.35	1.37	1.83	1.32
$CH_2CH_2C \rightarrow CH_2CHC+H$	54	0.46	0.60	0.97	0.07
$CH_2CH_2C \rightarrow CHCH_2C+H$	55	1.26	1.35	1.71	1.10
$CHCH_2CH \rightarrow CH_2CH+CH$	56	1.26	1.35	1.78	0.88
$CHCH_2CH \rightarrow CHCH_2C+H$	57	2.58	2.59	2.93	2.43
$CHCH_2CH \rightarrow CHCHCH+H$	58	1.91	1.92	2.31	1.71
$CH_2CHCH \rightarrow CH_2+CHCH$	59	0.87	0.98	1.42	0.55
$CH_2CHCH \rightarrow CH_2CH+CH$	60	1.38	1.53	1.95	1.06
$CH_2CHCH \rightarrow CH_2CHC+H$	61	0.41	0.57	0.98	0.08
$CH_2CHCH \rightarrow CH_2CCH+H$	62	-0.29	-0.06	0.31	-0.66
$CH_2CHCH \rightarrow CHCHCH+H$	63	0.69	0.93	1.30	0.35
$CH_2CCH_2 \rightarrow CH_2C+CH_2$	64	1.49	1.38	1.84	1.10
$CH_2CCH_2 \rightarrow CH_2CCH+H$	65	0.61	0.75	1.13	0.47
$CH_3CCH \rightarrow CH_3C+CH$	66	0.37	0.38	0.78	0.07
$CH_3CCH \rightarrow CH_3+CHC$	67	0.48	0.51	0.92	0.14
$CH_3CCH \rightarrow CH_3CC+H$	68	-0.03	0.02	0.38	-0.36
$CH_3CCH \rightarrow CH_2CCH+H$	69	-0.23	-0.03	0.34	-0.57
$CH_3CC \rightarrow CH_3+CC$	70	1.12	0.92	1.31	0.67
$CH_3CC \rightarrow CH_3C+C$	71	0.72	0.44	0.83	0.27
$CH_3CC \rightarrow CH_2CC+H$	72	0.23	0.16	0.51	-0.32
$CH_2CHC \rightarrow CH_2+CHC$	73	1.44	1.36	1.78	1.04

$CH_2CHC \rightarrow CH_2CH+C$	74	1.60	1.32	1.72	1.23
$CH_2CHC \rightarrow CH_2CC+H$	75	1.29	1.21	1.60	0.84
$CH_2CHC \rightarrow CHCHC+H$	76	1.18	1.11	1.45	0.76
$CHCH_2C \rightarrow CH+CH_2C$	77	1.44	1.86	2.26	1.79
$CHCH_2C \rightarrow CH_2CH+C$	78	1.51	1.22	1.62	1.01
$CHCH_2C \rightarrow CHCHC+H$	79	1.51	1.44	1.76	1.22
$CHCH_2C \rightarrow CCH_2C+H$	80	0.63	0.63	0.93	0.09
$CHCHCH \rightarrow CH+CHCH$	81	1.32	1.23	1.57	0.66
$CHCHCH \rightarrow CHCHC+H$	82	2.03	2.00	2.36	1.75
$CHCHCH \rightarrow CHCCH+H$	83	1.14	1.13	1.47	0.61
$CH_2CCH \rightarrow CH_2+CHC$	84	1.38	1.28	1.65	0.99
$CH_2CCH \rightarrow CH_2C+CH$	85	1.35	1.19	1.60	0.91
$CH_2CCH \rightarrow CH_2CC+H$	86	1.60	1.46	1.86	1.30
$CH_2CCH \rightarrow CHCCH+H$	87	1.35	1.28	1.67	1.24
$CH_2CC \rightarrow CH_2+CC$	88	0.96	0.56	0.97	0.50
$CH_2CC \rightarrow CHC+C$	89	2.26	1.72	2.06	1.71
$CH_2CC \rightarrow CHCC+H$	90	0.83	0.61	0.94	0.35
$CHCHC\rightarrow CH+CHC$	91	2.02	1.62	2.03	1.55
$CHCHC\rightarrow CHCH+C$	92	1.87	1.30	1.70	1.59
$CHCHC\rightarrow CHCC+H$	93	1.10	0.84	1.20	0.44
$CHCHC\rightarrow CCHC+H$	94	2.26	1.86	2.19	1.84
$CCH_2C \rightarrow C+CH_2C$	95	1.92	1.33	1.72	1.56
$CCH_2C \rightarrow CCHC+H$	96	2.29	1.94	2.26	1.86
$CHCCH \rightarrow CH+CCH$	97	0.98	0.66	0.99	0.53
$CHCCH \rightarrow CHCC+H$	98	2.03	1.63	2.03	1.68
$CCHC \rightarrow CHC+C$	99	1.47	0.90	1.23	1.01
$CCHC \rightarrow CCC+H$	100	2.51	2.01	2.35	1.98
$CHCC \rightarrow CH+CC$	101	1.51	0.92	1.28	1.01
$CHCC \rightarrow CHC+C$	102	1.39	0.77	1.09	0.98
$CHCC \rightarrow CCC+H$	103	1.50	0.98	1.34	0.87
$CCC \rightarrow C+CC$	104	2.10	1.22	1.58	1.37
$CH_4 \rightarrow CH_3+H$	105	0.56	1.20	1.30	0.94
$CH_3 \rightarrow CH_2+H$	106	0.38	0.89	0.97	0.45
$CH_2\rightarrow CH+H$	107	0.42	0.68	0.73	0.48
$CH \rightarrow C+H$	108	0.49	0.47	0.51	0.59
$CH_3CH_3 \rightarrow CH_3+CH_3$	109	2.24	2.99	3.33	2.73
$CH_3CH_3 \rightarrow CH_3CH_2+H$	110	0.76	1.51	1.78	1.19
$CH_3CH_2 \rightarrow CH_3+CH_2$	111	1.42	1.98	2.29	1.69
$CH_3CH_2 \rightarrow CH_3CH+H$	112	0.52	1.12	1.38	0.66
$CH_3CH_2 \rightarrow CH_2CH_2+H$	113	0.64	1.16	1.47	0.91
$CH_3CH \rightarrow CH_3+CH$	114	1.56	1.96	2.21	1.60
$CH_3CH \rightarrow CH_3C+H$	115	0.26	0.59	0.81	0.34
$CH_3CH \rightarrow CH_2CH+H$	116	0.56	1.06	1.28	0.55

$CH_3C \rightarrow CH_3+C$	117	1.01	1.01	1.27	1.15
$CH_3C \rightarrow CH_2C+H$	118	0.44	0.58	0.78	0.40
$CH_2CH_2 \rightarrow CH_2+CH_2$	119	1.52	1.87	2.20	1.59
$CH_2CH_2 \rightarrow CH_2CH+H$	120	0.38	0.83	1.08	0.33
$CH_2CH \rightarrow CH_2+CH$	121	0.89	1.13	1.36	0.60
$CH_2CH \rightarrow CH_2C+H$	122	0.61	0.26	0.98	0.50
$CH_2CH \rightarrow CHCH+H$	123	0.09	0.78	0.60	-0.11
$CH_2C \rightarrow CH_2+C$	124	1.26	1.07	1.29	1.00
$CH_2C \rightarrow CHC+H$	125	0.10	0.11	0.29	-0.26
$CHCH \rightarrow CH+CH$	126	0.55	0.51	0.73	0.20
$CHCH \rightarrow CHC+H$	127	0.03	0.03	0.20	-0.33
$CHC \rightarrow CH+C$	128	1.75	1.48	1.69	1.25
$CHC \rightarrow CC + H$	129	0.61	0.37	0.56	0.15
$CC \rightarrow C+C$	130	1.50	0.90	1.12	0.94

Table A.10: Free energies of adsorbed species on Pt(111) at 793 K, $P_{CH3CH2CH3}$ of 1 bar, and P_{H2} of 1 bar. Referenced to gaseous propane, hydrogen, and platinum surface.

Pt(111)		Free Energy of Adsorption, $\Delta G_{ads,i}$ (eV)			
Adsorbed Species	Adsorption Number (ADS #)	PBE-D3	BEEF-vdW	RPBE	SCAN-rVV10
$CH_3CH_2CH_3$	1	0.48	1.00	1.50	0.93
CH_3CHCH_3	2	0.40	0.92	1.52	0.56
$CH_3CH_2CH_2$	3	0.53	0.96	1.44	0.64
CH_3CHCH_2	4	0.16	0.55	1.13	0.07
CH_3CH_2CH	5	0.49	0.76	1.27	0.42
$CH_2CH_2CH_2$	6	0.35	0.79	1.37	0.19
CH_3CCH_3	7	0.13	0.49	1.07	0.05
CH_3CH_2C	8	-0.38	-0.32	0.15	-0.58
CH_2CH_2CH	9	0.57	0.80	1.33	0.22
CH_2CHCH_2	10	0.27	0.51	1.09	-0.01
CH_3CHCH	11	0.21	0.39	0.92	-0.08
CH_3CCH_2	12	0.08	0.27	0.81	-0.25
CH_3CHC	13	-0.03	-0.05	0.42	-0.43
CH_2CH_2C	14	0.24	0.26	0.72	-0.20
$CHCH_2CH$	15	0.25	0.33	0.87	-0.23
CH_2CHCH	16	1.09	1.18	1.67	0.28
CH_2CCH_2	17	0.27	0.29	0.81	-0.22
CH_3CCH	18	0.03	0.01	0.48	-0.39
CH_3CC	19	0.51	0.27	0.68	0.00
CH_2CHC	20	0.50	0.35	0.84	-0.11
$CHCHCH$	21	0.23	0.30	0.62	-0.52
$CHCH_2C$	22	1.50	1.27	1.74	0.93
CH_2CCH	23	0.13	0.00	0.49	-0.58
CH_2CC	24	0.56	0.29	0.73	-0.30
$CHCHC$	25	0.68	0.24	0.68	0.04
CCH_2C	26	1.02	0.55	0.98	0.34
$CHCCH$	27	0.39	0.11	0.55	-0.45
$CCHC$	28	0.89	0.32	0.74	-0.08
$CHCC$	29	1.25	0.65	1.08	0.37
CCC	30	1.88	1.05	1.51	0.95
CH_3CH_3	31	0.27	0.73	1.07	0.68
CH_3CH_2	32	0.26	0.64	1.02	0.37
CH_3CH	33	0.30	0.52	0.88	0.19
CH_3C	34	-0.45	-0.47	-0.17	-0.66
CH_2CH_2	35	0.09	0.37	0.75	-0.03
CH_2CH	36	0.13	0.23	0.57	-0.23
CH_2C	37	-0.16	-0.23	0.06	-0.74

CHCH	38	0.07	0.00	0.30	-0.48
CHC	39	0.74	0.43	0.70	0.13
CC	40	1.36	0.90	1.15	0.59
CH_4	41	-0.15	0.19	0.35	0.21
CH_3	42	0.17	0.48	0.69	0.22
CH_2	43	0.35	0.48	0.65	0.19
CH	44	-0.29	-0.38	-0.26	-0.61
C	45	0.32	0.07	0.19	-0.08
H	46	-0.04	0.27	0.14	-0.06

Table A.11: Free energies of Transition State Species on Pt(111) at 793 K, $P_{CH3CH2CH3}$ of 1 bar, and P_{H2} of 1 bar. Referenced to gaseous propane, hydrogen, and platinum surface.

Pt(111)		Free Energy of the Transition State, $\Delta G^{\ddagger}_{ads,j}$ (eV)			
Chemical Reaction	Reaction Number	PBE-D3	BEEF-vdW	RPBE	SCAN-rVV10
$CH_3CH_2CH_3 \rightarrow CH_3CHCH_3+H$	1	1.29	2.22	2.73	1.63
$CH_3CH_2CH_3 \rightarrow CH_3CH_2CH_2+H$	2	1.23	2.05	2.42	1.51
$CH_3CHCH_3 \rightarrow CH_3CHCH_2+H$	3	1.03	1.83	2.32	1.10
$CH_3CH_2CH_2 \rightarrow CH_3CHCH_2+H$	4	1.09	1.86	2.32	1.10
$CH_3CH_2CH_3 \rightarrow CH_3+CH_2CH_3$	5	2.93	3.74	4.21	3.25
$CH_3CHCH_3 \rightarrow CH_3CH+CH_3$	6	2.24	2.95	3.52	2.43
$CH_3CHCH_3 \rightarrow CH_3CCH_3+H$	7	1.01	1.76	2.27	0.99
$CH_3CH_2CH_2 \rightarrow CH_3CH_2+CH_2$	8	2.41	3.01	3.49	2.54
$CH_3CH_2CH_2 \rightarrow CH_3+CH_2CH_2$	9	2.76	3.55	4.11	2.89
$CH_3CH_2CH_2 \rightarrow CH_2CH_2CH_2+H$	10	1.18	2.06	2.55	1.19
$CH_3CH_2CH_2 \rightarrow CH_3CH_2CH+H$	11	1.20	1.85	2.26	1.18
$CH_3CH_2CH \rightarrow CH_3CH_2+CH$	12	2.77	3.37	3.89	2.75
$CH_3CH_2CH \rightarrow CH_3+CH_2CH$	13	2.64	3.18	3.70	2.60
$CH_3CH_2CH \rightarrow CH_3CH_2C+H$	14	0.87	1.36	1.78	0.82
$CH_3CH_2CH \rightarrow CH_3CHCH+H$	15	1.02	1.62	2.07	0.86
$CH_3CH_2CH \rightarrow CH_2CH_2CH+H$	16	1.24	1.92	2.36	1.07
$CH_2CH_2CH_2 \rightarrow CH_2+CH_2CH_2$	17	1.64	2.25	2.80	1.54
$CH_2CH_2CH_2 \rightarrow CH_2CH_2CH+H$	18	1.16	1.82	2.29	0.88
$CH_2CH_2CH_2 \rightarrow CH_2CHCH_2+H$	19	0.81	1.47	1.99	0.61
$CH_3CHCH_2 \rightarrow CH_3+CHCH_2$	20	1.89	2.47	3.01	1.84
$CH_3CHCH_2 \rightarrow CH_3CH+CH_2$	21	2.05	2.58	3.12	2.03
$CH_3CHCH_2 \rightarrow CH_3CCH_2+H$	22	0.91	1.56	2.03	0.71
$CH_3CHCH_2 \rightarrow CH_3CHCH+H$	23	0.90	1.50	1.98	0.67
$CH_3CHCH_2 \rightarrow CH_2CHCH_2+H$	24	0.86	1.49	2.02	0.79

$CH_3CCH_3 \rightarrow CH_3+CH_3C$	25	1.72	2.25	2.79	1.64
$CH_3CCH_3 \rightarrow CH_3CCH_2+H$	26	1.09	1.62	2.08	1.09
$CH_3CH_2C \rightarrow CH_3+CH_2C$	27	1.87	2.14	2.63	1.52
$CH_3CH_2C \rightarrow CH_3CH_2+C$	28	1.54	1.89	2.34	1.14
$CH_3CH_2C \rightarrow CH_2CH_2C+H$	29	1.02	1.45	1.86	0.76
$CH_3CH_2C \rightarrow CH_3CHC+H$	30	1.03	1.50	1.88	0.69
$CH_2CH_2CH \rightarrow CH_2+CH_2CH$	31	2.02	2.40	2.92	1.74
$CH_2CH_2CH \rightarrow CH_2CH_2+CH$	32	1.76	2.12	2.62	1.52
$CH_2CH_2CH \rightarrow CH_2CH2C+H$	33	1.07	1.49	1.92	0.71
$CH_2CH_2CH \rightarrow CH_2CHCH+H$	34	1.23	1.73	2.19	0.84
$CH_2CH_2CH \rightarrow CHCH_2CH+H$	35	1.68	2.13	2.57	1.35
$CH_2CHCH_2 \rightarrow CH_2+CH_2CH$	36	1.95	2.33	2.86	1.76
$CH_2CHCH_2 \rightarrow CH_2CHCH+H$	37	0.87	1.36	1.83	0.41
$CH_2CHCH_2 \rightarrow CH_2CCH_2+H$	38	1.22	1.68	2.14	0.82
$CH_3CHCH \rightarrow CH_3+CHCH$	39	2.00	2.42	2.92	1.68
$CH_3CHCH \rightarrow CH_3CH+CH$	40	1.64	1.88	2.36	1.34
$CH_3CHCH \rightarrow CH_3CHC+H$	41	0.73	1.13	1.54	0.44
$CH_3CHCH \rightarrow CH_3CCH+H$	42	0.83	1.23	1.67	0.53
$CH_3CHCH \rightarrow CH_2CHCH+H$	43	1.04	1.54	1.98	0.65
$CH_3CCH_2 \rightarrow CH_3+CH_2C$	44	1.83	2.19	2.69	1.50
$CH_3CCH_2 \rightarrow CH_3C+CH_2$	45	1.60	1.89	2.38	1.34
$CH_3CCH_2 \rightarrow CH_2CCH_2+H$	46	0.95	1.17	1.60	0.33
$CH_3CCH_2 \rightarrow CH_3CCH+H$	47	0.81	1.52	1.99	0.63
$CH_3CHC \rightarrow CH_3+CHC$	48	2.35	2.56	3.02	1.93
$CH_3CHC \rightarrow CH_3CH+C$	49	1.89	1.84	2.31	1.49
$CH_3CHC \rightarrow CH_3CC+H$	50	1.13	1.26	1.64	0.73
$CH_3CHC \rightarrow CH_2CHC+H$	51	1.01	1.33	1.71	0.52
$CH_2CH_2C \rightarrow CH_2CH_2+C$	52	1.76	1.74	2.23	1.24
$CH_2CH_2C \rightarrow CH_2+CH_2C$	53	1.62	1.78	2.21	1.22
$CH_2CH_2C \rightarrow CH_2CHC+H$	54	1.71	1.99	2.37	1.22
$CH_2CH_2C \rightarrow CHCH_2C+H$	55	1.91	2.16	2.55	1.44
$CHCH_2CH \rightarrow CH_2CH+CH$	56	1.91	2.01	2.49	1.43
$CHCH_2CH \rightarrow CHCH_2C+H$	57	2.02	2.27	2.67	1.51
$CHCH_2CH \rightarrow CHCHCH+H$	58	1.44	1.80	2.17	0.81
$CH_2CHCH \rightarrow CH_2+CHCH$	59	1.81	1.92	2.43	1.45
$CH_2CHCH \rightarrow CH_2CH+CH$	60	1.90	2.05	2.53	1.55
$CH_2CHCH \rightarrow CH_2CHC+H$	61	1.52	1.73	2.17	1.01
$CH_2CHCH \rightarrow CH_2CCH+H$	62	0.98	1.28	1.71	0.38
$CH_2CHCH \rightarrow CHCHCH+H$	63	1.10	1.42	1.84	0.41
$CH_2CCH_2 \rightarrow CH_2C+CH_2$	64	2.04	2.16	2.66	1.62
$CH_2CCH_2 \rightarrow CH_2CCH+H$	65	1.84	1.98	2.41	1.58
$CH_3CCH \rightarrow CH_3C+CH$	66	1.49	1.63	2.08	0.96
$CH_3CCH \rightarrow CH_3+CHC$	67	1.89	2.01	2.46	1.44

$CH_3CCH \rightarrow CH_3CC+H$	68	1.35	1.47	1.84	0.99
$CH_3CCH \rightarrow CH_2CCH+H$	69	0.93	1.21	1.62	0.33
$CH_3CC \rightarrow CH_3+CC$	70	3.07	2.98	3.44	2.35
$CH_3CC \rightarrow CH_3C+C$	71	1.44	1.29	1.68	0.79
$CH_3CC \rightarrow CH_2CC+H$	72	1.27	1.23	1.61	0.75
$CH_2CHC \rightarrow CH_2+CHC$	73	2.23	2.17	2.64	1.69
$CH_2CHC \rightarrow CH_2CH+C$	74	1.83	1.61	2.08	1.37
$CH_2CHC \rightarrow CH_2CC+H$	75	1.65	1.73	2.14	0.85
$CH_2CHC \rightarrow CHCHC+H$	76	1.34	1.29	1.68	0.80
$CHCH_2C \rightarrow CH+CH_2C$	77	1.82	1.63	2.10	1.28
$CHCH_2C \rightarrow CH_2CH+C$	78	2.19	2.09	2.56	1.59
$CHCH_2C \rightarrow CHCHC+H$	79	2.25	2.23	2.63	1.65
$CHCH_2C \rightarrow CCH_2C+H$	80	2.17	2.03	2.42	1.57
$CHCHCH \rightarrow CH+CHCH$	81	1.26	1.21	1.65	0.65
$CHCHCH \rightarrow CHCHC+H$	82	0.79	0.96	1.31	0.04
$CHCHCH \rightarrow CHCCH+H$	83	1.89	2.02	2.41	1.14
$CH_2CCH \rightarrow CH_2+CHC$	84	2.45	2.38	2.84	1.90
$CH_2CCH \rightarrow CH_2C+CH$	85	1.55	1.52	1.94	0.82
$CH_2CCH \rightarrow CH_2CC+H$	86	1.57	1.65	2.06	0.75
$CH_2CCH \rightarrow CHCCH+H$	87	1.62	1.71	2.08	0.75
$CH_2CC \rightarrow CH_2+CC$	88	2.97	2.63	3.12	2.12
$CH_2CC \rightarrow CHC+C$	89	2.09	1.72	2.15	1.33
$CH_2CC \rightarrow CHCC+H$	90	1.99	1.83	2.24	1.26
$CHCHC \rightarrow CH+CHC$	91	1.55	1.35	1.76	0.65
$CHCHC \rightarrow CHCH+C$	92	2.70	2.28	2.73	2.07
$CHCHC \rightarrow CHCC+H$	93	2.43	2.10	2.49	1.89
$CHCHC \rightarrow CCHC+H$	94	2.17	1.95	2.36	1.51
$CCH_2C \rightarrow C+CH_2C$	95	1.69	1.34	1.78	1.01
$CCH_2C \rightarrow CCHC+H$	96	2.42	2.13	2.47	1.77
$CHCCH \rightarrow CH+CCH$	97	2.01	1.78	2.18	1.24
$CHCCH \rightarrow CHCC+H$	98	1.77	1.56	1.95	0.97
$CCHC \rightarrow CHC+C$	99	2.16	1.66	2.08	1.34
$CCHC \rightarrow CCC+H$	100	2.92	2.50	2.87	2.02
$CHCC \rightarrow CH+CC$	101	2.69	2.14	2.52	1.72
$CHCC \rightarrow CHC+C$	102	2.61	2.10	2.50	1.79
$CHCC \rightarrow CCC+H$	103	2.85	2.40	2.75	2.08
$CCC \rightarrow C+CC$	104	3.22	2.44	2.85	2.21
$CH_4 \rightarrow CH_3+H$	105	0.88	1.64	1.75	0.86
$CH_3 \rightarrow CH_2+H$	106	0.95	1.50	1.60	0.73
$CH_2 \rightarrow CH+H$	107	0.49	0.88	0.93	0.20
$CH \rightarrow C+H$	108	0.91	1.14	1.17	0.52
$CH_3CH_3 \rightarrow CH_3+CH_3$	109	3.15	4.16	4.45	1.10
$CH_3CH_3 \rightarrow CH_3CH_2+H$	110	1.07	1.94	2.23	0.85

$CH_3CH_2 \rightarrow CH_3+CH_2$	111	1.96	2.57	2.92	0.20
$CH_3CH_2 \rightarrow CH_3CH+H$	112	1.04	1.70	1.99	0.40
$CH_3CH_2 \rightarrow CH_2CH_2+H$	113	1.09	1.71	2.01	3.50
$CH_3CH \rightarrow CH_3+CH$	114	1.66	2.07	2.38	1.35
$CH_3CH \rightarrow CH_3C+H$	115	0.69	1.07	1.32	2.08
$CH_3CH \rightarrow CH_2CH+H$	116	0.92	1.43	1.68	1.00
$CH_3C \rightarrow CH_3+C$	117	1.58	1.77	2.05	1.25
$CH_3C \rightarrow CH_2C+H$	118	0.82	1.12	1.35	1.62
$CH_2CH_2 \rightarrow CH_2+CH_2$	119	2.06	2.50	2.83	0.58
$CH_2CH_2 \rightarrow CH_2CH+H$	120	0.89	1.43	1.70	0.69
$CH_2CH \rightarrow CH_2+CH$	121	1.80	2.07	2.36	1.29
$CH_2CH \rightarrow CH_2C+H$	122	0.58	0.94	1.17	0.43
$CH_2CH \rightarrow CHCH+H$	123	0.86	1.23	1.46	2.00
$CH_2C \rightarrow CH_2+C$	124	1.89	1.86	2.12	0.62
$CH_2C \rightarrow CHC+H$	125	1.13	1.25	1.48	1.35
$CHCH \rightarrow CH+CH$	126	1.51	1.58	1.81	0.07
$CHCH \rightarrow CHC+H$	127	1.35	1.45	1.68	0.42
$CHC \rightarrow CH+C$	128	1.89	1.67	1.89	1.35
$CHC \rightarrow CC + H$	129	2.29	1.31	2.31	0.56
$CC \rightarrow C+C$	130	2.65	2.15	2.39	0.82

Table A.12: Free energies of adsorbed species on Pt(211) at 793 K, $P_{CH3CH2CH3}$ of 1 bar, and P_{H2} of 1 bar. Referenced to gaseous propane, hydrogen, and platinum surface.

Pt(211)		Free Energy of Adsorption, $\Delta G_{ads,i}$ (eV)			
Adsorbed Species	Adsorption Number (ADS #)	PBE-D3	BEEF-vdW	RPBE	SCAN-rVV10
$CH_3CH_2CH_3$	1	0.43	1.23	1.83	0.89
CH_3CHCH_3	2	0.35	1.06	1.71	0.44
$CH_3CH_2CH_2$	3	0.50	1.08	1.56	0.50
CH_3CHCH_2	4	0.04	0.54	1.04	0.07
CH_3CH_2CH	5	0.29	0.63	1.03	0.28
$CH_2CH_2CH_2$	6	0.33	0.85	1.28	0.25
CH_3CCH_3	7	-0.13	0.48	0.98	-0.21
CH_3CH_2C	8	-0.28	0.00	0.48	-0.52
CH_2CH_2CH	9	0.39	0.73	1.14	0.18
CH_2CHCH_2	10	-0.33	0.03	0.47	-0.59
CH_3CHCH	11	0.18	0.57	1.10	-0.16
CH_3CCH_2	12	0.01	0.40	0.92	-0.35
CH_3CHC	13	-0.09	0.02	0.48	-0.40
CH_2CH_2C	14	0.07	0.25	0.69	-0.34
$CHCH_2CH$	15	-0.36	-0.14	0.31	-0.87
CH_2CHCH	16	0.26	0.42	0.87	-0.26
CH_2CCH_2	17	-0.15	0.03	0.47	-0.66
CH_3CCH	18	-0.39	-0.05	0.52	-0.77
CH_3CC	19	-0.62	-0.71	-0.25	-1.02
CH_2CHC	20	-0.25	-0.21	0.27	-0.73
$CHCHCH$	21	-0.48	-0.38	0.08	-1.08
$CHCH_2C$	22	-0.21	-0.04	0.51	-0.76
CH_2CCH	23	-0.18	-0.10	0.44	-0.66
CH_2CC	24	-0.40	-0.67	-0.23	-0.94
$CHCHC$	25	-0.71	-0.87	-0.42	-1.37
CCH_2C	26	0.98	0.72	1.06	0.40
$CHCCH$	27	0.60	0.50	0.96	0.00
$CCHC$	28	0.88	0.51	0.89	0.01
$CHCC$	29	0.17	-0.26	0.15	-0.43
CCC	30	0.82	0.23	0.72	0.02
CH_3CH_3	31	0.33	0.99	1.25	0.56
CH_3CH_2	32	0.18	0.67	0.97	0.25
CH_3CH	33	-0.15	0.17	0.47	-0.17
CH_3C	34	-0.47	-0.35	-0.11	-0.67
CH_2CH_2	35	-0.22	0.17	0.42	-0.30
CH_2CH	36	0.13	0.39	0.69	-0.27
CH_2C	37	-0.09	-0.10	0.19	-0.52

CHCH	38	-0.22	-0.02	0.32	-0.59
CHC	39	-0.53	-0.69	-0.41	-0.94
CC	40	0.10	-0.28	0.01	-0.39
CH_4	41	0.00	0.48	0.59	0.21
CH_3	42	-0.07	0.35	0.47	-0.05
CH_2	43	-0.09	0.16	0.27	-0.17
CH	44	-0.20	-0.04	0.06	-0.53
C	45	0.31	0.18	0.34	-0.10
H	46	-0.17	0.25	0.17	-0.10

Table A.13: Free energies of transition state species on Pt(211) at 793 K, $P_{CH3CH2CH3}$ of 1 bar, and P_{H2} of 1 bar. Referenced to gaseous propane, hydrogen, and platinum surface.

Pt(211)		Free Energy of the Transition State, $\Delta G^{\ddagger}_{ads,j}$ (eV)			
Chemical Reaction	Reaction Number	PBE-D3	BEEF-vdW	RPBE	SCAN-rVV10
$CH_3CH_2CH_3 \rightarrow CH_3CHCH_3+H$	1	1.02	2.08	2.45	1.19
$CH_3CH_2CH_3 \rightarrow CH_3CH_2CH_2 +H$	2	1.19	2.10	2.34	1.41
$CH_3CHCH_3 \rightarrow CH_3CHCH_2+H$	3	0.66	1.58	1.92	0.70
$CH_3CH_2CH_2 \rightarrow CH_3CHCH_2+H$	4	0.71	1.55	1.85	0.75
$CH_3CH_2CH_3 \rightarrow CH_3+CH_2CH_3$	5	2.93	4.06	4.63	3.39
$CH_3CHCH_3 \rightarrow CH_3CH+CH_3$	6	2.16	3.07	3.66	2.27
$CH_3CHCH_3 \rightarrow CH_3CCH_3+H$	7	1.06	1.99	2.50	1.02
$CH_3CH_2CH_2 \rightarrow CH_3CH_2+CH_2$	8	2.21	3.00	3.50	2.31
$CH_3CH_2CH_2 \rightarrow CH_3+CH_2CH_2$	9	2.32	3.18	3.83	2.39
$CH_3CH_2CH_2 \rightarrow CH_2CH_2CH_2+H$	10	0.93	1.94	2.36	1.31
$CH_3CH_2CH_2 \rightarrow CH_3CH_2CH +H$	11	1.24	2.12	2.52	0.70
$CH_3CH_2CH \rightarrow CH_3CH_2+CH$	12	1.59	2.59	3.01	1.88
$CH_3CH_2CH \rightarrow CH_3+CH_2CH$	13	1.89	2.15	2.49	1.54
$CH_3CH_2CH \rightarrow CH_3CH_2C +H$	14	0.72	1.24	1.55	0.64
$CH_3CH_2CH \rightarrow CH_3CHCH+H$	15	0.82	1.56	1.95	0.69
$CH_3CH_2CH \rightarrow CH_2CH_2CH+H$	16	0.81	1.64	2.03	0.73
$CH_2CH_2CH_2 \rightarrow CH_2+CH_2CH_2$	17	1.41	2.08	2.48	1.43
$CH_2CH_2CH_2 \rightarrow CH_2CH_2CH+H$	18	1.40	2.14	2.47	1.37
$CH_2CH_2CH_2 \rightarrow CH_2CHCH_2+H$	19	0.66	1.52	2.02	0.35
$CH_3CHCH_2 \rightarrow CH_3+CHCH_2$	20	1.68	2.44	2.96	1.57
$CH_3CHCH_2 \rightarrow CH_3CH+CH_2$	21	1.75	2.58	3.11	1.60
$CH_3CHCH_2 \rightarrow CH_3CCH_2+H$	22	0.81	1.65	2.11	0.52
$CH_3CHCH_2 \rightarrow CH_3CHCH+H$	23	0.80	1.63	2.09	0.51
$CH_3CHCH_2 \rightarrow CH_2CHCH_2+H$	24	0.90	1.75	2.17	0.77
$CH_3CCH_3 \rightarrow CH_3+CH_3C$	25	1.42	2.08	2.57	1.30
$CH_3CCH_3 \rightarrow CH_3CCH_2+H$	26	1.54	2.23	2.52	1.49
$CH_3CH_2C \rightarrow CH_3+CH_2C$	27	1.37	1.77	2.79	1.68
$CH_3CH_2C \rightarrow CH_3CH_2+C$	28	1.60	2.02	2.51	1.32
$CH_3CH_2C \rightarrow CH_2CH_2C+H$	29	0.69	1.24	1.63	0.29
$CH_3CH_2C \rightarrow CH_3CHC+H$	30	1.66	2.34	2.76	1.43
$CH_2CH_2CH \rightarrow CH_2+CH_2CH$	31	1.28	1.74	2.13	1.14
$CH_2CH_2CH \rightarrow CH_2CH_2+CH$	32	1.51	2.03	2.43	1.18
$CH_2CH_2CH \rightarrow CH_2CH2C+H$	33	1.22	1.84	2.11	1.02
$CH_2CH_2CH \rightarrow CH_2CHCH+H$	34	1.44	2.04	2.39	1.17
$CH_2CH_2CH \rightarrow CHCH_2CH+H$	35	1.40	2.02	2.36	1.06
$CH_2CHCH_2 \rightarrow CH_2+CH_2CH$	36	1.49	2.00	2.40	1.19
$CH_2CHCH_2 \rightarrow CH_2CHCH+H$	37	0.62	1.24	1.60	0.30

$CH_2CHCH_2 \rightarrow CH_2CCH_2+H$	38	0.55	1.20	1.69	0.13
$CH_3CHCH \rightarrow CH_3+CHCH$	39	1.75	2.28	2.78	1.51
$CH_3CHCH \rightarrow CH_3CH+CH$	40	1.60	2.08	2.57	1.38
$CH_3CHCH \rightarrow CH_3CHC+H$	41	0.59	1.24	1.69	0.22
$CH_3CHCH \rightarrow CH_3CCH+H$	42	0.79	1.43	1.89	0.49
$CH_3CHCH \rightarrow CH_2CHCH+H$	43	1.14	1.81	2.23	0.82
$CH_3CCH_2 \rightarrow CH_3+CH_2C$	44	1.46	2.02	2.52	1.15
$CH_3CCH_2 \rightarrow CH_3C+CH_2$	45	1.42	1.85	2.34	1.07
$CH_3CCH_2 \rightarrow CH_2CCH_2+H$	46	0.55	1.14	1.57	0.22
$CH_3CCH_2 \rightarrow CH_3CCH+H$	47	1.01	1.64	2.02	0.70
$CH_3CHC \rightarrow CH_3+CHC$	48	2.09	2.47	2.93	1.75
$CH_3CHC \rightarrow CH_3CH+C$	49	1.68	1.82	2.25	1.32
$CH_3CHC \rightarrow CH_3CC+H$	50	0.96	1.25	1.63	0.63
$CH_3CHC \rightarrow CH_2CHC+H$	51	1.12	1.51	1.96	1.01
$CH_2CH_2C \rightarrow CH_2CH_2+C$	52	1.66	1.84	2.49	1.49
$CH_2CH_2C \rightarrow CH_2+CH_2C$	53	1.70	1.98	2.47	1.46
$CH_2CH_2C \rightarrow CH_2CHC+H$	54	1.32	1.78	2.12	0.80
$CH_2CH_2C \rightarrow CHCH_2C+H$	55	1.83	2.34	2.71	1.56
$CHCH_2CH \rightarrow CH_2CH+CH$	56	1.79	2.22	2.67	1.39
$CHCH_2CH \rightarrow CHCH_2C+H$	57	1.12	1.56	1.90	0.55
$CHCH_2CH \rightarrow CHCHCH+H$	58	1.34	1.74	2.11	0.86
$CH_2CHCH \rightarrow CH_2+CHCH$	59	1.57	1.83	2.23	1.20
$CH_2CHCH \rightarrow CH_2CH+CH$	60	1.68	2.03	2.45	1.22
$CH_2CHCH \rightarrow CH_2CHC+H$	61	1.24	1.83	2.30	0.63
$CH_2CHCH \rightarrow CH_2CCH+H$	62	0.88	1.31	1.67	0.39
$CH_2CHCH \rightarrow CHCHCH+H$	63	0.43	0.91	1.25	-0.23
$CH_2CCH_2 \rightarrow CH_2C+CH_2$	64	1.76	2.04	2.45	1.33
$CH_2CCH_2 \rightarrow CH_2CCH+H$	65	0.68	1.15	1.46	0.23
$CH_3CCH \rightarrow CH_3C+CH$	66	1.30	1.56	1.92	0.87
$CH_3CCH \rightarrow CH_3+CHC$	67	1.29	1.58	2.05	0.85
$CH_3CCH \rightarrow CH_3CC+H$	68	0.61	0.98	1.45	0.22
$CH_3CCH \rightarrow CH_2CCH+H$	69	0.35	0.84	1.29	-0.11
$CH_3CC \rightarrow CH_3+CC$	70	1.20	1.25	1.66	0.78
$CH_3CC \rightarrow CH_3C+C$	71	1.47	1.41	1.78	0.98
$CH_3CC \rightarrow CH_2CC+H$	72	0.17	0.31	0.67	-0.31
$CH_2CHC \rightarrow CH_2+CHC$	73	2.30	2.42	2.85	1.93
$CH_2CHC \rightarrow CH_2CH+C$	74	1.72	1.83	2.30	1.21
$CH_2CHC \rightarrow CH_2CC+H$	75	0.22	0.39	0.76	-0.19
$CH_2CHC \rightarrow CHCHC+H$	76	-0.15	0.14	0.50	-0.67
$CHCH_2C \rightarrow CH+CH_2C$	77	1.65	1.83	2.33	1.06
$CHCH_2C \rightarrow CH_2CH+C$	78	1.96	2.10	2.51	1.45
$CHCH_2C \rightarrow CHCHC+H$	79	0.83	1.13	1.42	0.04
$CHCH_2C \rightarrow CCH_2C+H$	80	0.55	0.91	1.28	-0.12

CHCHCH → CH+CHCH	81	1.58	1.74	2.11	1.05
CHCHCH → CHCHC+H	82	0.93	1.21	1.54	0.24
CHCHCH → CHCCH+H	83	0.99	1.26	1.57	0.25
$CH_2CCH \rightarrow CH_2+CHC$	84	2.12	2.25	2.65	1.48
$CH_2CCH \rightarrow CH_2C+CH$	85	1.47	1.40	1.81	1.11
$CH_2CCH \rightarrow CH_2CC+H$	86	0.91	1.06	1.51	0.33
$CH_2CCH \rightarrow CHCCH+H$	87	1.07	1.24	1.59	0.48
$CH_2CC \rightarrow CH_2+CC$	88	1.96	1.78	2.18	1.40
$CH_2CC \rightarrow CHC+C$	89	1.28	1.16	1.54	0.68
$CH_2CC \rightarrow CHCC+H$	90	1.50	1.70	2.03	0.85
CHCHC→ CH+CHC	91	1.01	1.00	1.41	0.18
CHCHC→ CHCH+C	92	1.42	1.28	1.71	0.76
CHCHC→ CHCC+H	93	2.04	1.98	2.31	1.42
CHCHC→ CCHC+H	94	0.73	0.84	1.47	0.01
$CCH_2C \rightarrow C+CH_2C$	95	1.51	1.33	1.29	0.95
$CCH_2C \rightarrow CCHC+H$	96	1.76	1.73	2.04	1.18
CHCCH → CH+CCH	97	1.80	1.68	2.07	1.86
CHCCH → CHCC+H	98	1.95	2.05	2.43	1.42
CCHC → CHC+C	99	1.86	1.48	1.96	1.10
CCHC → CCC+H	100	1.64	1.50	1.92	0.91
CHCC → CH+CC	101	1.46	1.15	1.48	0.78
CHCC → CHC+C	102	2.62	2.37	2.80	1.72
CHCC → CCC+H	103	1.42	1.24	1.64	0.71
CCC → C+CC	104	2.74	2.07	2.52	1.80
$CH_4 \rightarrow CH_3+H$	105	0.54	1.41	1.44	0.73
$CH_3 \rightarrow CH_2+H$	106	0.35	1.06	1.08	0.31
$CH_2 \rightarrow CH+H$	107	0.45	0.98	0.97	0.25
CH → C+H	108	0.84	1.07	1.16	0.53
$CH_3CH_3 \rightarrow CH_3+CH_3$	109	1.87	2.79	3.11	2.21
$CH_3CH_3 \rightarrow CH_3CH_2+H$	110	0.94	1.86	2.05	1.18
$CH_3CH_2 \rightarrow CH_3+CH_2$	111	1.36	2.09	2.32	1.45
$CH_3CH_2 \rightarrow CH_3CH+H$	112	1.00	1.83	2.13	0.88
$CH_3CH_2 \rightarrow CH_2CH_2+H$	113	0.51	1.32	1.49	0.58
$CH_3CH \rightarrow CH_3+CH$	114	1.25	1.82	2.02	1.18
$CH_3CH \rightarrow CH_3C+H$	115	0.54	1.02	1.19	0.44
$CH_3CH \rightarrow CH_2CH+H$	116	0.67	1.32	1.54	0.42
$CH_3C \rightarrow CH_3+C$	117	1.37	1.70	1.97	1.20
$CH_3C \rightarrow CH_2C+H$	118	0.71	1.14	1.34	0.40
$CH_2CH_2 \rightarrow CH_2+CH_2$	119	1.39	1.92	2.14	1.32
$CH_2CH_2 \rightarrow CH_2CH+H$	120	0.38	0.97	1.16	0.17
$CH_2CH \rightarrow CH_2+CH$	121	1.27	1.67	1.88	0.92
$CH_2CH \rightarrow CH_2C+H$	122	0.60	1.06	1.28	0.18
$CH_2CH \rightarrow CHCH+H$	123	0.70	1.16	1.40	0.32

$CH_2C \rightarrow CH_2+C$	124	1.58	1.72	1.93	1.08
$CH_2C \rightarrow CHC+H$	125	1.18	1.45	1.65	0.72
CHCH → CH+CH	126	1.48	1.79	1.36	0.40
CHCH → CHC+H	127	0.86	1.10	1.35	0.42
CHC → CH+C	128	1.06	1.01	1.26	0.55
CHC → CC + H	129	0.62	0.62	0.84	0.23
CC → C+C	130	1.75	1.45	1.64	0.98

Table A.14: Free energies of gas species at 793 K, $P_{CH3CH2CH3}$ of 1 bar, and P_{H2} of 1 bar. Referenced to gaseous propane and hydrogen.

	Free Energy (eV) of Product Gas Species.			
Gas Species	PBE-D3	BEEF-vdw	RPBE	SCAN-rVV10
Propylene	0.28	0.04	0.12	0.36
Propyne	1.16	0.84	0.81	1.32
Ethane	-0.02	0.01	-0.06	-0.01
Ethylene	0.34	0.17	0.14	0.41
Acetylene	1.57	1.22	1.22	1.72
Methane	-0.56	-0.51	-0.60	-0.56

Table A.15: Activation barriers of selected reactions at 793K on Pt(100), $P_{CH3CH2CH3}$ of 1 bar, and P_{H2} of 1 bar. Referenced to the reactant of each reaction.

Activation barriers (eV) for selected surface reactions				
	Pt(100)			
Chemical Reaction on Surface	PBE-D3	BEEF-vdw	RPBE	SCAN-rVV10
$CH_3CH_2CH_3 \rightarrow CH_3CHCH_3+H$	0.43	0.78	0.58	0.15
$CH_3CH_2CH_3 \rightarrow CH_3CH_2CH_2 +H$	0.49	0.89	0.58	0.30
$CH_3CHCH_3 \rightarrow CH_3CHCH_2+H$	0.36	0.70	0.48	0.47
$CH_3CH_2CH_2 \rightarrow CH_3CHCH_2+H$	0.30	0.66	0.51	0.33
$CH_3CH_2CH_3 \rightarrow CH_3+CH_2CH_3$	2.22	2.82	2.57	2.06
$CH_3CHCH_3 \rightarrow CH_3CH+CH_3$	1.31	1.57	1.44	1.33
$CH_3CHCH_3 \rightarrow CH_3CCH_3+H$	0.31	0.58	0.38	0.12
$CH_3CH_2CH_2 \rightarrow CH_3CH_2+CH_2$	1.21	1.55	1.45	1.23
$CH_3CH_2CH_2 \rightarrow CH_3+CH_2CH_2$	2.26	2.81	2.66	2.19
$CH_3CH_2CH_2 \rightarrow CH_2CH_2CH_2+H$	0.42	0.93	0.82	0.36
$CH_3CH_2CH_2 \rightarrow CH_3CH_2CH +H$	0.27	0.64	0.46	0.15
$CH_3CHCH_2 \rightarrow CH_3+CHCH_2$	1.18	1.37	1.33	1.13
$CH_3CHCH_2 \rightarrow CH_3CH+CH_2$	1.17	1.46	1.39	1.14
$CH_3CHCH_2 \rightarrow CH_3CCH_2+H$	0.41	0.67	0.58	0.25
$CH_3CHCH_2 \rightarrow CH_3CHCH+H$	0.35	0.58	0.46	0.23
$CH_3CHCH_2 \rightarrow CH_2CHCH_2+H$	0.42	0.70	0.62	0.38

Table A.16. Activation barriers of selected reactions at 793K on Pt(111) , $P_{CH3CH2CH3}$ of 1 bar, and P_{H2} of 1 bar. Referenced to the reactant of each reaction.

Activation barriers (eV) for selected surface reactions				
	Pt(111)			
Chemical Reaction on Surface	PBE-D3	BEEF-vdw	RPBE	SCAN-rVV10
$CH_3CH_2CH_3 \rightarrow CH_3CHCH_3+H$	0.75	1.66	2.13	1.03
$CH_3CH_2CH_3 \rightarrow CH_3CH_2CH_2 +H$	0.73	1.52	1.86	0.94
$CH_3CHCH_3 \rightarrow CH_3CHCH_2+H$	0.61	1.52	1.98	0.75
$CH_3CH_2CH_2 \rightarrow CH_3CHCH_2+H$	0.53	1.41	1.83	0.62
$CH_3CH_2CH_3 \rightarrow CH_3+CH_2CH_3$	2.45	3.24	3.67	2.71
$CH_3CHCH_3 \rightarrow CH_3CH+CH_3$	1.82	2.63	3.17	2.08
$CH_3CHCH_3 \rightarrow CH_3CCH_3+H$	0.61	1.47	1.95	0.68
$CH_3CH_2CH_2 \rightarrow CH_3CH_2+CH_2$	1.85	2.55	3.00	2.05
$CH_3CH_2CH_2 \rightarrow CH_3+CH_2CH_2$	2.17	3.08	3.60	2.38
$CH_3CH_2CH_2 \rightarrow CH_2CH_2CH_2+H$	0.59	1.58	2.03	0.67
$CH_3CH_2CH_2 \rightarrow CH_3CH_2CH +H$	0.64	1.41	1.78	0.70
$CH_3CHCH_2 \rightarrow CH_3+CHCH_2$	1.71	2.54	3.05	1.87
$CH_3CHCH_2 \rightarrow CH_3CH+CH_2$	1.90	2.68	3.18	2.10
$CH_3CHCH_2 \rightarrow CH_3CCH_2+H$	0.73	1.62	2.06	0.74
$CH_3CHCH_2 \rightarrow CH_3CHCH+H$	0.72	1.56	2.02	0.71
$CH_3CHCH_2 \rightarrow CH_2CHCH_2+H$	0.71	1.57	2.07	0.84

Table A.17: Activation barriers of selected reactions at 793K on Pt(211) , $P_{CH3CH2CH3}$ of 1 bar, and P_{H2} of 1 bar. Referenced to the reactant of each reaction.

Activation barriers (eV) for selected surface reactions				
	Pt(211)			
Chemical Reaction on Surface	PBE-D3	BEEF-vdw	RPBE	SCAN-rVV10
$CH_3CH_2CH_3 \rightarrow CH_3CHCH_3+H$	0.57	0.82	0.59	0.27
$CH_3CH_2CH_3 \rightarrow CH_3CH_2CH_2 +H$	0.72	0.82	0.47	0.47
$CH_3CHCH_3 \rightarrow CH_3CHCH_2+H$	0.31	0.51	0.21	0.26
$CH_3CH_2CH_2 \rightarrow CH_3CHCH_2+H$	0.20	0.45	0.28	0.23
$CH_3CH_2CH_3 \rightarrow CH_3+CH_2CH_3$	2.45	2.77	2.74	2.45
$CH_3CHCH_3 \rightarrow CH_3CH+CH_3$	1.81	2.00	1.95	1.82
$CH_3CHCH_3 \rightarrow CH_3CCH_3+H$	0.71	0.92	0.78	0.57
$CH_3CH_2CH_2 \rightarrow CH_3CH_2+CH_2$	1.69	1.89	1.91	1.79
$CH_3CH_2CH_2 \rightarrow CH_3+CH_2CH_2$	1.78	2.05	2.23	1.85
$CH_3CH_2CH_2 \rightarrow CH_2CH_2CH_2+H$	0.37	0.79	0.74	0.75
$CH_3CH_2CH_2 \rightarrow CH_3CH_2CH +H$	0.73	1.02	0.95	0.18
$CH_3CHCH_2 \rightarrow CH_3+CHCH_2$	1.82	2.07	2.10	1.68
$CH_3CHCH_2 \rightarrow CH_3CH+CH_2$	1.85	2.18	2.21	1.67
$CH_3CHCH_2 \rightarrow CH_3CCH_2+H$	0.90	1.24	1.20	0.58
$CH_3CHCH_2 \rightarrow CH_3CHCH+H$	0.90	1.22	1.19	0.58
$CH_3CHCH_2 \rightarrow CH_2CHCH_2+H$	1.00	1.35	1.27	0.84

A.2.2 Prior Construction for Model Variances

As the results of model evidence and Mahalanobis distances are dependent on the prior distribution, care was taken when choosing hyperparameters so not to bias the prior and resulting posterior distributions towards any of the six models studied in this paper. When developing the variances, we chose inverse gamma distributions to sample the variances in the model. Inverse gamma functions are the conjugate prior to Gaussian distributions, and only sample positive real numbers for the variances. These inverse gamma hyperparameters, for the shape, α, and scale, β, were informed by the prior experiments conducted by Walker[2], while keeping them non-informative with respect to the current experimental datasets and simulation settings. These hyperparameters for these distributions can be read in Appendix A A.18. In addition, in Figure A.1, an inverse gamma distribution with shape and scale of 3 and 1 is graphically depicted.

Table A.18: Model variances through hyperparameters for shape and scale of the inverse gamma prior distributions.

Hyperparameters	Log10 (TOF)	Logit (Selectivity)	Propane Reaction Order	Hydrogen Reaction Order	Apparent Activation Energy
A	3	3	3	3	3
B	1	1	0.5	0.5	0.5

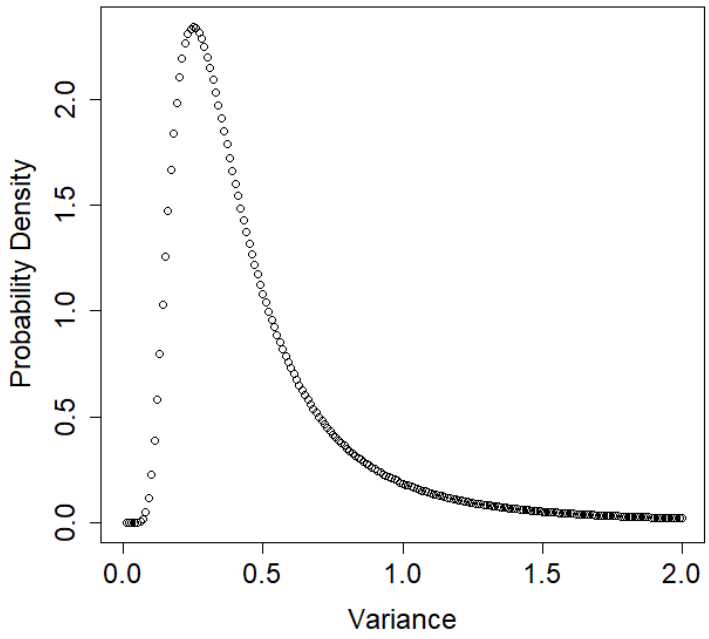

Figure A.1: An inverse gamma distribution with shape of 3 and scale of 1

A.2.3 χ^2 Goodness-of-Fit and Jeffery's Scale for Bayes Factor

χ^2, or chi-squared, is a measure of the goodness-of-fit for how well the data matches a particular reported value.[9-11] For multinormal data, that this study generates, the squared Mahalanobis distance is used to evaluate the goodness of fit. In this study, a model is rejected if it fails to be less than a χ^2 value at a significance level of 0.05, as referred to as $\chi^2_{0.05}$. Table A.19 lists the χ^2 values as given by Brerenton.[11]

Table A.19: $\chi^2_{0.05}$table for evaluating Squared Mahalanobis Distance.[9-11]

Degrees of Freedom (DOF)	Corresponding Experiment to DOF	$\chi_{0.05}^2$
1		3.84
2	D3	5.99
3		7.82
4	D1	9.49
5	D2	11.07

The Bayes factor is a comparative model evaluation statistic comparing evidence between two models, in this case, Model 1 (M_1), and Model 2, (M_2).[12] In this study, the models may either be the surfaces, or the functional methodologies used. Values can be found in Table A.20.

Table A.20. Jeffery's Scale for Bayes Factors, $B_{12} = p(D|M_1)/p(D|M_2)$ [12]

B_{12}	Evidence for M_1
1 - 3.2	Not worth more than a bare mention
3.2 – 10	Positive
10 – 100	Strong
> 100	Very strong

A.2.4 Confidence Intervals around the Relative Free Energy for Pt(100), Pt(111), and Pt(211)

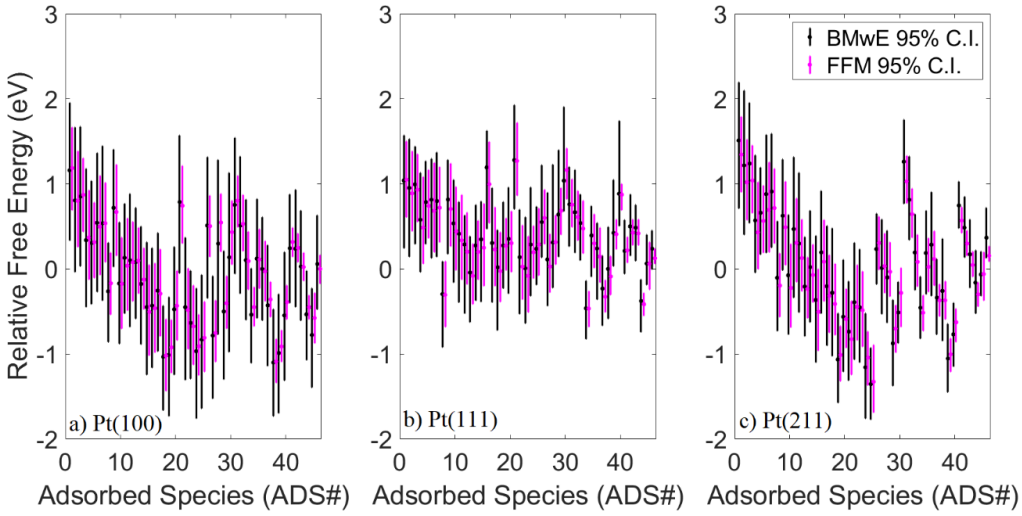

Figure A.2: 95% Confidence intervals around each adsorbed species on a) Pt(100), b) Pt(111), and c) Pt(211) using the Four Functional Model (FFM) and the BEEF-vdW Model with Ensembles (BMwE). Adsorbed species numbers can be found in Table A.2.

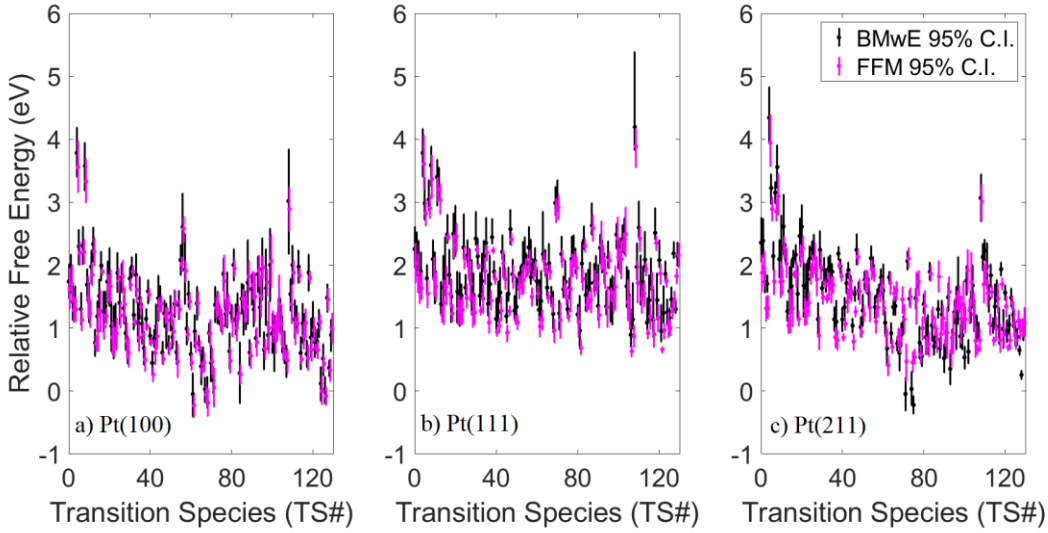

Figure A.3: 95% Confidence intervals around each transition state species on a) Pt(100), b) Pt(111), and c) Pt(211) using the Four Functional Model (FFM) and the BEEF-vdW Model with Ensembles (BMwE). Transition state species numbers can be found in Table A.3.

A.2.5 Likelihood Functions for Experimental Conditions D2 and D3

In addition to the full likelihood function for experiment D1[13] explained in the main paper, likelihood functions for D2[14] and D3[15] can also be derived. For D2, the selectivity to propylene was one of the quantities of interested data. When evaluating model errors to the selectivity to propylene, a logit function was chosen to transform this function, as selectivity, by definition, must be within the bounds of [0,1]. This transformation changes the range of the function to (-∞, ∞) to include and analyze the errors properly. The logit function for selectivity is defined in the following.[16]

$$logit(Selectivity) = \ln\left(\frac{Selectivity}{1 - Selectivity}\right) \qquad (A.1)$$

The expanded likelihood function for D2 then becomes equation A.2.

$$\begin{aligned} p(D_2|\theta, M) = {} & \frac{1}{\sqrt{2\pi\sigma_{TOF}^2}}\exp\left(-\frac{1}{2}\frac{(log_{10}TOF - log_{10}TOF^*)^2}{\sigma_{TOF}^2}\right) \\ & * \frac{1}{\sqrt{2\pi\sigma_{\alpha_{propane}}^2}}\exp\left(-\frac{1}{2}\frac{\left(\alpha_{propane} - \alpha_{propane}{}^*\right)^2}{\sigma_{\alpha_{propane}}^2}\right) \\ & * \frac{1}{\sqrt{2\pi\sigma_{\alpha_{H_2}}^2}}\exp\left(-\frac{1}{2}\frac{\left(\alpha_{H_2} - \alpha_{H_2}{}^*\right)^2}{\sigma_{\alpha_{H_2}}^2}\right) \\ & * \frac{1}{\sqrt{2\pi\sigma_{E_{apparent}}^2}}\exp\left(-\frac{1}{2}\frac{\left(E_{apparent} - E_{apparent}{}^*\right)^2}{\sigma_{E_{apparent}}^2}\right) \\ & * \frac{1}{\sqrt{2\pi\sigma_{logit(Selectivity)}^2}}\exp\left(-\frac{1}{2}\frac{(logit(Selectivity) - logit(Selectivity)^*)^2}{\sigma_{logit(Selectivity)}^2}\right) \end{aligned} \qquad (A.2)$$

For D3, as there exist only two reported quantities of interest, this is condensed to equation A.3.

$$p(D_3|\theta, M) = \frac{1}{\sqrt{2\pi\sigma_{TOF}^2}} \exp\left(-\frac{1}{2}\frac{(log_{10}TOF - log_{10}TOF^*)^2}{\sigma_{TOF}^2}\right)$$

$$* \frac{1}{\sqrt{2\pi\sigma_{logit(Selectivity)}^2}} \exp\left(-\frac{1}{2}\frac{(logit(Selectivity) - logit(Selectivity)^*)^2}{\sigma_{logit(Selectivity)}^2}\right) \quad (A.3)$$

A.3 Experimental Data

Table A.21. Experimental conditionals and reported results for the experiments D1,[13] D2,[14] and D3,[15] as replicated in this study. Data in black was not reported by the specific experiment.

Reported Experimental Information	D1	D2	D3
Temperature (K)	633	793	792
$P_{Propane}$ (bar)	0.04	0.03	0.29
P_{H2} (bar)	2.00	0.03	0.09
TOF (1/s)	0.035	0.45	0.2
Selectivity to Propylene		90%	85%
Propane reaction order	1	1	
Hydrogen reaction order	-1.1	-0.51	
Apparent activation energy (eV)	1.25	0.98	

A.4 Additional Information for Microkinetic Modeling

A.4.1 Site Occupation by Surface

We studied the same reaction pathways on each of the surfaces. However, the geometry and number of occupied sites for the lowest energy adsorbed species depends on the surface, as the surface facets are different from each other. This study defines that one Pt atom is one site. We used this methodology for all carbon containing species. For atomic hydrogen, we assumed that one H atom covers 1 site, regardless of the most stable adsorption site, due to its small size and weak self-interactions on each of the surfaces. This information can be read in Table A.22.

Table A.22: Number of sites occupied by each adsorbed species on Pt(100), Pt(111), Pt(211)

	Number of Sites Occupied		
Adsorbed Species	Pt(100)	Pt(111)	Pt(211)
$CH_3CH_2CH_3$	1	1	1
CH_3CHCH_3	1	1	1
$CH_3CH_2CH_2$	1	1	1
CH_3CHCH_2	2	2	2
CH_3CH_2CH	2	2	2
$CH_2CH_2CH_2$	2	2	2
CH_3CCH_3	2	2	2
CH_3CH_2C	4	3	3
CH_2CH_2CH	3	3	2
CH_2CHCH_2	2	3	2
CH_3CHCH	3	3	3
CH_3CCH_2	3	3	3
CH_3CHC	3	3	3
CH_2CH_2C	4	3	3
$CHCH_2CH$	4	3	4
CH_2CHCH	3	3	3
CH_2CCH_2	3	4	3
CH_3CCH	4	3	3
CH_3CC	4	3	4
CH_2CHC	3	3	4
CHCHCH	4	4	4
$CHCH_2C$	4	4	4

CH_2CCH	3	4	4
CH_2CC	4	4	4
CHCHC	4	3	4
CCH_2C	4	5	5
CHCCH	4	5	4
CCHC	6	5	4
CHCC	4	5	4
CCC	6	5	4
CH_3CH_3	1	1	1
CH_3CH_2	1	1	1
CH_3CH	2	2	2
CH_3C	4	3	3
CH_2CH_2	2	2	2
CH_2CH	2	3	3
CH_2C	3	3	3
CHCH	4	3	4
CHC	4	4	4
CC	4	4	4
CH_4	1	1	1
CH_3	1	1	1
CH_2	2	2	2
CH	4	3	3
C	4	3	4
H	1	1	1

A.4.2 Lateral Interactions

To describe the lateral interactions on all of our surfaces, we used the same methodology as in Zare et al.[17]

$$G_{ads,i}(\theta_j) = G_{ads,i}(0) + \sum_j \alpha_{i,j}\theta_j \qquad (A.4)$$

where $G_{ads,i}(\theta_j)$ is the adsorption free energy of species i, with coverage of species j, $G_{ads}(0)$ is the energy of the adsorbed species on a clean slab, θ_j is the coverage of species j on the surface, and $\alpha_{i,j}$ is the lateral interaction parameter between species i and j. All lateral interactions are calculated at a coverage of 25%, with the exception of the interactions between other species and CHC* on Pt(211), which was calculated at 33% due to the different number of surface atoms and site coverage of CHC*.

$$\alpha_{i,j} = \frac{1}{\theta_j}(G_{ads,i}(\theta_j) - G_{ads,i}(0) \qquad (A.5)$$

The lateral interaction parameter is $\alpha_{i,j}$, which is calculated as the difference between the adsorption energy of species i with the lateral interaction species j at coverage of θ_j and the adsorption energy of species i at 0 species j coverage. For all species, save CHC* on Pt(211), a coverage of 25% was used to generate the lateral interaction term. For CHC* on Pt(211), we used a coverage of 33%.

After calculating $\alpha_{i,j}$, we proceed to calculate the transition state energy, using the following equations:

$$G_k^{TS}(\theta_j) = G_k^{TS}(0) + \sum_j (\beta_{k,j}\theta_j) \qquad (A.6)$$

$$\beta_{k,j} = \frac{1}{2} * \sum_i {\alpha_{i,j}}^k \qquad (A.7)$$

where $G_k^{TS}(\theta_j)$ is the transition state energy for reaction k at surface coverage of species j, $G_k^{TS}(0)$ is the transition state energy for reaction k on the clean surface, and $\beta_{k,j}$ is the lateral interaction term for reaction k over all species i involved in the reaction described by transition state k. Thus, $\beta_{k,j}$ is calculated as the sum of the products and reactants lateral interactions and divided by 2, as we assume that the transition states are half of the products and half of the reactant states.

Table A.23: Lateral interactions on Pt(100).

Pt(100)	Lateral Interaction Paramters (eV/coverage)		
Adsorbed Species (i)	$\alpha_{i,H}$	$\alpha_{i,CHCH}$	$\alpha_{i,C}$
$CH_3CH_2CH_3$	0.20	-0.09	0.08
CH_3CHCH_3	0.18	0.45	0.02
$CH_3CH_2CH_2$	0.02	0.19	-0.05
CH_3CHCH_2	0.31	0.57	-0.04
CH_3CH_2CH	0.16	0.73	0.22
$CH_2CH_2CH_2$	0.08	0.61	0.26
CH_3CCH_3	0.28	0.68	0.01
CH_3CH_2C	-0.03	0.39	-0.04
CH_2CH_2CH	0.38	0.92	0.11
CH_2CHCH_2	-0.05	0.81	0.18
CH_3CHCH	0.26	0.58	-0.01
CH_3CCH_2	0.09	0.79	0.15
CH_3CHC	0.36	0.73	0.22
CH_2CH_2C	0.02	0.30	-0.13
$CHCH_2CH$	-0.15	0.57	0.04
CH_2CHCH	0.56	0.65	0.27
CH_2CCH_2	0.14	0.58	0.04
CH_3CCH	0.01	0.47	0.06
CH_3CC	-0.06	0.39	0.18
CH_2CHC	0.14	0.68	0.17

CHCHCH	0.10	0.52	0.55
$CHCH_2C$	0.17	1.03	0.05
CH_2CCH	0.18	0.66	0.30
CH_2CC	0.26	0.38	0.18
CHCHC	-0.22	0.81	0.35
CCH_2C	0.27	0.78	0.37
CHCCH	0.35	0.46	0.25
CCHC	0.23	0.39	0.00
CHCC	0.27	0.87	0.54
CCC	0.12	0.38	0.06
CH_3CH_3	0.09	0.14	0.04
CH_3CH_2	0.14	0.80	0.56
CH_3CH	0.29	0.40	0.23
CH_3C	0.09	0.21	-0.08
CH_2CH_2	0.11	0.24	0.10
CH_2CH	0.32	0.37	0.22
CH_2C	-0.08	0.19	0.01
CHCH	0.01	0.19	-0.01
CHC	-0.02	0.15	0.19
CC	0.17	0.26	0.16
CH_4	0.03	0.18	0.05
CH_3	0.13	0.33	0.06
CH_2	0.13	0.28	0.10
CH	-0.10	0.15	0.02
C	-0.16	0.01	-0.04
H	0.05	0.11	-0.02

Table A.24 Lateral interactions on Pt(111).

Pt(111)	Lateral Interaction Parameters (eV/coverage)			
Adsorbed Species (i)	$\alpha_{i,H}$	$\alpha_{i,CH}$	$\alpha_{i,CH3C}$	$\alpha_{i,CH3CH2C}$
$CH_3CH_2CH_3$	0.28	0.15	0.00	0.08
CH_3CHCH_3	0.52	0.42	0.52	0.90
$CH_3CH_2CH_2$	0.47	0.31	0.60	0.76
CH_3CHCH_2	0.42	0.64	0.76	1.06
CH_3CH_2CH	0.67	0.42	1.01	1.48
$CH_2CH_2CH_2$	0.38	0.80	0.81	1.06
CH_3CCH_3	0.82	1.57	0.93	1.57
CH_3CH_2C	0.57	0.74	0.93	1.10
CH_2CH_2CH	0.49	0.67	1.05	1.31
CH_2CHCH_2	0.67	0.52	1.01	1.12
CH_3CHCH	0.82	0.59	0.93	1.39
CH_3CCH_2	0.62	0.61	0.98	1.12
CH_3CHC	0.63	0.70	1.10	1.31
CH_2CH_2C	0.37	0.76	1.23	1.39
$CHCH_2CH$	0.76	0.80	1.08	1.23
CH_2CHCH	0.87	0.98	1.00	1.35
CH_2CCH_2	1.14	0.73	1.16	1.21
CH_3CCH	0.66	0.60	0.58	1.09
CH_3CC	0.73	0.73	1.29	1.45
CH_2CHC	-0.13	0.76	1.62	1.97
CHCHCH	0.58	0.76	0.98	1.46
$CHCH_2C$	0.83	0.77	0.85	1.39
CH_2CCH	0.83	0.70	1.00	1.26
CH_2CC	1.00	0.84	0.95	1.21
CHCHC	0.68	0.77	1.14	1.33
CCH_2C	0.37	0.84	0.93	1.42
CHCCH	1.59	0.93	1.47	1.79
CCHC	0.92	0.88	1.11	1.45
CHCC	0.74	0.88	1.01	1.42
CCC	0.83	0.81	0.93	1.31
CH_3CH_3	0.20	0.17	0.36	0.49
CH_3CH_2	0.25	1.27	0.66	0.79
CH_3CH	0.43	0.75	1.07	1.17
CH_3C	0.66	1.14	0.62	1.24
CH_2CH_2	0.45	0.52	0.56	1.05
CH_2CH	0.55	0.76	0.72	1.27
CH_2C	0.62	0.69	0.76	1.26
CHCH	0.60	0.80	0.98	1.08
CHC	0.79	0.60	0.90	1.08

CC	0.85	0.83	0.98	1.23
CH_4	0.25	0.31	0.29	0.50
CH_3	0.28	-0.08	0.09	0.41
CH_2	0.39	0.37	0.94	1.13
CH	0.51	0.44	0.92	1.15
C	0.56	0.51	0.24	0.80
H	0.21	0.23	0.58	0.85

Table A.25: Lateral interactions on Pt(211).

Pt(211)	Lateral Interactions Parameters (eV/coverage)		
Molecule	$\alpha_{i,H}$	$\alpha_{i,CH3C}$	$\alpha_{i,CHC}$
$CH_3CH_2CH_3$	-0.06	0.54	0.56
CH_3CHCH_3	0.14	0.40	0.74
$CH_3CH_2CH_2$	0.25	0.62	0.73
CH_3CHCH_2	0.18	0.09	0.22
CH_3CH_2CH	-0.16	0.08	0.68
$CH_2CH_2CH_2$	-0.12	0.14	0.98
CH_3CCH_3	0.25	0.38	0.96
CH_3CH_2C	0.17	0.11	0.67
CH_2CH_2CH	0.09	0.21	0.96
CH_2CHCH_2	0.01	0.25	0.97
CH_3CHCH	0.44	0.18	1.05
CH_3CCH_2	0.47	0.23	1.00
CH_3CHC	0.17	-0.02	0.91
CH_2CH_2C	0.21	0.10	1.08
$CHCH_2CH$	0.50	0.16	0.91
CH_2CHCH	0.24	0.14	1.04
CH_2CCH_2	0.40	0.37	1.03
CH_3CCH	0.67	0.25	0.50
CH_3CC	0.33	0.09	1.36
CH_2CHC	0.10	0.00	1.22
CHCHCH	0.23	0.19	0.26
$CHCH_2C$	0.41	0.34	1.76
CH_2CCH	0.16	0.13	0.98
CH_2CC	0.11	0.08	1.35
CHCHC	0.22	0.06	1.16
CCH_2C	0.51	0.28	1.08
CHCCH	0.31	0.37	0.81
CCHC	0.53	0.08	0.99
CHCC	0.51	0.27	1.11
CCC	0.52	-0.06	0.97
CH_3CH_3	0.59	0.16	0.67
CH_3CH_2	0.60	-0.03	0.85
CH_3CH	0.39	0.51	0.72
CH_3C	0.40	0.56	1.11
CH_2CH_2	0.54	0.10	0.70
CH_2CH	0.38	0.24	1.05
CH_2C	0.40	0.09	1.02
CHCH	0.20	0.18	0.17
CHC	0.15	-0.08	0.23
CC	0.44	0.03	0.53

CH_4	0.51	0.06	0.66
CH_3	0.46	-0.19	0.42
CH_2	0.44	0.07	0.69
CH	0.25	0.10	0.99
C	0.24	0.09	0.84
H	0.11	0.81	0.83

For the lateral interactions between high coverage species and all other surface species, we calculated the ddG of adsorption, or the change of adsorption energy as the number of adsorbed species increased. Figures A.4 – A.13 describe these lateral interactions for the self-interaction of various species.

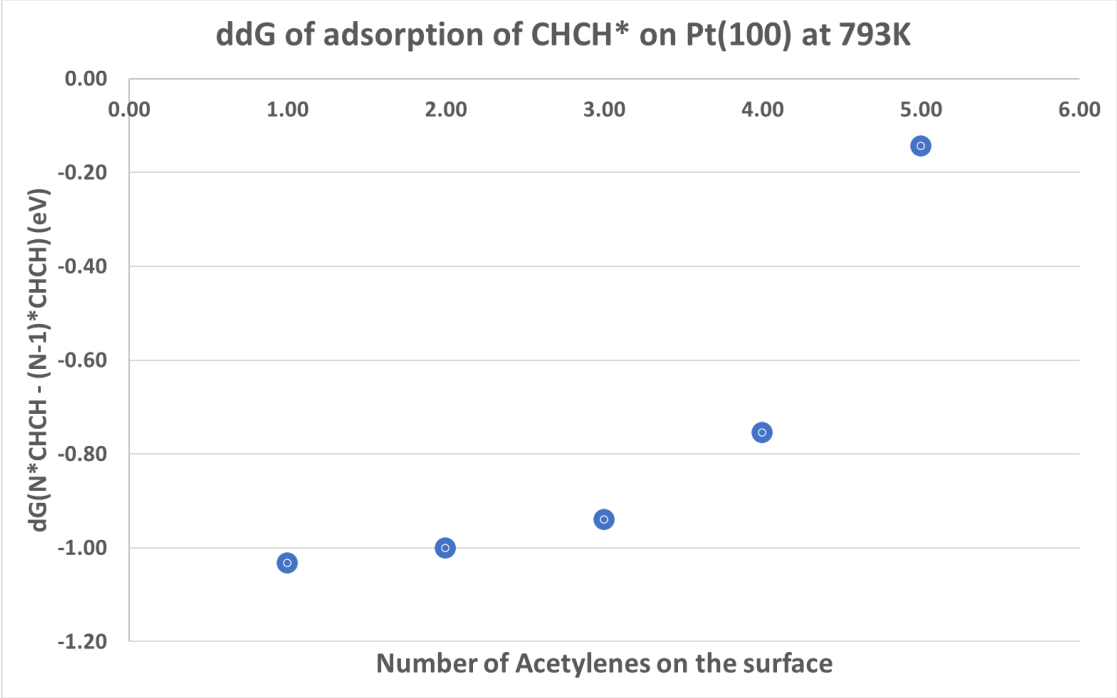

Figure A.4: Differential adsorption energies of acetylene as a function of the number of acetylene molecules adsorbing onto the Pt(100) surface. Lateral interaction parameters were calculated from 0% acetylene coverage to 75% acetylene coverage (3 CHCH species on the surface slab).

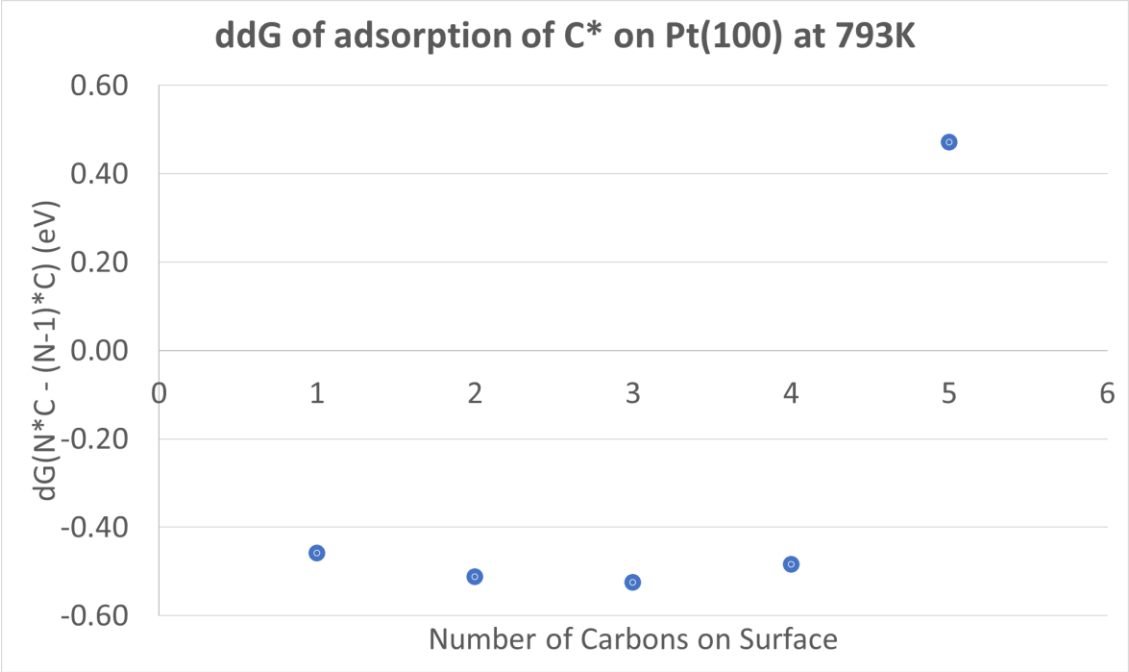

Figure A.5: Differential adsorption energies of atomic carbon as a function of the number of carbon atoms adsorbing onto the Pt(100) surface. Lateral interactions were calculated from 0% coverage to 100% C* coverage (4 C species on the surface slab).

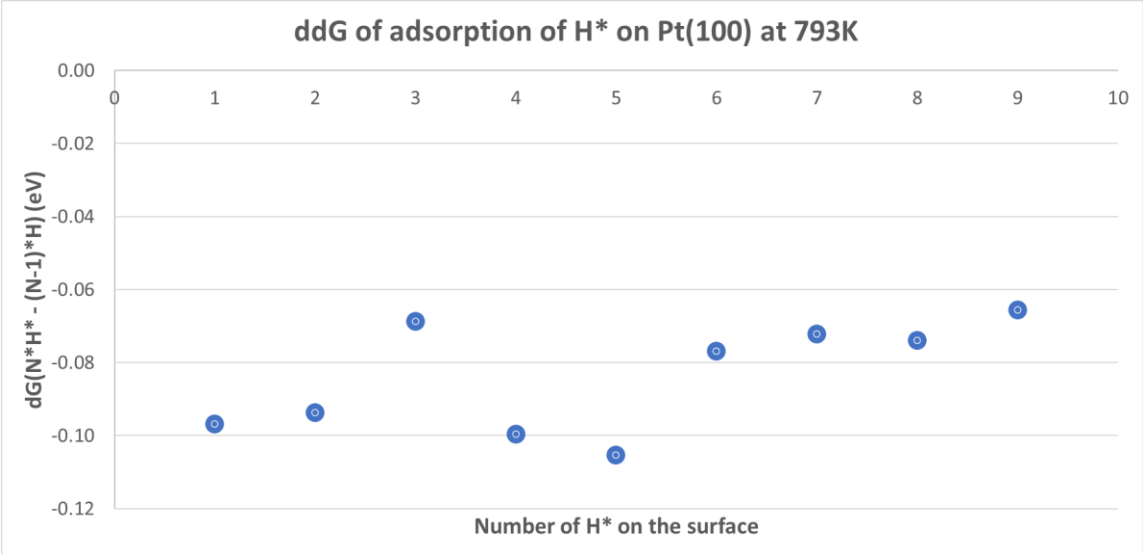

Figure A.6: Differential adsorption energies of atomic hydrogen as a function of the number of hydrogen atoms adsorbing onto the Pt(100) surface. Lateral interactions were calculated from 0% coverage to 50% H* coverage (8 H species on the surface slab).

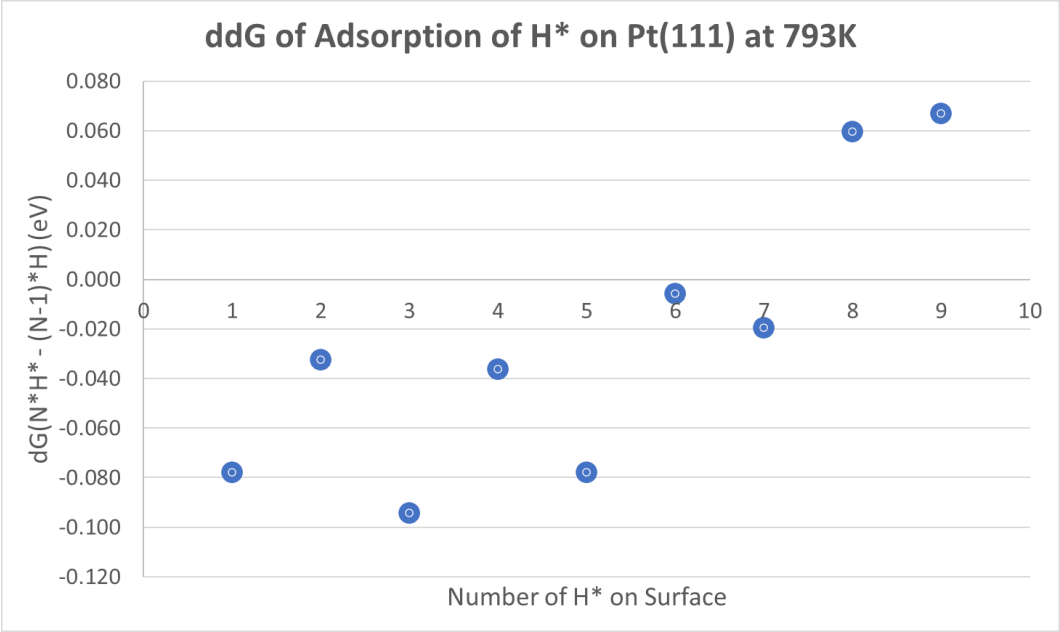

Figure A.7: Differential adsorption energies of atomic hydrogen as a function of the number of hydrogen atoms adsorbing onto the Pt(111) surface. Lateral interactions were calculated from 0% coverage to 50% H* coverage (8 H species on the surface slab).

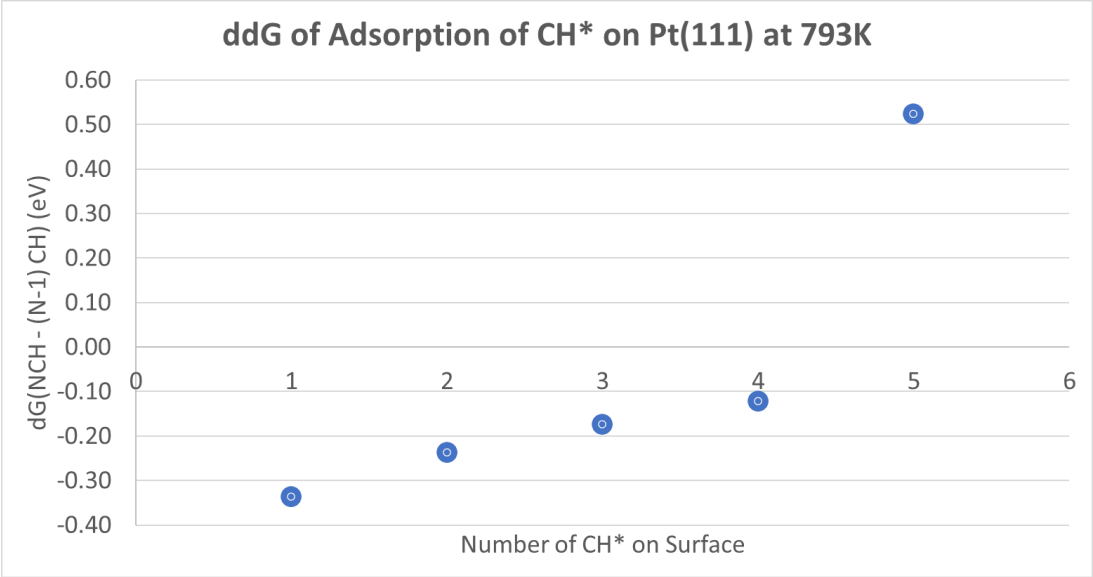

Figure A.8: Differential adsorption energies of CH* as a function of the number of CH* species adsorbing onto the Pt(111) surface. Lateral interactions were calculated from 0% coverage to 75% coverage of CH* (4 CH species on the surface slab).

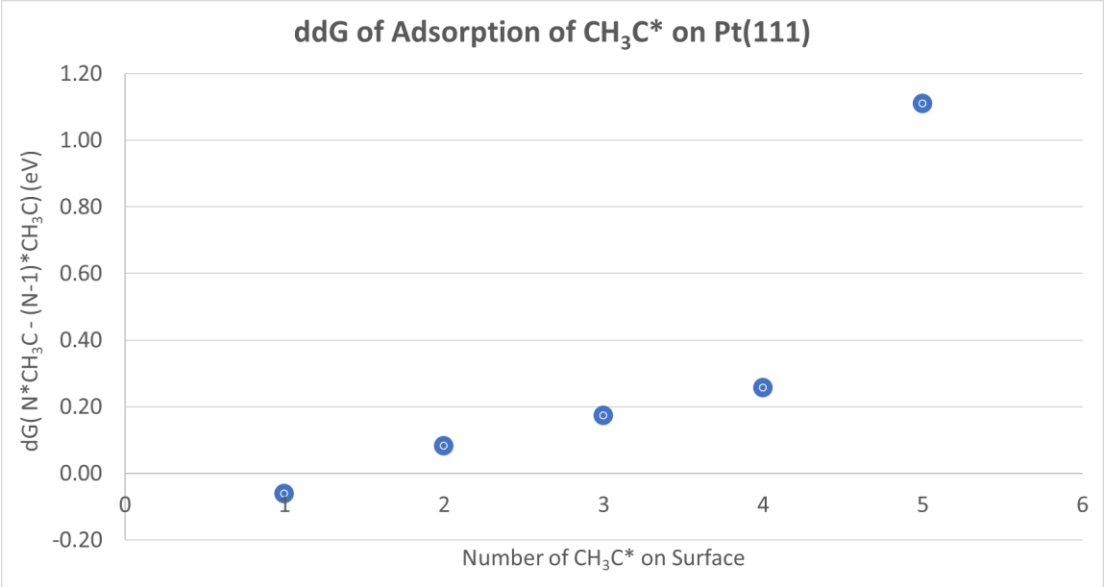

Figure A.9: Differential adsorption energies of CH_3C^* as a function of the number of CH_3C^* species adsorbing onto the Pt(111) surface. Lateral interactions were calculated from 0% coverage to 75% CH_3C^* coverage (4 CH_3C species on the surface slab).

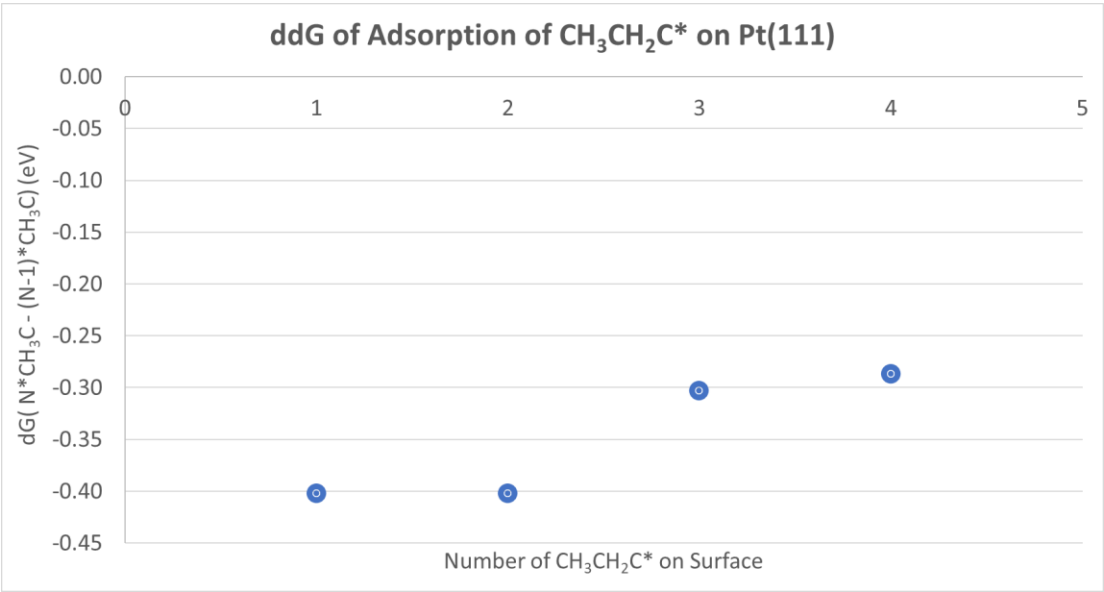

Figure A.10: Differential adsorption energies of $CH_3CH_2C^*$ as a function of the number of $CH_3CH_2C^*$ species adsorbing onto the Pt(111) surface. Lateral interactions were calculated from 0% coverage to 75% $CH_3CH_2C^*$ coverage (4 CH_3CH_2C species on the surface slab).

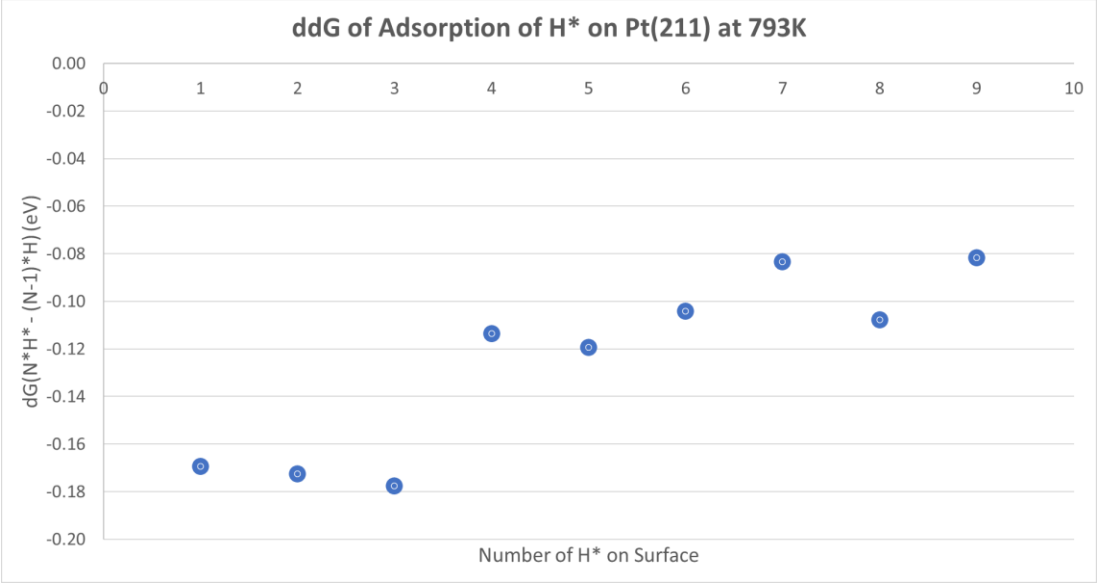

Figure A.11: Differential adsorption energies of atomic hydrogen as a function of the number of hydrogen atoms adsorbing onto the Pt(211) surface. Lateral interactions were calculated between 0% and 33% H* coverage (8 H species on the surface slab).

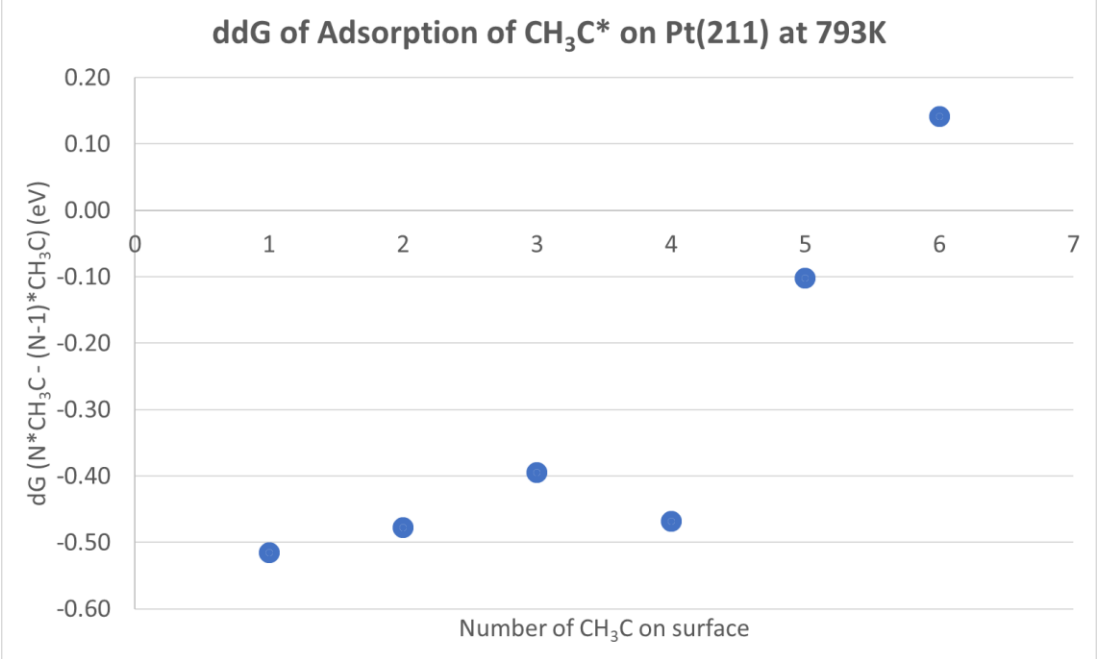

Figure A.12: Differential adsorption energies of CH_3C^* as a function of the number of CH_3C^* adsorbing onto the Pt(211) surface. Lateral interactions were calculated between 0% and 38% CH_3C^* coverage (3 CH_3C species on the surface slab).

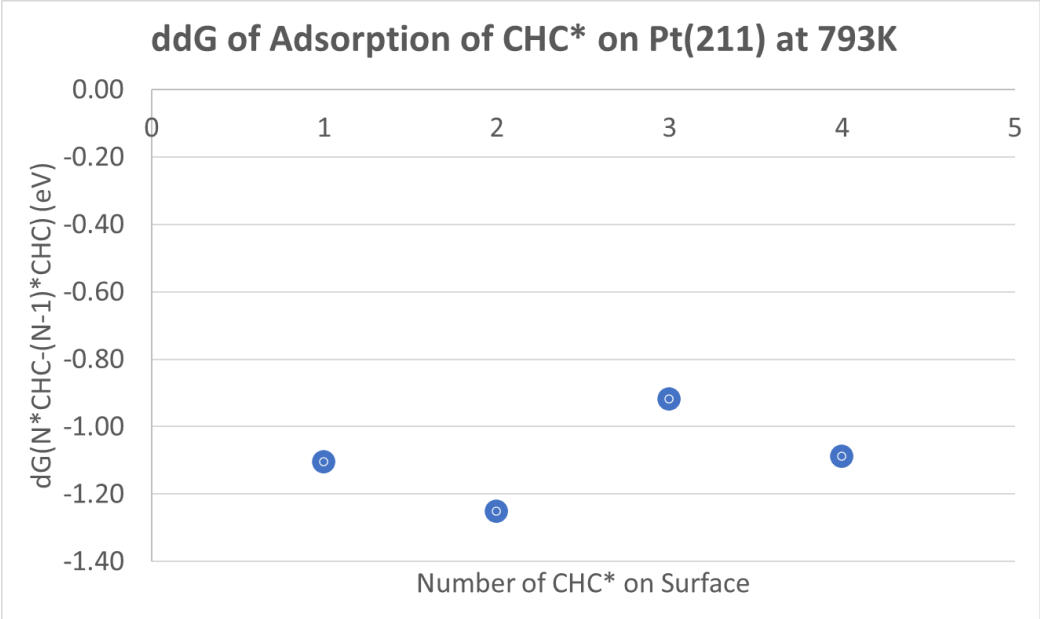

Figure A.13. Differential adsorption energies of CHC* as a function of the number of CHC* adsorbing onto the Pt(211) surface. Lateral interactions were calculated from 0% coverage to 50% CHC* coverage (4 CHC species on the surface slab).

A.4.3 Uncertainty within Site Occupancy

A challenge of mean-field microkinetic modelling includes determining site occupancies for each adsorbed species, which can have cascading effects on results. In this study, the site occupancies given in Table A.22 are what the study uses for all of the calculations. These occupancies have been derived from how many platinum atoms are being directly affected by each species through bonding. However, a one-site model in which a site is either occupied or unoccupied might not be correct for a system with many different types of sites, and considerable uncertainty exists in calculating the species site occupancy. To determine if the species occupancies affected the results, the Pt(100) microkinetic model was modified such that all species occupancies that were greater than 2 were reduced by 1, such that a species occupying 3 sites now occupies 2 sites etc. Table A.26 reports the results of this model that ran at D2 conditions, which again can be compared to Table A.28. Table A.26 shows that site occupancies do affect the resulting predicted experimental data; however, in this study we hypothesize that these errors are small relative to the DFT functional error.

Table A.26: Evaluating two different microkinetic models for the effect of changing the surface occupancies of the microkinetic model from the current to the modified model.

Experimental Quantities of Interest	Reaction Conditions of D2	
D2 Dataset	Modified Microkinetic Model, PBE-D3	Current Microkinetic Model
TOF (Propylene) (1/s)	0.77	6.60
Selectivity to Propylene	67.9%	76.1%
Apparent Activation Energy (eV)	1.31	1.30
Propane Reaction Order	0.33	0.61
H_2 Reaction Order	1.02	0.67

A.5 Selectivity towards different Gas Species, Prior, forward-only problem.

Table A.27. Average selectivity towards gas-phase species at experimental conditions, prior models only.

Average Selectivity towards Gas-Phase Species (%), No Calibration									
	Four Functional Model (FFM)								
	D1 conditions			D2 conditions			D3 conditions		
Species	Pt(100)	Pt(111)	Pt(211)	Pt(100)	Pt(111)	Pt(211)	Pt(100)	Pt(111)	Pt(211)
Propylene	74.7	77.0	98.3	23.7	53.4	98.7	27.3	60.8	98.0
Propyne	0.92	3.33	0.00	0.00	0.07	0.26	0.00	0.04	0.00
Ethane	4.76	5.19	0.02	0.24	0.00	0.00	0.57	0.00	0.00
Ethylene	9.25	6.71	0.02	29.3	23.4	1.37	38.5	19.7	0.02
Acetylene	0.00	0.63	0.00	0.00	0.16	0.00	0.00	0.02	0.25
Methane	7.22	6.27	0.12	43.3	19.9	0.00	31.2	17.8	0.00
	BEEF Model with Ensembles (BMwE)								
	D1 conditions			D2 conditions			D3 conditions		
Species	Pt(100)	Pt(111)	Pt(211)	Pt(100)	Pt(111)	Pt(211)	Pt(100)	Pt(111)	Pt(211)
Propylene	65.1	84.7	88.7	25.4	44.0	96.0	33.0	40.7	97.9
Propyne	0.73	0.00	0.02	0.00	4.64	0.00	0.05	1.08	0.00
Ethane	0.65	0.00	1.11	0.13	0.00	0.00	0.11	0.00	0.00
Ethylene	11.5	4.98	1.19	36.4	25.7	0.57	38.9	26.5	0.20
Acetylene	0.01	2.94	0.00	0.01	3.16	0.00	0.00	0.44	0.00
Methane	21.9	5.36	7.11	30.4	20.5	1.16	24.3	27.1	0.90
Experiment	Reaction Conditions								
D1[2]	$PCH_3CH_2CH_3$ = 0.04 bar, PH_2 = 2 bar, T = 633K								
D2[4]	$PCH_3CH_2CH_3$ = 0.03 bar, PH_2 = 0.03 bar, T = 793K								
D3[3]	$PCH_3CH_2CH_3$ = 0.29 bar, PH_2 = 0.09 bar, T = 792K								

A.6 Surface Microkinetic Model Results for Each Functional, No Uncertainty

Table A.28: Microkinetic model results using each functional separately, no uncertainty, on Pt(100).

Experimental Quanties of Interest	Pt(100)			
D1 Dataset	PBE-D3	BEEF-vdw	RPBE	SCAN-rVV10
TOF (Propylene) (1/s)	9.67×10^{-4}	5.49×10^{-7}	6.60×10^{-11}	7.81×10^{-5}
Apparent Activation Energy (eV)	1.86	2.24	2.73	1.93
Propane Reaction Order	1.00	1.00	1.00	1.00
H_2 Reaction Order	-2.01	-1.76	-1.93	-1.77
D2 Dataset	PBE-D3	BEEF-vdw	RPBE	SCAN-rVV10
TOF (Propylene) (1/s)	6.60	2.98×10^{-4}	8.29×10^{-5}	1.96×10^{-3}
Selectivity to Propylene	76.1%	68.0%	47.2%	11.0%
Apparent Activation Energy (eV)	1.30	2.34	2.54	1.66
Propane Reaction Order	0.61	0.65	0.54	0.16
H_2 Reaction Order	0.67	0.61	0.88	1.17
D3 Dataset	PBE-D3	BEEF-vdw	RPBE	SCAN-rVV10
TOF (Propylene) (1/s)	1.91×10^{2}	1.70×10^{-2}	3.41×10^{-4}	6.06×10^{-1}
Selectivity to Propylene	93.4%	87.1%	51.4%	60.6%

Table A.29: Microkinetic model results using each functional separately, no uncertainty, on Pt(111).

Experimental Quanties of Interest	Pt(111)			
D1 Dataset	PBE-D3	BEEF-vdw	RPBE	SCAN-rVV10
TOF (Propylene) (1/s)	4.76×10^{-5}	9.64×10^{-9}	6.57×10^{-14}	6.30×10^{-6}
Apparent Activation Energy (eV)	1.98	2.36	3.04	2.08
Propane Reaction Order	1.00	1.00	1.00	1.00
H_2 Reaction Order	-2.31	-2.02	-2.27	-2.33
D2 Dataset	PBE-D3	BEEF-vdw	RPBE	SCAN-rVV10
TOF (Propylene) (1/s)	3.35×10^{1}	4.64×10^{-5}	6.315×10^{-7}	2.02×10^{-2}
Selectivity to Propylene	91.4%	34.9%	24.9%	55.2%
Apparent Activation Energy (eV)	1.48	2.39	2.66	2.02
Propane Reaction Order	0.64	0.52	0.68	0.50
H_2 Reaction Order	0.25	0.53	0.23	0.396
D3 Dataset	PBE-D3	BEEF-vdw	RPBE	SCAN-rVV10
TOF (Propylene) (1/s)	1.54×10^{3}	1.15×10^{-3}	3.12×10^{-5}	1.00
Selectivity to Propylene	98.7%	40.3%	23.0%	64.4%

Table A.30: Microkinetic model results using each functional separately, no uncertainty, on Pt(211).

Experimental Quanties of Interest	Pt(211)			
D1 Dataset	PBE-D3	BEEF-vdw	RPBE	SCAN-rVV10
TOF (Propylene) (1/s)	2.46×10^{-1}	2.11×10^{-5}	3.60×10^{-8}	6.67×10^{-4}
Apparent Activation Energy (eV)	1.50	2.00	2.35	1.85
Propane Reaction Order	1.00	1.00	1.00	1.00
H_2 Reaction Order	-1.72	-0.51	-0.85	-1.96
D2 Dataset	PBE-D3	BEEF-vdw	RPBE	SCAN-rVV10
TOF (Propylene) (1/s)	8.41	1.55×10^{-3}	2.20×10^{-5}	4.08
Selectivity to Propylene	95.1%	99.7%	99.9%	95.4%
Apparent Activation Energy (eV)	1.04	2.39	2.67	1.24
Propane Reaction Order	0.31	1.00	1.00	0.54
H_2 Reaction Order	0.46	-0.02	-0.07	0.30
D3 Dataset	PBE-D3	BEEF-vdw	RPBE	SCAN-rVV10
TOF (Propylene) (1/s)	7.48×10^{2}	1.46×10^{-1}	2.03×10^{-3}	9.87
Selectivity to Propylene	97.6%	99.7%	99.9%	91.0%

Table A.31: Degree of Kinetic Rate Control for Pt(111) and Pt(211) at D2 conditions around the direct Propane to Propylene Dehydrogenation Pathway for various DFT functionals.

Degree of Kinetic Rate Control for Propane and Propylene on Pt(111) and Pt(211)								
Pt(111)								
	PBE-D3		BEEF-vdw		RPBE		SCAN-rVV10	
Reaction	Propane	Propylene	Propane	Propylene	Propane	Propylene	Propane	Propylene
$CH_3CH_2CH_3 \rightarrow CH_3CHCH_3$+H	0.21	0.23	0.06	0.15	0.01	0.01	0.09	0.16
$CH_3CH_2CH_3 \rightarrow CH_3CH_2CH_2$ +H	0.42	0.42	0.45	0.34	0.65	0.59	0.40	0.32
$CH_3CHCH_3 \rightarrow CH_3CHCH_2$+H	0.03	0.04	0.01	0.04	0.00	0.01	0.01	0.02
$CH_3CH_2CH_2 \rightarrow CH_3CHCH_2$+H	0.20	0.24	0.15	0.69	0.09	0.83	0.25	0.65
Total	0.86	0.92	0.67	1.22	0.75	1.44	0.75	1.15
Pt(211)								
	PBE-D3		BEEF-vdw		RPBE		SCAN-rVV10	
Reaction	Propane	Propylene	Propane	Propylene	Propane	Propylene	Propane	Propylene
$CH_3CH_2CH_3 \rightarrow CH_3CHCH_3$+H	0.29	0.31	0.57	0.57	0.18	0.18	0.61	0.61
$CH_3CH_2CH_3 \rightarrow CH_3CH_2CH_2$ +H	0.00	0.00	0.38	0.38	0.82	0.82	-0.39	-0.39
$CH_3CHCH_3 \rightarrow CH_3CHCH_2$+H	0.00	0.03	0.00	0.00	0.00	0.00	0.00	0.00
$CH_3CH_2CH_2 \rightarrow CH_3CHCH_2$+H	0.03	0.03	0.03	0.03	0.00	0.00	0.29	0.29
Propylene Desorption	0.66	0.67	0.00	0.00	0.00	0.00	0.36	0.36
Total	0.98	1.04	0.98	0.98	1.00	1.00	0.87	0.87

A.7 BMwE and FFM Calibration model probability distributions

A.7.1 Forward-only probability distributions

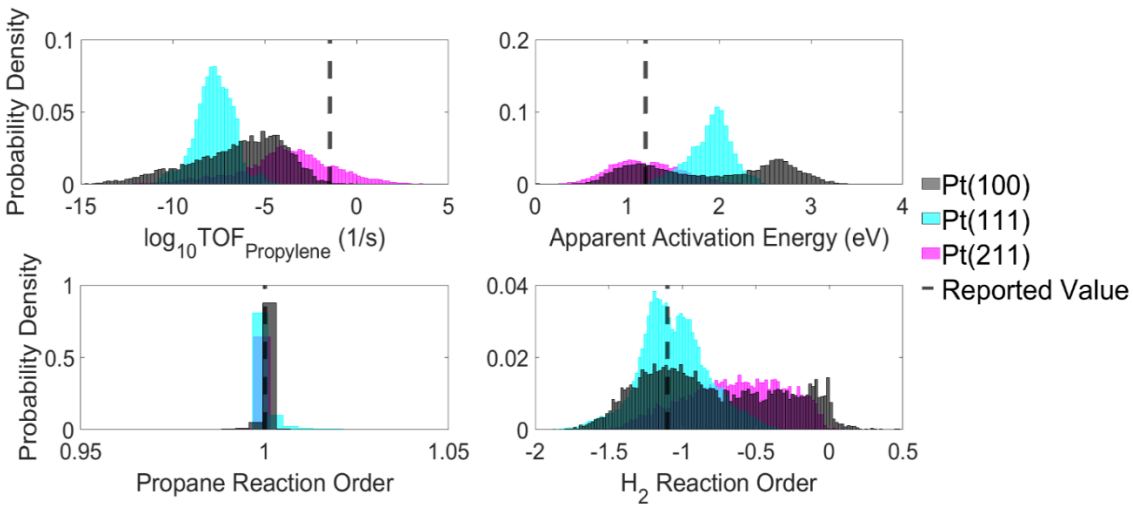

Figure A.14: Probability Distributions for Quantities of interest at D1 conditions using the BMwE model.

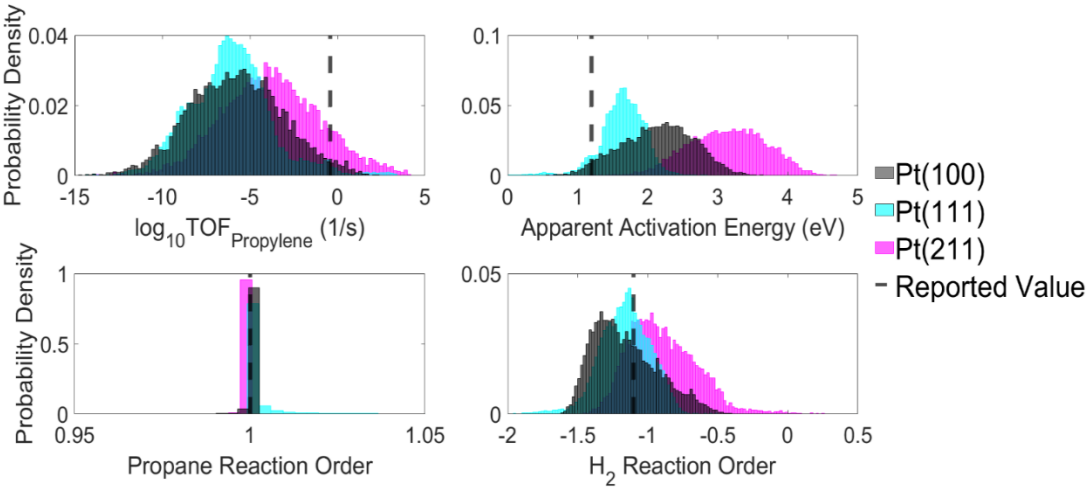

Figure A.15: Probability Distributions for Quantities of Interest at D1 conditions using the FFM model.

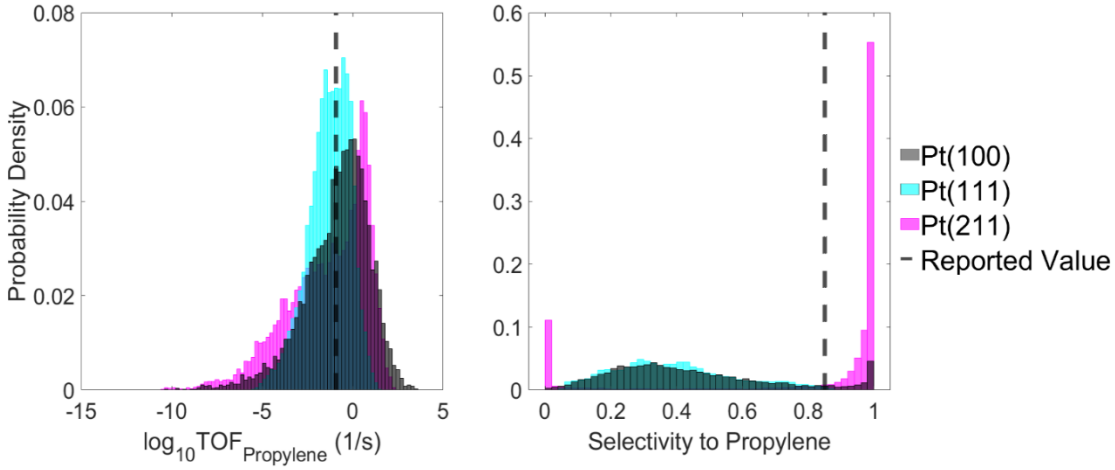

Figure A.16. Probability Distributions for Quantities of Interest at D3 conditions using the BMwE model.

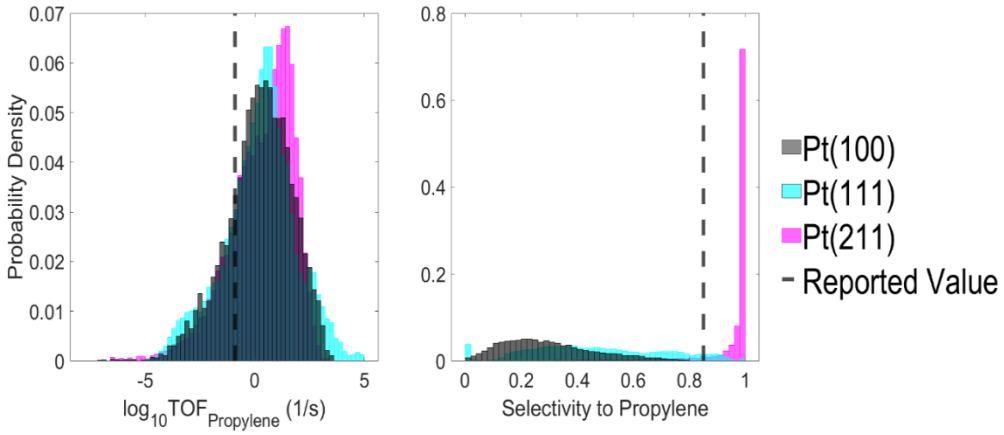

Figure A.17. Probability Distributions for Quantities of Interest at D3 conditions using the FFM model.

A.7.2 Calibrated Probability Distributions

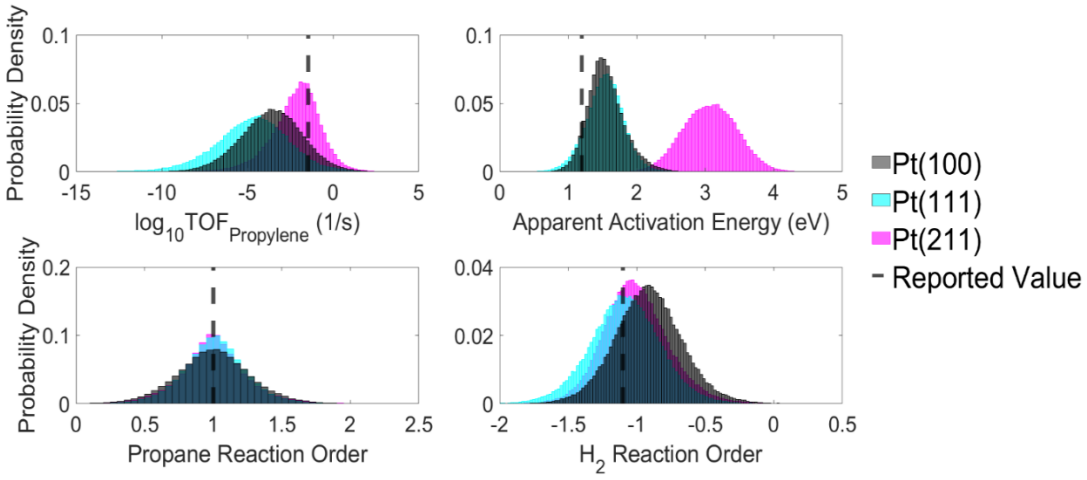

Figure A.18: Probability Distributions for Quantities of Interest calibrating on D1 and D2 and verifying on D1 using the FFM model.

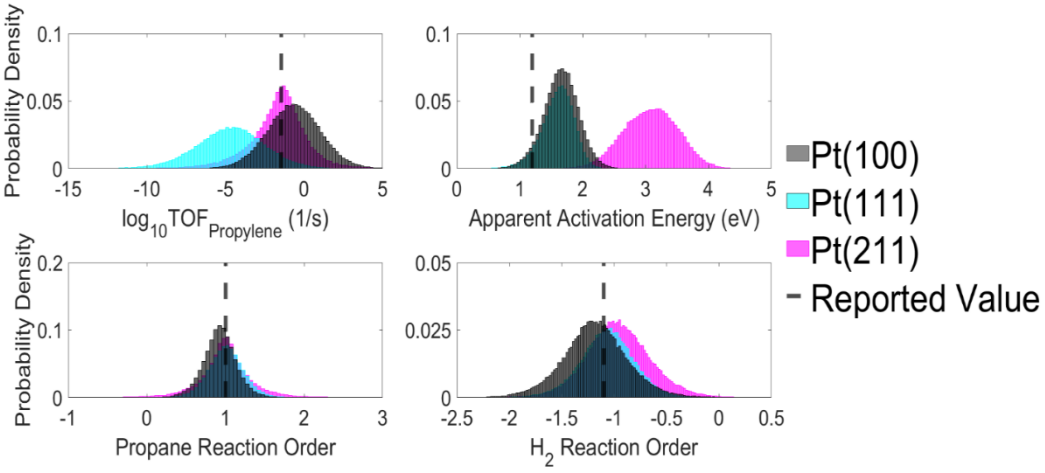

Figure A.19: Probability Distributions for Quantities of Interest calibrating on D1 and D3 and verifying on D1 using the FFM model.

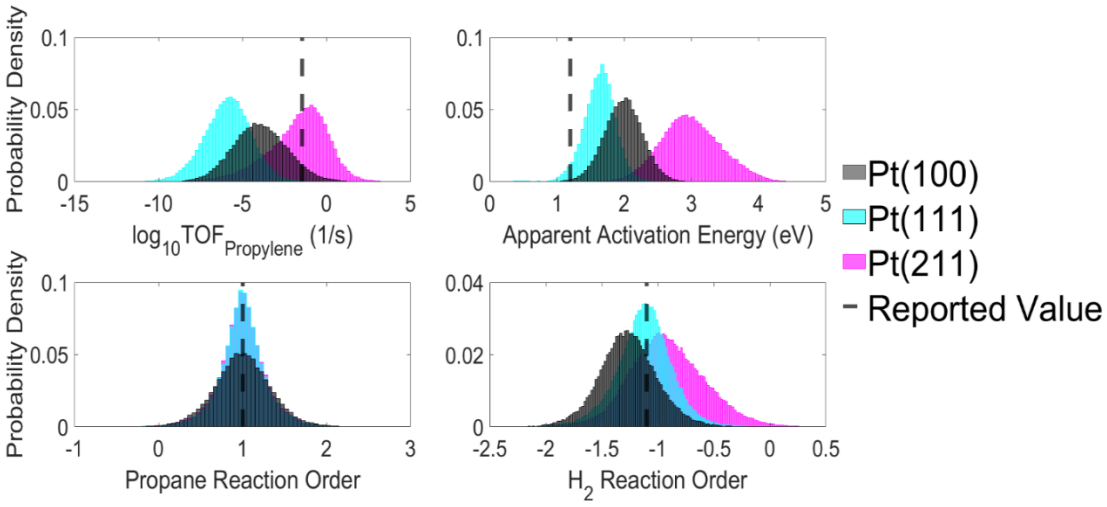

Figure A.20: Probability Distributions for Quantities of Interest calibrating on D2 and D3 and validating on D1 using the FFM model.

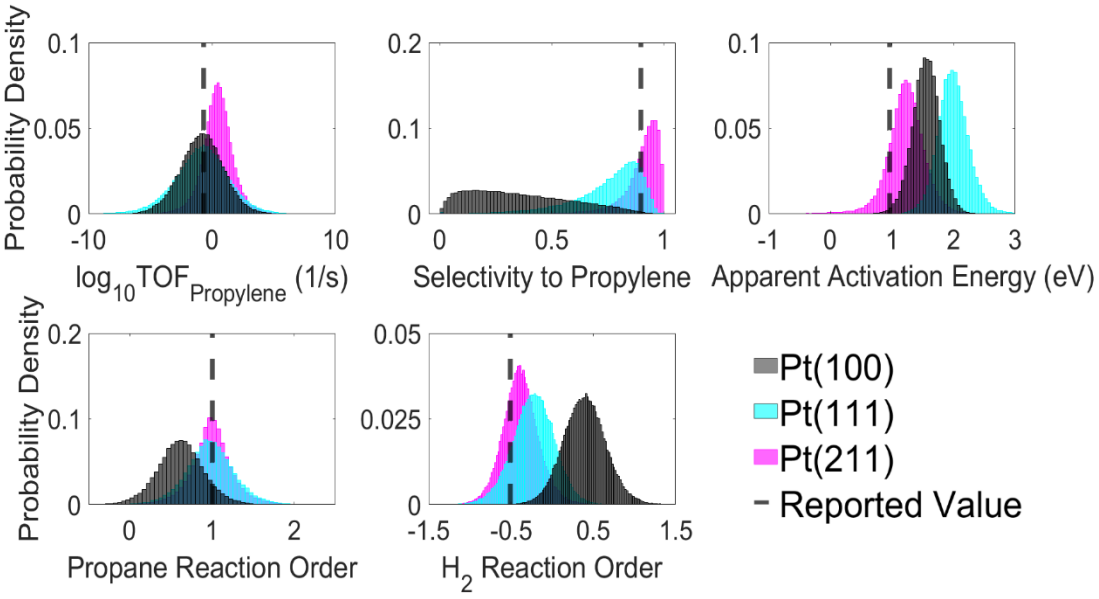

Figure A.21. Probability Distributions for Quantities of Interest calibrating on D1 and D2 and verifying on D2 using the FFM model.

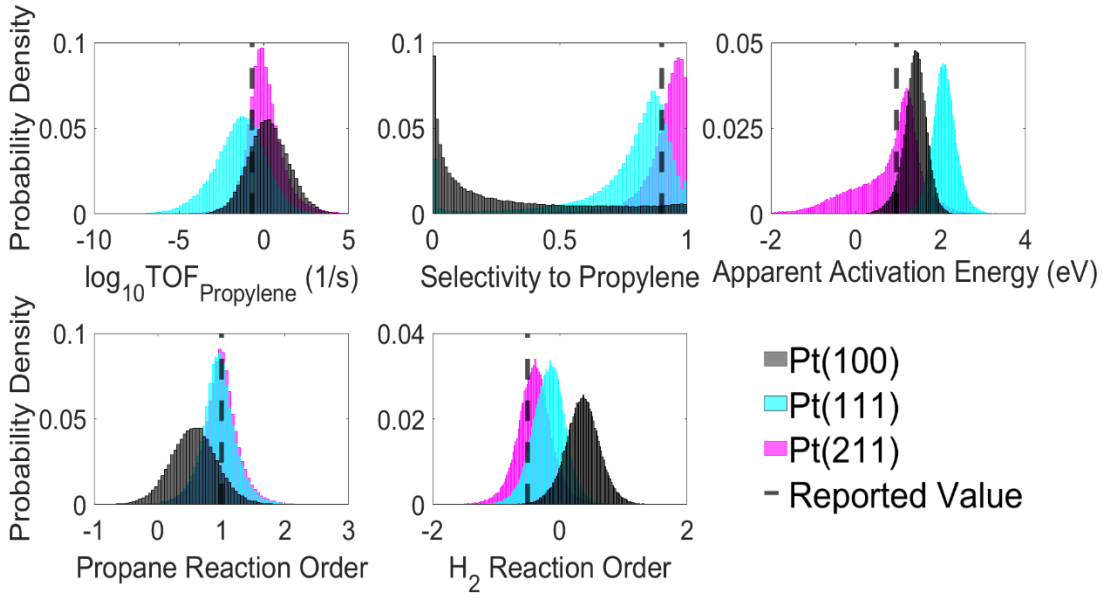

Figure A.22: Probability Distributions for Quantities of Interest calibrating on D2 and D3 and verifying on D2 using the FFM model.

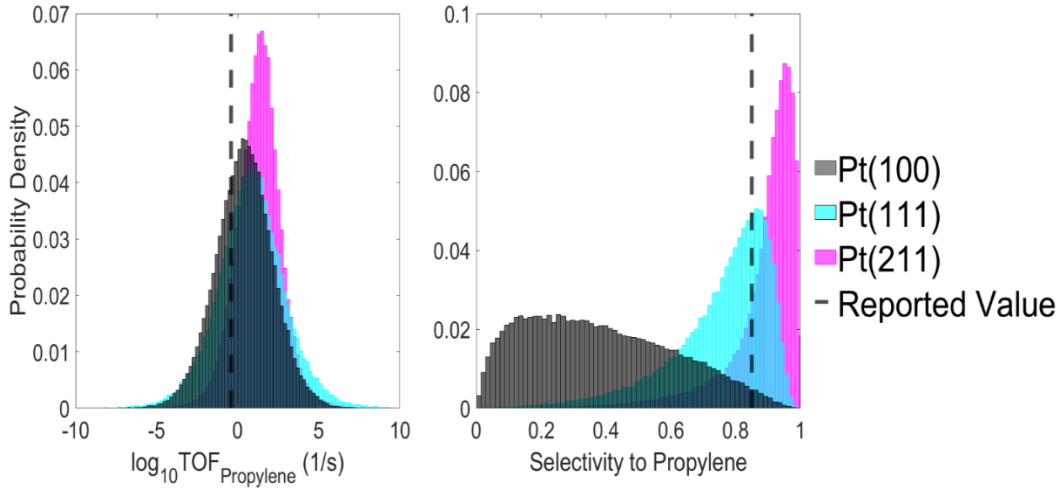

Figure A.23. Probability Distributions for Quantities of Interest calibrating on D1 and D2 and validating on D3 using the FFM model.

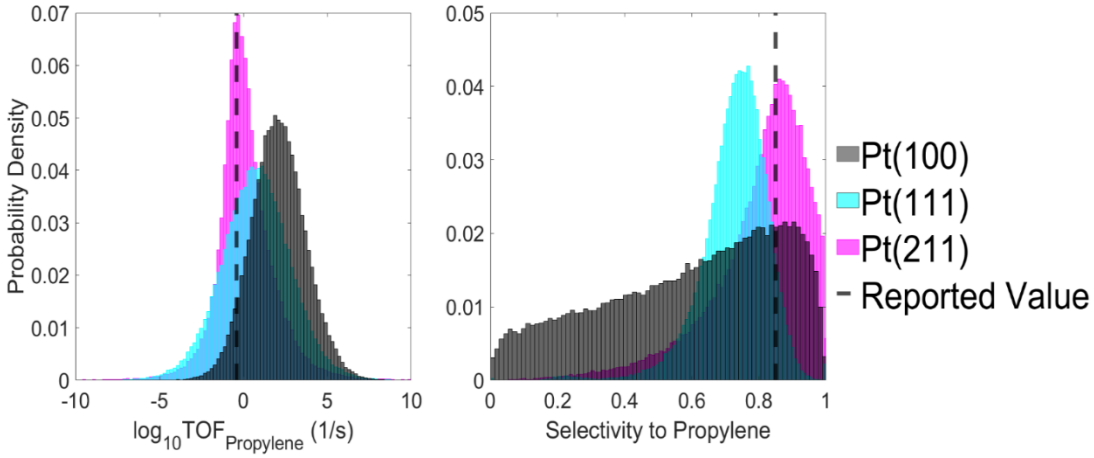

Figure A.24. Probability Distributions for Quantities of Interest calibrating on D1 and D3 and verifying on D3 using the FFM model

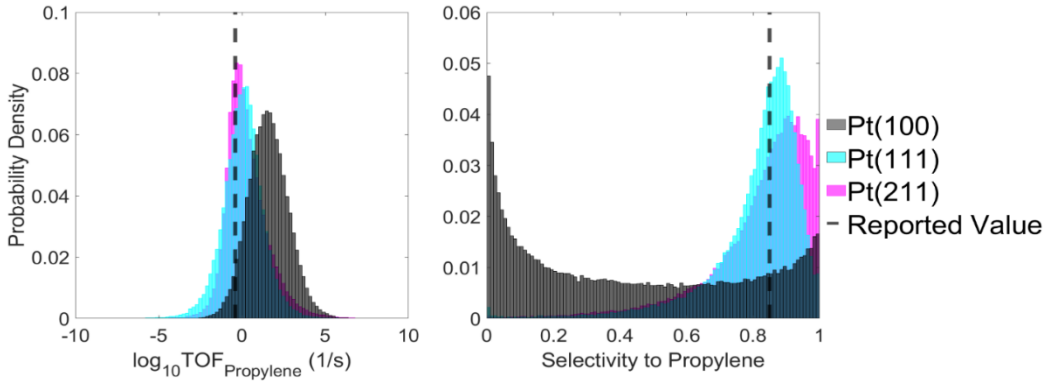

Figure A.25: Probability Distributions for Quantities of Interest calibrating on D2 and D3 and verifying on D3 using the FFM model

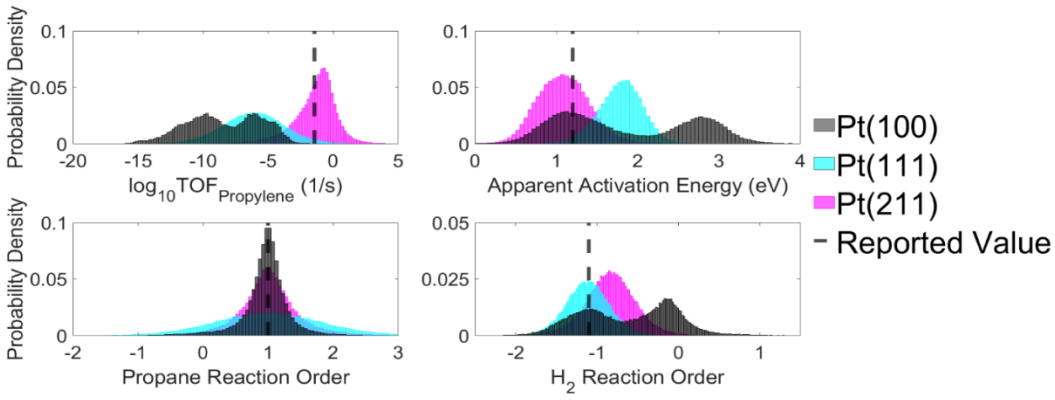

Figure A.26: Probability Distributions for Quantities of Interest calibrating on D1 and D2 and verifying on D1 using the BMwE model.

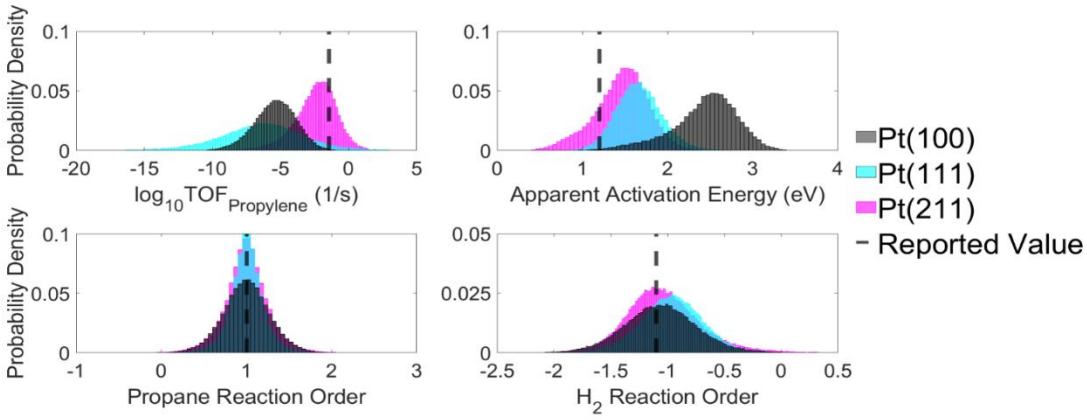

Figure A.27: Probability Distributions for Quantities of Interest calibrating on D1 and D3 and verifying on D1 using the BMwE model.

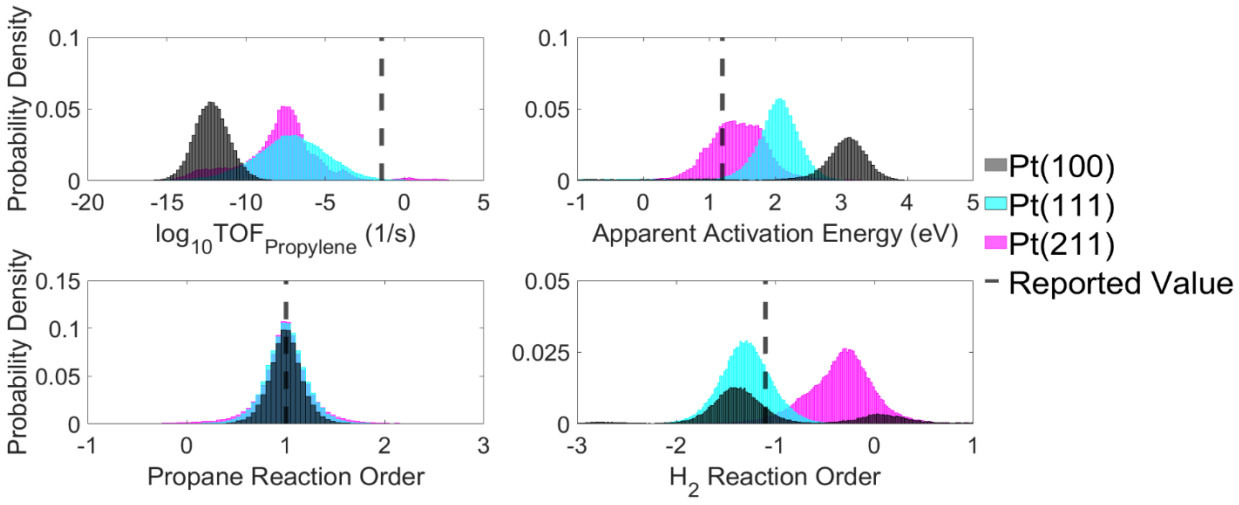

Figure A.28: Probability Distributions for Quantities of Interest calibrating on D2 and D3 and challenging on D1 using the BMwE model.

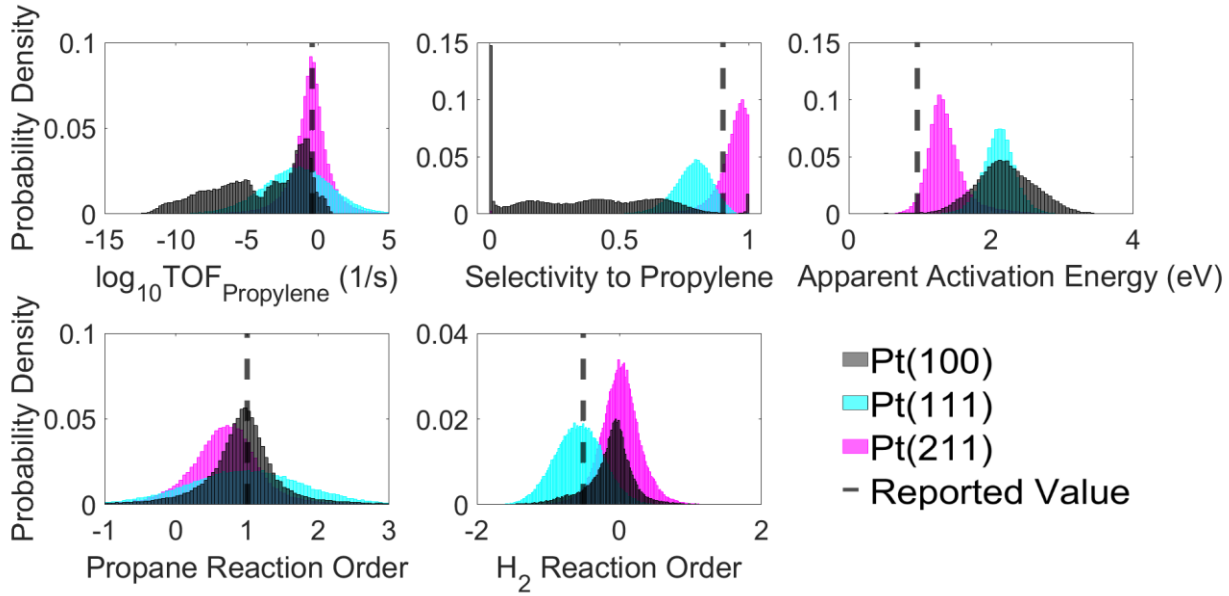

Figure A.29: Probability Distributions for Quantities of Interest calibrating on D1 and D2 and verifying on D2 using the BMwE model.

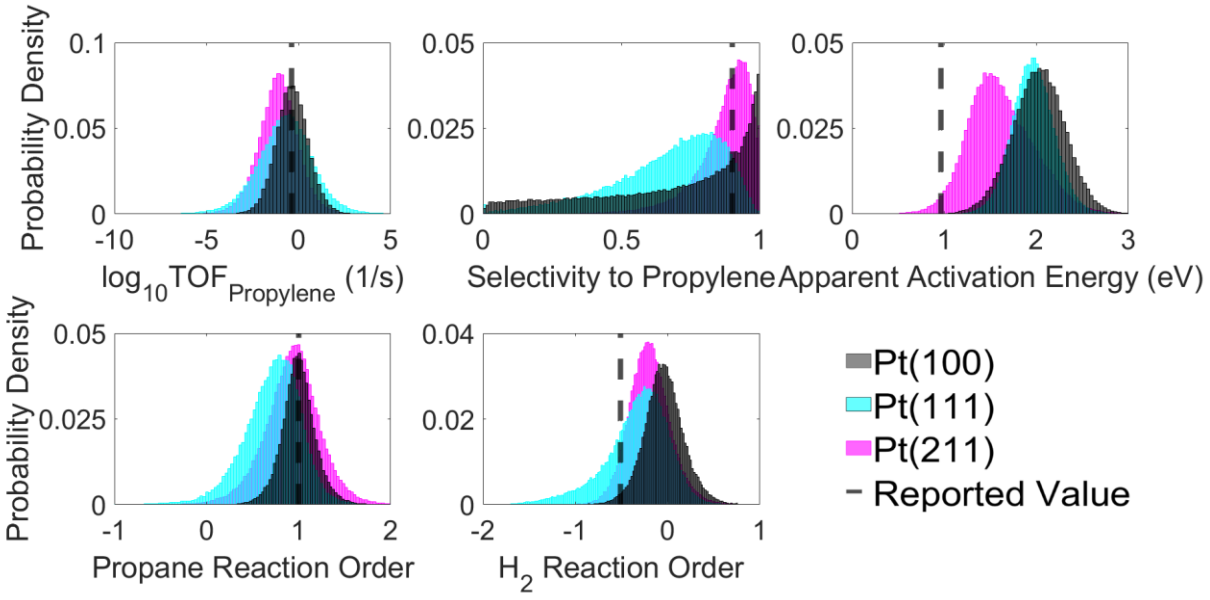

Figure A.30: Probability Distributions for Quantities of Interest calibrating on D2 and D3 and verifying on D2 using the BMwE model.

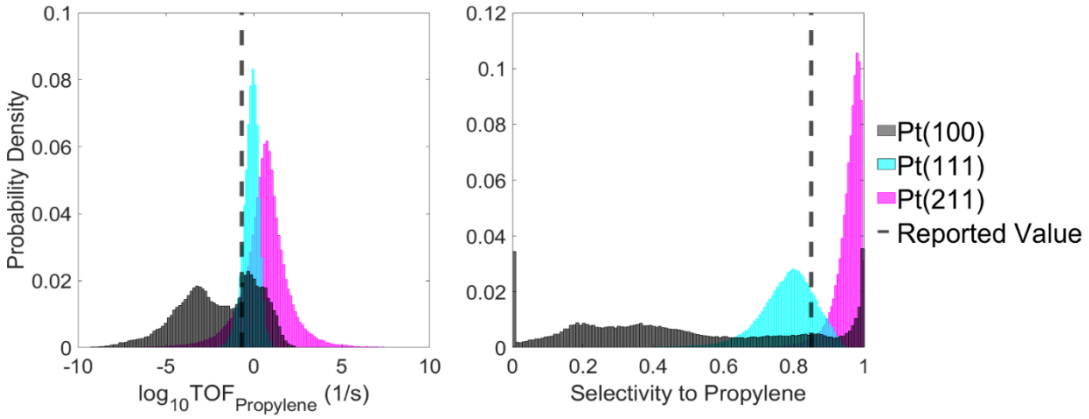

Figure A.31: Probability Distributions for Quantities of Interest calibrating on D1 and D2 and challenging on D3 using the BMwE model.

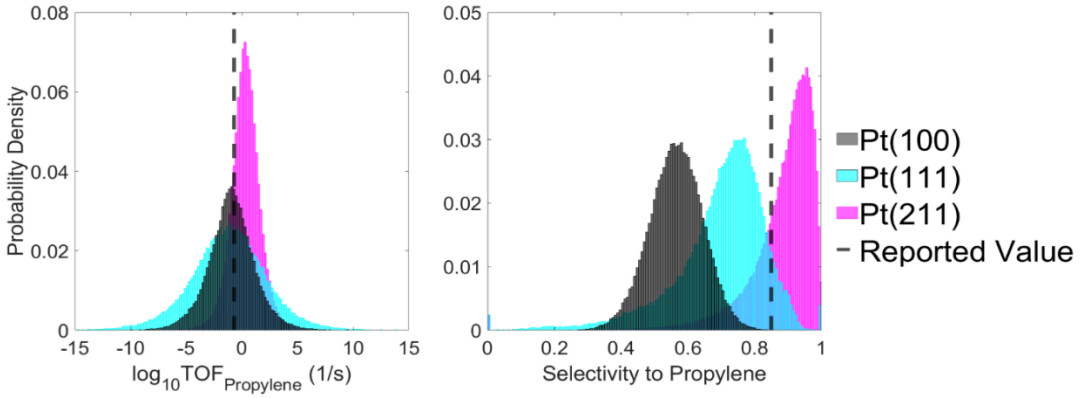

Figure A.32: Probability Distributions for Quantities of Interest calibrating on D1 and D3 and verifying on D3 using the BMwE model.

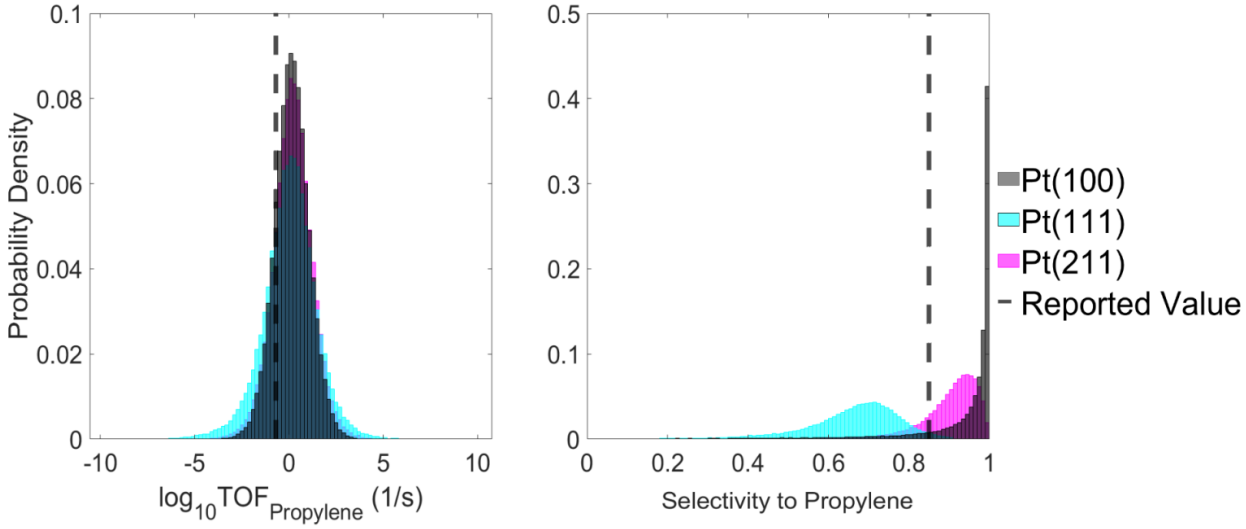

Figure A.33: Probability Distributions for Quantities of Interest calibrating on D2 and D3 and verifying on D3 using the BMwE model.

A.8 Bibliography

1. Walker, E.; Ammal, S. C.; Terejanu, G. A.; Heyden, A. Uncertainty Quantification Framework Applied to the Water–Gas Shift Reaction over Pt-Based Catalysts. *J. Phys. Chem C.* , **2016**, *120*, 10328-10339

2. Waker, E.; Mitchell, D.; Terejanu, G. A.; Heyden, A. Identifying Active Sites of the Water-Gas Shift Reaction over Titania Supported Platinum Catalysts under Uncertainty. *ACS Catal.*, **2018**, *8*, 3990-3998

3. Perdew, J. P.; Burke, K.; Ernzerhof, M. Generalized Gradient Approximation Made Simple. *Phys. Rev. Lett*., **1996**, *77*, 3865-3868

4. Grimme, S.; Antony, J.; Ehrlich, S.; Krieg, S. A consistent and accurate ab initio parametrization of density functional dispersion correction (DFT-D) for the 94 elements H-Pu. *J. Chem. Phys*., **2010**, *132*, 154104

5. Wellendorff, J; Lundgaard, K.T; Møgelhøj, A.; Petzold, V.; Landis, D.D.; Nørskov, J.K; Bligaard, T.; Jacobsen, K.W. Density functionals for surface science: Exchange-correlation model development with Bayesian error estimation. *Phys. Rev. B*, **2012**, *85*, 235149

6. Hammer, B.; Hansen, L. B.; Norskov, J. K. Improved Adsorption Energetics within Density- Functional Theory Using Revised Perdew-Burke-Ernzerhof Functionals. *Phys. Rev. B*., **1999**, *59*, 7413-7421

7. Peng, H.; Yang, Z.H.; Sun, J.; Perdew, J.P. Versatile van der Waals Density Functional Based on a Meta-Generalized Gradient Approximation. *Phys. Rev. X*, **2016**, *6*, 041005

8. Bernardo, J.; Smith. A; *Bayesian Theory*. John Wiley, 1994

9. Mahalanobis, P.C. On the generalised distance in statistics. *Proceedings of the National Institute of Science of India*, **1936**, vol 12, pp. 49-55

10. Warren, R; Smith, R. E.; Cybenko, A. K. Use of Mahalanobis Distance for Detecting Outliers and Outlier Clusters in Markedly Non-Normal Data: a Vehicular Traffic Example. Wright-Patterson Air Force Base, 2011.

11. Brerenton, R. G. The chi squared and multinormal distributions. *J. Chemometr*., **2015**; *29*, 9-12.

12. Jeffreys, H., *The Theory of Probability*; Oxford University Press:Oxford, **1939**; pp 356−357.

13. Biloen, P.; Dautzenberger, F. M.; Sachtler, W.M.H. Catalytic Dehydrogenation of Propane to Propene over Platinum and Platinum-Gold Alloys. *J. Catal.*, **1977**, *50* ,77-86

14. Zhu, J. ; Yang, M.; Yu, Y.; Zhu, Y.; Sui, Z.; Zhou, X.; Holmen, A.; Chen, D. Size-Dependent Reaction Mechanism and Kinetics for Propane Dehydrogenation over Pt Catalysts, *ACS Catal*. **2015**, *5*, 6310−6319

15. Barias, O. A.; Holmen, A.; Blekkan, E.A. Propane Dehydrogenation over Supported Pt and Pt–Sn Catalysts: Catalyst Preparation, Characterization, and Activity Measurements. *J. Catal.*, **1996**, *158*, 1–12

16. Cramer, J. S. Logit Models from Economics and Other Fields; Cambridge University Press: Cambridge, 2003; pp 149–157.

17. Zare, M.; Solomon, R. V; Yang, W.; Yonge, A.; Heyden, A.; "Theoretical Investigation of Solvent Effects on the Hydrodeoxygenation of Propionic Acid over a Ni(111) Catalyst Model. *J. Phys. Chem. C.* ,**2020,** *124* (30), 16488-16500

APPENDIX B

SUPPORTING INFORMATION FOR MODELING THE EFFECT OF SURFACE PLATINUM-TIN ALLOYS ON PROPANE DEHYDROGENATION ON PLATINUM-TIN CATALYSTS

B.1 Energies of Adsorbed State Species and Transition State Species

Table B.1: Free energies of adsorbed species at 792 K, $P_{CH3CH2CH3}$ of 1 bar, and P_{H2} of 1 bar, referenced to gaseous propane, hydrogen, and corresponding platinum-tin surface slab.

		Free Energy of Adsorption (eV)			
Adsorbed Species	Adsorption Number (ADS #)	Pt_3Sn/ Pt(100)	PtSn/ Pt(100)	Pt_3Sn/ Pt(111)	Pt_2Sn/ Pt(211)
$CH_3CH_2CH_3$	1	0.80	0.84	0.92	1.00
CH_3CHCH_3	2	0.93	1.13	1.19	1.20
$CH_3CH_2CH_2$	3	0.95	1.09	1.18	1.14
CH_3CHCH_2	4	0.69	0.86	1.13	0.98
CH_3CH_2CH	5	0.66	1.63	1.25	1.72
$CH_2CH_2CH_2$	6	0.97	1.36	1.37	1.50
CH_3CCH_3	7	0.69	1.28	1.12	1.23
CH_3CH_2C	8	0.49	1.80	0.46	1.10
CH_2CH_2CH	9	1.02	1.97	1.59	2.05
CH_2CHCH_2	10	0.47	1.16	0.91	1.01
CH_3CHCH	11	0.61	1.74	1.15	1.39
CH_3CCH_2	12	0.50	1.49	1.03	1.61
CH_3CHC	13	0.42	1.56	0.79	0.95
CH_2CH_2C	14	0.89	2.28	1.25	1.62
$CHCH_2CH$	15	0.98	2.06	1.28	2.27
CH_2CHCH	16	0.36	1.46	2.09	2.20
CH_2CCH_2	17	1.11	1.48	1.14	1.33
CH_3CCH	18	0.18	1.29	0.79	1.09
CH_3CC	19	0.43	1.56	1.13	1.28
CH_2CHC	20	0.87	1.93	1.34	1.61
CHCHCH	21	0.45	1.30	2.44	2.34
$CHCH_2C$	22	1.37	2.98	1.17	2.02
CH_2CCH	23	0.71	1.61	1.50	1.20
CH_2CC	24	1.09	1.63	2.00	1.44

CHCHC	25	1.13	2.08	1.58	1.76
CCH_2C	26	2.07	2.41	2.75	2.42
CHCCH	27	1.14	1.54	1.62	1.90
CCHC	28	1.31	2.48	2.37	2.21
CHCC	29	1.10	1.84	1.97	1.58
CCC	30	1.67	2.30	2.48	2.12
CH_3CH_3	31	0.47	0.46	0.58	0.56
CH_3CH_2	32	0.64	0.79	0.91	0.84
CH_3CH	33	0.50	1.45	1.03	1.33
CH_3C	34	0.17	1.55	0.32	0.85
CH_2CH_2	35	0.57	0.73	0.93	0.62
CH_2CH	36	0.60	1.44	1.02	1.25
CH_2C	37	0.33	1.47	0.68	1.33
CHCH	38	0.08	1.23	0.84	1.16
CHC	39	0.41	1.54	1.43	1.18
CC	40	1.01	1.83	2.13	1.61
CH_4	41	0.10	0.07	0.05	0.17
CH_3	42	0.31	0.43	0.69	0.49
CH_2	43	0.36	1.30	0.95	1.09
CH	44	0.28	1.47	0.46	0.85
C	45	0.30	1.73	0.85	1.19
H	46	0.09	0.17	0.20	0.46

Table B.2: Free energies of transition state species at 792 K, $P_{CH3CH2CH3}$ of 1 bar, and P_{H2} of 1 bar, referenced to gaseous propane, hydrogen, and corresponding platinum-tin surface slab.

		Free Energy of the Transition State, (eV)			
Chemical Reaction	Reaction Number	Pt_3Sn/ Pt(100)	PtSn/ Pt(100)	Pt_3Sn/ Pt(111)	Pt_2Sn/ Pt(211)
$CH_3CH_2CH_3 \rightarrow CH_3CHCH_3+H$	1	1.77	2.20	2.22	2.22
$CH_3CH_2CH_3 \rightarrow CH_3CH_2CH_2 +H$	2	1.85	2.17	2.22	2.05
$CH_3CHCH_3 \rightarrow CH_3CHCH_2+H$	3	1.75	2.61	2.20	2.12
$CH_3CH_2CH_2 \rightarrow CH_3CHCH_2+H$	4	1.71	2.58	2.21	2.23
$CH_3CH_2CH_3 \rightarrow CH_3+CH_2CH_3$	5	3.23	3.15	3.55	3.15
$CH_3CHCH_3 \rightarrow CH_3CH+CH_3$	6	2.79	3.59	3.23	3.42
$CH_3CHCH_3 \rightarrow CH_3CCH_3+H$	7	1.51	2.89	2.13	2.18
$CH_3CH_2CH_2 \rightarrow CH_3CH_2+CH_2$	8	2.58	3.48	3.15	3.22
$CH_3CH_2CH_2 \rightarrow CH_3+CH_2CH_2$	9	3.22	3.98	3.93	4.00
$CH_3CH_2CH_2 \rightarrow CH_2CH_2CH_2+H$	10	1.99	2.50	2.45	2.40
$CH_3CH_2CH_2 \rightarrow CH_3CH_2CH +H$	11	1.61	2.45	2.18	2.41
$CH_3CH_2CH \rightarrow CH_3CH_2+CH$	12	2.47	4.33	2.78	3.35
$CH_3CH_2CH \rightarrow CH_3+CH_2CH$	13	2.92	3.74	3.57	3.45
$CH_3CH_2CH \rightarrow CH_3CH_2C +H$	14	1.38	3.40	1.84	2.61
$CH_3CH_2CH \rightarrow CH_3CHCH+H$	15	1.52	2.21	2.15	2.40
$CH_3CH_2CH \rightarrow CH_2CH_2CH+H$	16	1.94	3.03	2.60	3.72
$CH_2CH_2CH_2 \rightarrow CH_2+CH_2CH_2$	17	2.52	3.16	3.02	2.64
$CH_2CH_2CH_2 \rightarrow CH_2CH_2CH+H$	18	1.79	2.57	3.24	2.57
$CH_2CH_2CH_2 \rightarrow CH_2CHCH_2+H$	19	1.87	3.09	2.06	2.75

$CH_3CHCH_2 \rightarrow CH_3+CHCH_2$	20	2.18	4.03	3.14	2.88
$CH_3CHCH_2 \rightarrow CH_3CH+CH_2$	21	2.59	3.36	3.14	3.11
$CH_3CHCH_2 \rightarrow CH_3CCH_2+H$	22	1.60	2.60	2.12	2.40
$CH_3CHCH_2 \rightarrow CH_3CHCH+H$	23	1.47	2.19	2.14	2.52
$CH_3CHCH_2 \rightarrow CH_2CHCH_2+H$	24	1.62	1.79	2.18	1.92
$CH_3CCH_3 \rightarrow CH_3+CH_3C$	25	2.52	3.88	2.88	3.08
$CH_3CCH_3 \rightarrow CH_3CCH_2+H$	26	1.59	2.67	2.09	2.56
$CH_3CH_2C \rightarrow CH_3+CH_2C$	27	2.55	4.01	3.28	3.41
$CH_3CH_2C \rightarrow CH_3CH_2+C$	28	2.25	3.63	2.82	2.95
$CH_3CH_2C \rightarrow CH_2CH_2C+H$	29	1.90	3.63	3.08	2.15
$CH_3CH_2C \rightarrow CH_3CHC+H$	30	1.37	2.74	1.78	3.20
$CH_2CH_2CH \rightarrow CH_2+CH_2CH$	31	2.66	4.33	3.17	3.61
$CH_2CH_2CH \rightarrow CH_2CH_2+CH$	32	2.26	3.60	2.79	3.59
$CH_2CH_2CH \rightarrow CH_2CH2C+H$	33	1.96	3.27	2.41	3.07
$CH_2CH_2CH \rightarrow CH_2CHCH+H$	34	1.63	3.23	2.58	3.14
$CH_2CH_2CH \rightarrow CHCH_2CH+H$	35	1.74	2.82	2.96	3.00
$CH_2CHCH_2 \rightarrow CH_2+CH_2CH$	36	2.94	3.42	2.92	2.87
$CH_2CHCH_2 \rightarrow CH_2CHCH+H$	37	1.52	2.28	3.16	2.60
$CH_2CHCH_2 \rightarrow CH_2CCH_2+H$	38	2.74	3.24	2.00	2.50
$CH_3CHCH \rightarrow CH_3+CHCH$	39	2.06	4.21	2.82	2.99
$CH_3CHCH \rightarrow CH_3CH+CH$	40	2.43	4.27	2.92	4.27
$CH_3CHCH \rightarrow CH_3CHC+H$	41	1.62	2.54	1.68	1.98

$CH_3CHCH \rightarrow CH_3CCH+H$	42	1.98	3.51	2.07	1.96
$CH_3CHCH \rightarrow CH_2CHCH+H$	43	1.98	2.91	2.42	2.43
$CH_3CCH_2 \rightarrow CH_3+CH_2C$	44	2.20	3.91	2.49	2.98
$CH_3CCH_2 \rightarrow CH_3C+CH_2$	45	1.61	3.98	2.93	3.74
$CH_3CCH_2 \rightarrow CH_2CCH_2+H$	46	1.51	2.40	2.15	1.96
$CH_3CCH_2 \rightarrow CH_3CCH+H$	47	1.45	3.25	1.95	2.89
$CH_3CHC \rightarrow CH_3+CHC$	48	2.70	3.92	3.27	3.98
$CH_3CHC \rightarrow CH_3CH+C$	49	2.54	4.73	3.15	3.44
$CH_3CHC \rightarrow CH_3CC+H$	50	1.35	3.11	2.27	2.57
$CH_3CHC \rightarrow CH_2CHC+H$	51	1.72	2.77	2.15	2.43
$CH_2CH_2C \rightarrow CH_2CH_2+C$	52	2.04	3.60	2.63	3.02
$CH_2CH_2C \rightarrow CH_2+CH_2C$	53	2.22	3.92	2.61	3.05
$CH_2CH_2C \rightarrow CH_2CHC+H$	54	2.16	3.84	2.67	3.34
$CH_2CH_2C \rightarrow CHCH_2C+H$	55	1.96	3.71	3.10	2.97
$CHCH_2CH \rightarrow CH_2CH+CH$	56	2.83	4.30	3.63	3.69
$CHCH_2CH \rightarrow CHCH_2C+H$	57	2.79	3.08	3.39	3.44
$CHCH_2CH \rightarrow CHCHCH+H$	58	2.27	3.95	3.60	3.12
$CH_2CHCH \rightarrow CH_2+CHCH$	59	2.21	3.44	2.74	3.18
$CH_2CHCH \rightarrow CH_2CH+CH$	60	2.67	3.63	2.66	3.98
$CH_2CHCH \rightarrow CH_2CHC+H$	61	1.79	2.73	2.35	3.28
$CH_2CHCH \rightarrow CH_2CCH+H$	62	1.61	3.86	2.54	3.00
$CH_2CHCH \rightarrow CHCHCH+H$	63	1.62	2.22	2.36	3.78

$CH_2CCH_2 \rightarrow CH_2C+CH_2$	64	2.95	3.82	2.90	3.47
$CH_2CCH_2 \rightarrow CH_2CCH+H$	65	1.13	2.30	2.70	2.14
$CH_3CCH \rightarrow CH_3C+CH$	66	1.97	4.26	2.54	3.56
$CH_3CCH \rightarrow CH_3+CHC$	67	2.21	3.37	3.02	2.89
$CH_3CCH \rightarrow CH_3CC+H$	68	1.94	2.85	2.16	2.19
$CH_3CCH \rightarrow CH_2CCH+H$	69	1.80	2.85	2.50	2.45
$CH_3CC \rightarrow CH_3+CC$	70	2.93	3.63	4.01	4.53
$CH_3CC \rightarrow CH_3C+C$	71	2.34	4.53	4.01	4.15
$CH_3CC \rightarrow CH_2CC+H$	72	1.88	2.78	2.41	2.95
$CH_2CHC \rightarrow CH_2+CHC$	73	2.30	3.80	2.96	3.27
$CH_2CHC \rightarrow CH_2CH+C$	74	2.52	3.36	2.61	2.77
$CH_2CHC \rightarrow CH_2CC+H$	75	1.79	3.54	3.05	3.68
$CH_2CHC \rightarrow CHCHC+H$	76	1.52	3.01	3.71	2.81
$CHCH_2C \rightarrow CH+CH_2C$	77	2.96	4.61	3.26	2.57
$CHCH_2C \rightarrow CH_2CH+C$	78	2.45	4.15	3.63	3.35
$CHCH_2C \rightarrow CHCHC+H$	79	2.57	4.22	3.53	2.91
$CHCH_2C \rightarrow CCH_2C+H$	80	2.61		3.82	3.45
$CHCHCH \rightarrow CH+CHCH$	81	2.53	4.36	2.72	3.01
$CHCHCH \rightarrow CHCHC+H$	82	1.74	2.94	1.87	2.65
$CHCHCH \rightarrow CHCCH+H$	83	2.76	3.68	3.58	3.57
$CH_2CCH \rightarrow CH_2+CHC$	84	2.30	3.65	3.34	3.83
$CH_2CCH \rightarrow CH_2C+CH$	85	2.80	4.30	3.65	4.19

$CH_2CCH \rightarrow CH_2CC+H$	86	1.79	2.49	3.19	3.25
$CH_2CCH \rightarrow CHCCH+H$	87	2.01	2.17	2.60	2.80
$CH_2CC \rightarrow CH_2+CC$	88	2.07	3.76	3.67	3.83
$CH_2CC \rightarrow CHC+C$	89	2.23	3.75	4.01	4.23
$CH_2CC \rightarrow CHCC+H$	90	2.51	2.99	2.85	3.12
$CHCHC \rightarrow CH+CHC$	91	2.29	4.55	3.27	3.84
$CHCHC \rightarrow CHCH+C$	92	1.95	4.35	2.44	2.67
$CHCHC \rightarrow CHCC+H$	93	2.64	3.87	3.62	3.34
$CHCHC \rightarrow CCHC+H$	94	2.49	3.67	3.03	3.42
$CCH_2C \rightarrow C+CH_2C$	95	2.57	5.18	2.88	3.80
$CCH_2C \rightarrow CCHC+H$	96	2.46	4.67	4.37	4.23
$CHCCH \rightarrow CH+CCH$	97	2.15	4.74	3.28	3.78
$CHCCH \rightarrow CHCC+H$	98	1.87	2.65	2.87	3.02
$CCHC \rightarrow CHC+C$	99	2.03	4.41	3.11	3.06
$CCHC \rightarrow CCC+H$	100	1.76	4.76	4.28	3.40
$CHCC \rightarrow CH+CC$	101	2.44	4.84	4.14	3.80
$CHCC \rightarrow CHC+C$	102	1.85	4.11	3.67	4.74
$CHCC \rightarrow CCC+H$	103	2.67	3.76	3.35	2.84
$CCC \rightarrow C+CC$	104	2.42	5.57	4.02	3.94
$CH_4 \rightarrow CH_3+H$	105	1.25	1.56	1.70	1.48
$CH_3 \rightarrow CH_2+H$	106	1.10	1.96	1.70	1.73
$CH_2 \rightarrow CH+H$	107	1.30	2.56	1.51	2.20
$CH \rightarrow C+H$	108	1.35	2.58	1.82	2.60
$CH_3CH_3 \rightarrow CH_3+CH_3$	109	2.97	3.40	3.55	2.94
$CH_3CH_3 \rightarrow CH_3CH_2+H$	110	1.58	1.95	2.15	1.88
$CH_3CH_2 \rightarrow CH_3+CH_2$	111	2.26	3.52	2.81	2.81

$CH_3CH_2 \rightarrow CH_3CH+H$	112	1.43	2.26	2.05	2.08
$CH_3CH_2 \rightarrow CH_2CH_2+H$	113	1.42	2.38	1.98	1.86
$CH_3CH \rightarrow CH_3+CH$	114	2.26	3.81	2.59	2.98
$CH_3CH \rightarrow CH_3C+H$	115	1.40	3.18	1.66	2.36
$CH_3CH \rightarrow CH_2CH+H$	116	1.56	2.87	2.03	2.29
$CH_3C \rightarrow CH_3+C$	117	1.89	3.19	2.48	2.64
$CH_3C \rightarrow CH_2C+H$	118	1.50	2.59	1.66	1.93
$CH_2CH_2 \rightarrow CH_2+CH_2$	119	2.27	3.87	3.10	2.80
$CH_2CH_2 \rightarrow CH_2CH+H$	120	1.35	2.13	1.96	2.15
$CH_2CH \rightarrow CH_2+CH$	121	2.66	3.99	2.95	3.14
$CH_2CH \rightarrow CH_2C+H$	122	1.49	2.19	1.67	2.26
$CH_2CH \rightarrow CHCH+H$	123	1.66	2.50	1.99	1.99
$CH_2C \rightarrow CH_2+C$	124	2.53	4.17	3.04	3.41
$CH_2C \rightarrow CHC+H$	125	1.61	2.79	2.39	2.02
$CHCH \rightarrow CH+CH$	126	2.07	4.97	3.10	3.31
$CHCH \rightarrow CHC+H$	127	1.47	2.86	2.43	2.30
$CHC \rightarrow CH+C$	128	2.45	4.66	3.36	3.50
$CHC \rightarrow CC + H$	129	1.88	2.89	3.02	3.01
$CC \rightarrow C+C$	130	3.01	5.13	4.37	3.76

B.2 Hyperparameters and Experimental Dataset

B.2.1 Hyperparameters for Model Variances

As the results of calibration problems are dependent on both the prior distribution and the hyperparameters chosen to represent the variances, non-informative hyperparameters were chosen for these models.[1-3]

Table B.3: Hyperparameters for shape and scale of the inverse gamma prior distributions to describe the variances in the models.

Hyperparameters	Log_{10}(TOF)	Logit(Selectivity)
α	3	3
β	1	1

B.2.2 Experimental Dataset

Table B.4: Experimental conditions and reported results for the experiment as replicated in this study.[4]

Reported Experimental Data	
Temperature (K)	792
$P_{Propane}$ (bar)	0.29
P_{H2} (Bar)	0.09
TOF (1/s)	0.6
Selectivity to Propylene	98%

B.3 Additional Information for Microkinetic Modeling

B.3.1 Site Occupation by Surface

We studied the same reaction pathways on each of the surfaces, with the exception of transition state #80 for PtSn/Pt(100), where the transition state was not found. We note that the geometry and number of occupied sites for the lowest energy adsorbed species depends on the surface, as the surface facets are different from each other. This study defines that one Pt or Sn atom is one site. We used this methodology for all carbon containing species. For atomic hydrogen, we assumed that one H atom covers one site, regardless of the most stable adsorption site, due to its small size and weak self-interactions on each of the surfaces. This information can be read in Table B.5.

Table B.5: Number of sites occupied by each adsorbed species on Pt(100), Pt(111), Pt(211)

	Number of Sites Occupied			
Adsorbed Species	Pt_3Sn/Pt(100)	PtSn/Pt(100)	Pt_3Sn /Pt(111)	Pt_2Sn /Pt(211)
$CH_3CH_2CH_3$	1	1	1	1
CH_3CHCH_3	1	1	1	1
$CH_3CH_2CH_2$	1	1	1	1
CH_3CHCH_2	2	2	2	2
CH_3CH_2CH	2	2	2	2
$CH_2CH_2CH_2$	2	2	2	2
CH_3CCH_3	2	2	2	2
CH_3CH_2C	4	4	3	3
CH_2CH_2CH	3	3	3	2
CH_2CHCH_2	2	2	3	2
CH_3CHCH	3	3	3	3
CH_3CCH_2	3	3	3	3
CH_3CHC	3	3	3	3
CH_2CH_2C	4	4	3	3
$CHCH_2CH$	4	4	3	4
CH_2CHCH	3	3	3	3
CH_2CCH_2	3	3	4	3
CH_3CCH	4	4	3	3
CH_3CC	4	4	3	4
CH_2CHC	3	3	3	4

CHCHCH	4	4	4	4
$CHCH_2C$	4	4	4	4
CH_2CCH	3	3	4	4
CH_2CC	4	4	4	4
CHCHC	4	4	3	4
CCH_2C	4	4	5	5
CHCCH	4	4	5	4
CCHC	6	6	5	4
CHCC	4	4	5	4
CCC	6	6	5	4
CH_3CH_3	1	1	1	1
CH_3CH_2	1	1	1	1
CH_3CH	2	2	2	2
CH_3C	4	4	3	3
CH_2CH_2	2	2	2	2
CH_2CH	2	2	3	3
CH_2C	3	3	3	3
CHCH	4	4	3	4
CHC	4	4	4	4
CC	4	4	4	4
CH_4	1	1	1	1
CH_3	1	1	1	1
CH_2	2	2	2	2
CH	4	4	3	3
C	4	4	3	4
H	1	1	1	1

B.3.2 Lateral Interactions

To describe the lateral interactions on all of our surfaces, we used the same methodology as in Zare et al. and Fricke et al.[1,5]

$$G_{ads,i}(\theta_j) = G_{ads,i}(0) + \sum_j \alpha_{i,j}\theta_j \qquad (B.1)$$

where $G_{ads,i}(\theta_j)$ is the adsorption free energy of species i, with coverage of species j, $G_{ads}(0)$ is the energy of the adsorbed species on a clean slab, θ_j is the coverage of species j on the surface, and $\alpha_{i,j}$ is the lateral interaction parameter between species i and j. All lateral interactions are calculated between coverages of 25% and 50%.

$$\alpha_{i,j} = \frac{1}{\theta_j}(G_{ads,i}(\theta_j) - G_{ads,i}(0) \qquad (B.2)$$

The lateral interaction parameter, $\alpha_{i,j}$, is calculated as the difference between the adsorption energy of species i and the lateral interaction species j at coverage of θ_j and the adsorption energy of species i at 0 species j coverage.

From finding $\alpha_{i,j}$, we calculate the transition state free energy, using the below equations:

$$G_k^{TS}(\theta_j) = G_k^{TS}(0) + \sum_j (\beta_{k,j}\theta_j) \qquad (B.3)$$

$$\beta_{k,j} = \frac{1}{2} * \sum_i {\alpha_{i,j}}^k \qquad (B.4)$$

where $G_k^{TS}(\theta_j)$ is the transition state energy for reaction k at surface coverage of species j, $G_k^{TS}(0)$ is the transition state energy for reaction k on the clean surface, and $\beta_{k,j}$ is the

lateral interaction term for reaction k over all species i involved in the reaction described by transition state k. Thus, $\beta_{k,j}$ is calculated as the sum of the products and reactants lateral interactions and divided by 2, as we assume that the transition states are half of the reactant and product states.

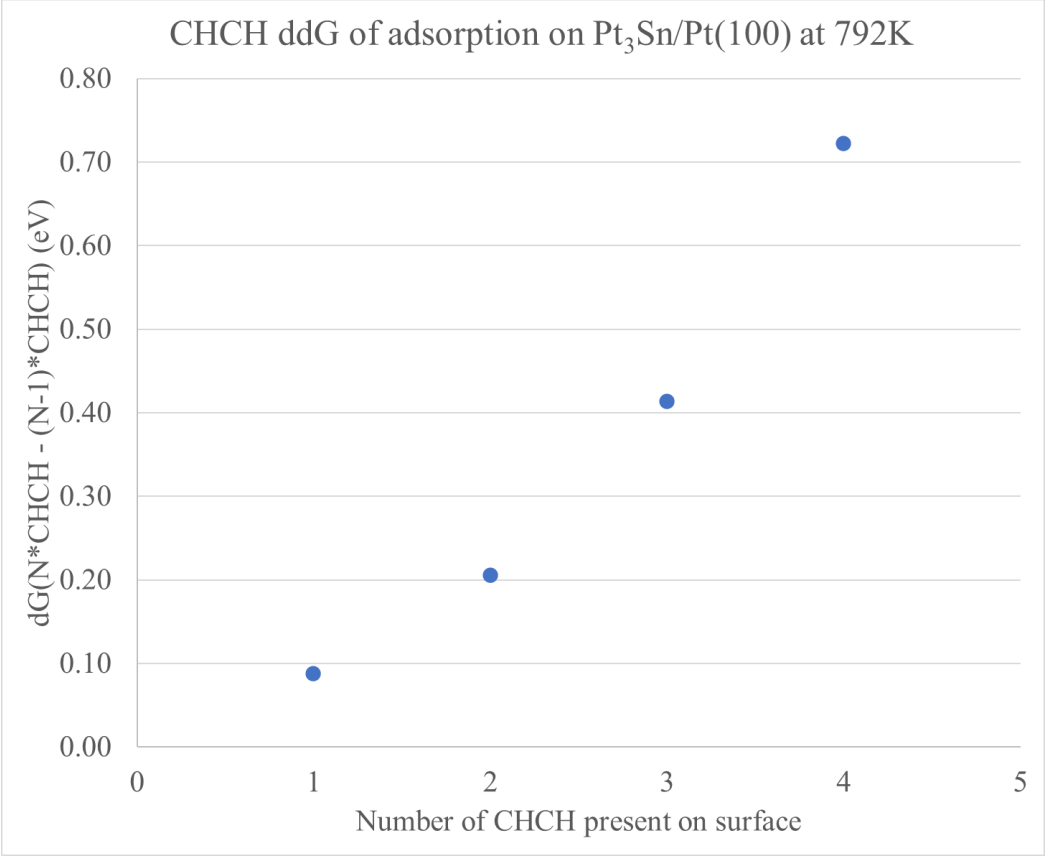

Figure B.1: Differential Gibbs free energy of adsorption of acetylene on $Pt_3Sn/Pt(100)$. Lateral interactions for acetylene were calculated between 1 and 3 acetylenes on the surface.

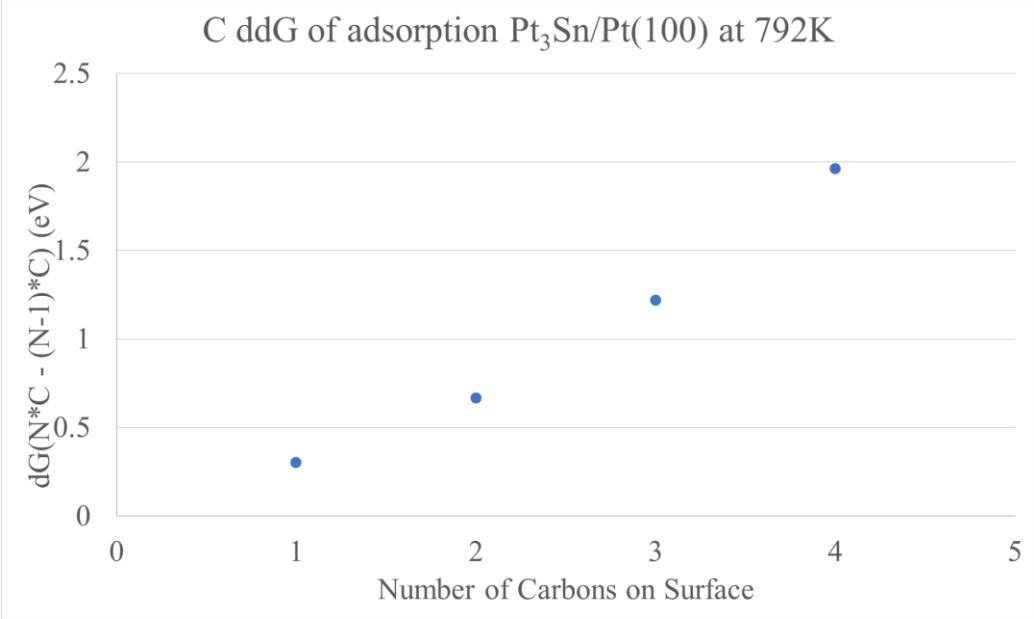

Figure B.2: Differential Gibbs free energy of adsorption of carbon on $Pt_3Sn/Pt(100)$. Lateral interactions for carbon were calculated between 1 and 3 carbons on the surface.

Table B.6. Lateral interactions on $Pt_3Sn/Pt(100)$.

Pt(100)	Lateral Interaction Parameters (eV/coverage)	
Adsorbed Species (i)	$\alpha_{i,CHCH}$	$\alpha_{i,C}$
$CH_3CH_2CH_3$	0.01	0.19
CH_3CHCH_3	0.36	0.36
$CH_3CH_2CH_2$	0.19	0.30
CH_3CHCH_2	0.20	-0.15
CH_3CH_2CH	0.30	0.62
$CH_2CH_2CH_2$	0.31	-0.47
CH_3CCH_3	0.15	0.28
CH_3CH_2C	0.23	-0.35
CH_2CH_2CH	0.01	0.28
CH_2CHCH_2	0.31	0.64
CH_3CHCH	0.19	0.45
CH_3CCH_2	0.19	1.08
CH_3CHC	0.20	0.65
CH_2CH_2C	0.21	0.41
$CHCH_2CH$	0.23	0.55
CH_2CHCH	0.38	1.03
CH_2CCH_2	0.46	0.88
CH_3CCH	1.17	1.53
CH_3CC	0.34	0.57
CH_2CHC	0.33	0.74
CHCHCH	0.37	0.70
$CHCH_2C$	0.46	0.55
CH_2CCH	0.27	-0.15
CH_2CC	0.63	-0.54
CHCHC	0.76	0.49
CCH_2C	1.23	-0.07
CHCCH	0.02	0.40
CCHC	1.82	2.14
CHCC	0.99	1.11
CCC	0.23	-0.30
CH_3CH_3	0.25	0.35
CH_3CH_2	0.77	0.99
CH_3CH	0.36	-0.31
CH_3C	0.31	0.35
CH_2CH_2	0.18	0.47
CH_2CH	0.33	0.62
CH_2C	0.26	0.51
CHCH	0.88	0.44
CHC	0.31	0.66
CC	0.27	0.50

CH_4	0.12	0.11
CH_3	0.34	0.37
CH_2	0.24	0.46
CH	0.29	0.49
C	0.38	0.55
H	0.10	0.40

B.4 Microkinetic Modeling Results without Uncertainty Quantification

Table B.7: BEEF-vdW (without uncertainty quantification) predicted turnover frequencies (TOF), selectivity to propylene, and free sites on surface.

	Pt_3Sn/Pt(100)	PtSn/Pt(100)	Pt_3Sn/Pt(111)	Pt_2Sn/Pt211
TOF Propane Consumption (1/s)	7.08	4.08×10^{-3}	2.17×10^{-2}	1.33×10^{-1}
TOF Propylene (1/s)	7.68×10^{-1}	3.96×10^{-3}	1.48×10^{-2}	1.27×10^{-1}
TOF Propyne (1/s)	6.80×10^{-8}	6.20×10^{-6}	5.59×10^{-4}	4.86×10^{-3}
TOF Ethane (1/s)	1.14×10^{-3}	1.49×10^{-8}	4.32×10^{-7}	5.07×10^{-6}
TOF Ethylene (1/s)	6.23	1.10×10^{-4}	5.83×10^{-3}	6.42×10^{-4}
TOF Ethyne (1/s)	2.57×10^{-3}	5.46×10^{-6}	3.87×10^{-4}	1.21×10^{-5}
TOF Methane (1/s)	6.38	1.15×10^{-4}	6.28×10^{-3}	6.59×10^{-4}
Selectivity to Propylene	10.9%	97.0%	68.6%	95.8%
Free Sites on Surface	92.4%	99.3%	99.5%	100.0%

Table B.8: BEEF-vdW (without uncertainty quantification) predicted apparent activation energies

Apparent Activation Energy (eV)				
	Pt_3Sn/Pt(100)	PtSn/Pt(100)	Pt_3Sn/Pt(111)	Pt_2Sn/Pt(211)
Propane Consumption	1.83	2.52	2.36	2.26
Propylene	2.02	2.51	2.37	2.25
Propyne	2.65	2.95	2.04	2.44
Ethane	2.20	3.35	2.83	2.84
Ethylene	1.80	2.86	2.39	2.65
Ethyne	1.97	3.13	1.95	2.78
Methane	1.81	2.87	2.37	2.65

Table B.9: BEEF-vdW (without uncertainty quantification) predicted reaction orders in propane

Propane Reaction Order				
	Pt_3Sn/Pt(100)	PtSn/Pt(100)	Pt_3Sn/Pt(111)	Pt_2Sn/Pt(211)
Propane Consumption	0.77	1.00	1.01	1.00
Propylene	0.86	1.00	1.01	1.00
Propyne	1.42	1.00	1.01	1.00
Ethane	0.75	1.00	1.02	1.00
Ethylene	0.76	1.00	1.01	1.00
Ethyne	0.95	1.00	1.01	1.00
Methane	0.75	1.00	1.01	1.00

Table B.10: BEEF-vdW (without uncertainty quantification) predicted reaction orders in H_2

H_2 Reaction Order				
	Pt_3Sn/Pt(100)	PtSn/Pt(100)	Pt_3Sn/Pt(111)	Pt_2Sn/Pt(211)
Propane Consumption	0.35	-0.46	-0.02	-0.29
Propylene	0.51	-0.41	0.04	-0.28
Propyne	-1.24	-0.51	-0.48	-0.56
Ethane	1.43	-0.27	0.95	-0.32
Ethylene	0.28	-1.58	-0.05	-0.83
Ethyne	-0.65	-2.15	-1.01	-1.75
Methane	0.32	-1.61	-0.12	-0.84

Table B.11: BEEF-vdW (without uncertainty quantification) predicted degree of kinetic rate control for the propane to propylene dehydrogenation pathway on Pt_3Sn/Pt(100)

	D_{KRC}, Pt_3Sn/Pt(100)			
	$CH_3CH_2CH_3 \rightarrow CH_3CHCH_3+H$	$CH_3CH_2CH_3 \rightarrow CH_3CH_2CH_2+H$	$CH_3CHCH_3 \rightarrow CH_3CHCH_2+H$	$CH_3CH_2CH_2 \rightarrow CH_3CHCH_2+H$
Propane Consumption	0.57	0.21	0.01	0.01
Propylene	0.34	0.50	0.25	0.34
Propyne	1.33	0.08	-0.05	-0.02
Ethane	0.62	0.13	-0.03	-0.03
Ethylene	0.60	0.17	-0.02	-0.03
Ethyne	0.80	0.16	-0.03	-0.03
Methane	0.59	0.17	-0.02	-0.03

Table B.12: BEEF-vdW (without uncertainty quantification) predicted degree of kinetic rate control for the propane to propylene dehydrogenation pathway on PtSn/Pt(100)

	D_{KRC}, PtSn/Pt(100)				
	$CH_3CH_2CH_3 \rightarrow CH_3CHCH_3+H$	$CH_3CH_2CH_3 \rightarrow CH_3CH_2CH_2+H$	$CH_3CHCH_3 \rightarrow CH_3CHCH_2+H$	$CH_3CH_2CH_2 \rightarrow CH_3CHCH_2+H$	$CH_3CH_2CH_2 \rightarrow CH_3CH_2CH+H$
Propane Consumption	0.00	0.17	0.09	0.11	0.61
Propylene	0.00	0.17	0.09	0.11	0.63
Propyne	0.03	0.00	-0.02	0.00	0.01
Ethane	0.00	0.00	0.00	0.00	-0.03
Ethylene	0.00	0.18	0.00	0.00	-0.15
Ethyne	0.00	0.18	0.00	-0.02	-0.15
Methane	0.00	0.18	0.00	-0.03	-0.15

Table B.13: BEEF-vdW (without uncertainty quantification) degree of kinetic rate control for the propane to propylene dehydrogenation pathway on Pt_3Sn/Pt(111)

	D_{KRC}, Pt_3Sn/Pt(111)			
	$CH_3CH_2CH_3 \rightarrow CH_3CHCH_3+H$	$CH_3CH_2CH_3 \rightarrow CH_3CH_2CH_2+H$	$CH_3CHCH_3 \rightarrow CH_3CHCH_2+H$	$CH_3CH_2CH_2 \rightarrow CH_3CHCH_2+H$
Propane Consumption	0.49	0.48	0.00	0.01
Propylene	0.66	0.31	0.02	0.16
Propyne	0.68	0.30	-0.19	-0.11
Ethane	0.08	0.89	-0.02	-0.36
Ethylene	0.05	0.92	-0.01	-0.38
Ethyne	0.08	0.89	-0.02	-0.36
Methane	0.05	0.92	-0.01	-0.37

Table B.14: BEEF-vdW (without uncertainty quantification) degree of kinetic rate control for the propane to propylene dehydrogenation pathway on Pt_2Sn/Pt(211)

	D_{KRC}, Pt_2Sn/Pt(211)			
	$CH_3CH_2CH_3 \rightarrow CH_3CHCH_3+H$	$CH_3CH_2CH_3 \rightarrow CH_3CH_2CH_2+H$	$CH_3CHCH_3 \rightarrow CH_3CHCH_2+H$	$CH_3CH_2CH_2 \rightarrow CH_3CHCH_2+H$
Propane Consumption	0.25	0.16	0.02	0.52
Propylene	0.27	0.16	0.02	0.55
Propyne	0.04	0.21	-0.04	-0.20
Ethane	0.00	0.22	0.00	-0.21
Ethylene	0.00	0.22	0.00	-0.21
Ethyne	0.00	0.22	0.00	-0.21
Methane	0.00	0.22	0.00	-0.21

B.5 BEEF-vdW with Ensembles (BMwE) Forward-Only Additional Results

Table B.15: Site coverages for prior models

	Average Site Coverages (%)			
Species	Pt_3Sn/Pt(100)	PtSn/Pt(100)	Pt_3Sn/Pt(111)	Pt_2Sn/Pt(211)
Free Sites	81.8	96.0	95.7	99.2
CHCH	3.24	0.00	0.00	0.00
C	4.79	0.03	0.23	0.00
H	3.59	3.75	1.18	0.27
Other	7.32	0.19	2.90	0.50

Table B.16: Selectivity to different products for prior models

	Mean Selectivity (%)			
Species	Pt_3Sn/Pt(100)	PtSn/Pt(100)	Pt_3Sn/Pt(111)	Pt_2Sn/Pt(211)
Propylene	36.3	31.3	61.6	85.7
Propyne	1.30	0.36	7.63	7.36
Ethane	0.05	0.13	0.03	0.05
Ethylene	38.3	6.47	12.9	1.13
Ethyne	4.29	39.1	8.12	3.37
Methane	19.9	22.8	9.7	2.41

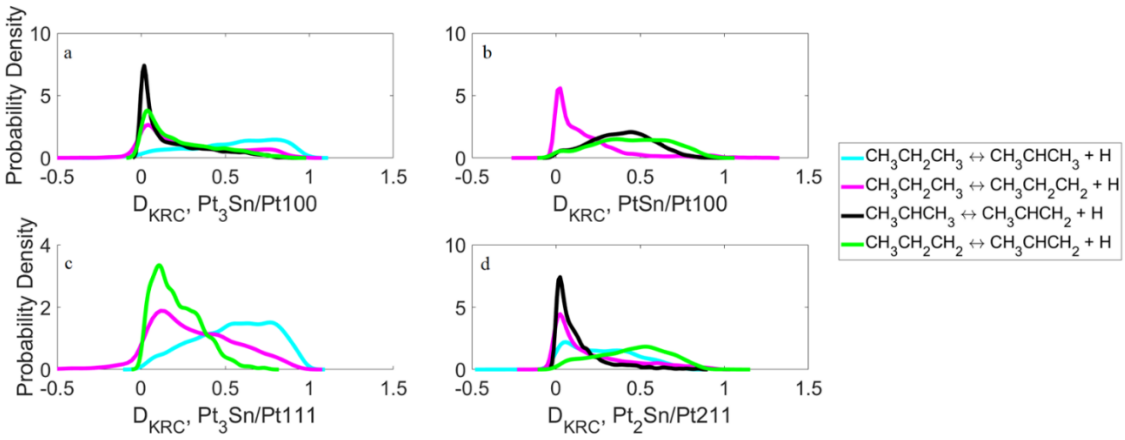

Figure B.3: Degree of kinetic rate control (D_{KRC}) measuring $TOF_{Propylene}$ for the prior only model for elementary steps with generally positive D_{KRC}.

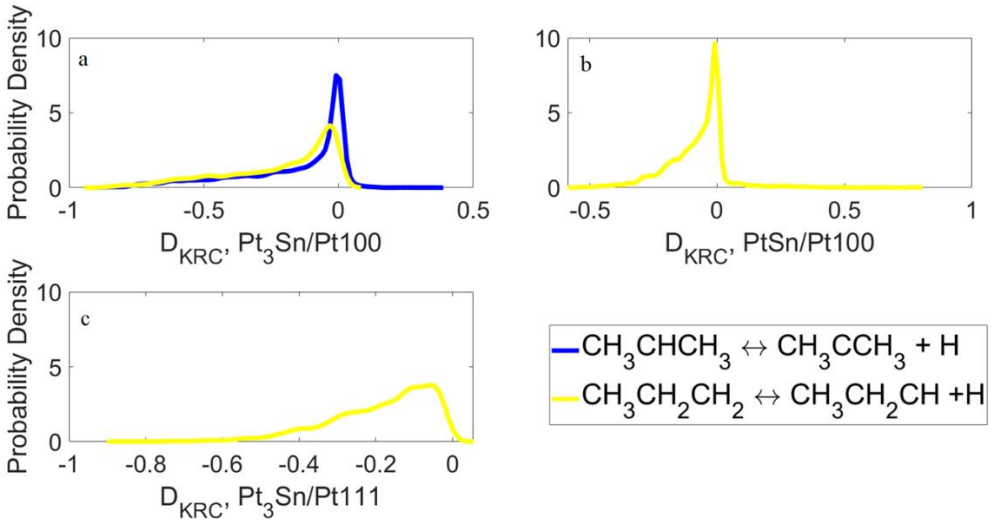

Figure B.4: Degree of kinetic rate control (D_{KRC}) measuring $TOF_{Propylene}$ for the prior only model for elementary steps with generally negative D_{KRC}.

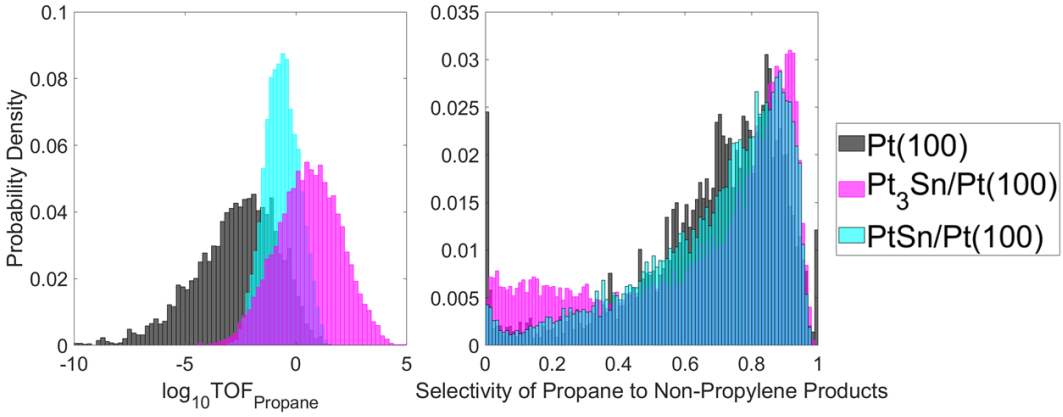

Figure B.5: TOF of propane conversion and selectivity of propane to non-propylene products for the prior model on Pt(100), Pt_3Sn/Pt(100), and PtSn/Pt(100).

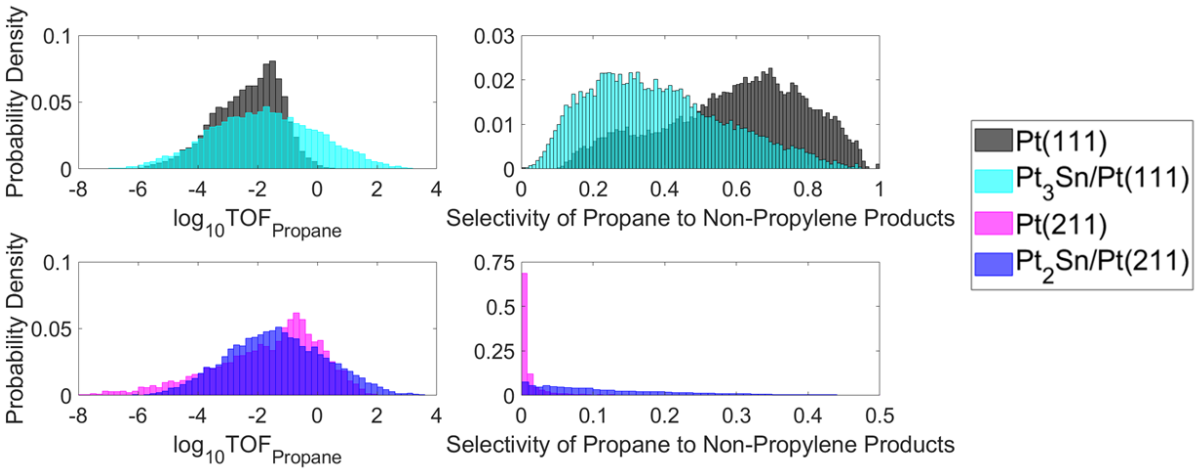

Figure B.6: TOF of propane conversion and selectivity of propane to non-propylene products for the prior model on Pt(111), Pt_3Sn/Pt(111), Pt(211), and Pt_2Sn/Pt(211).

B.5 BEEF-vdW with Ensembles (BMwE) Calibrated Additional Results

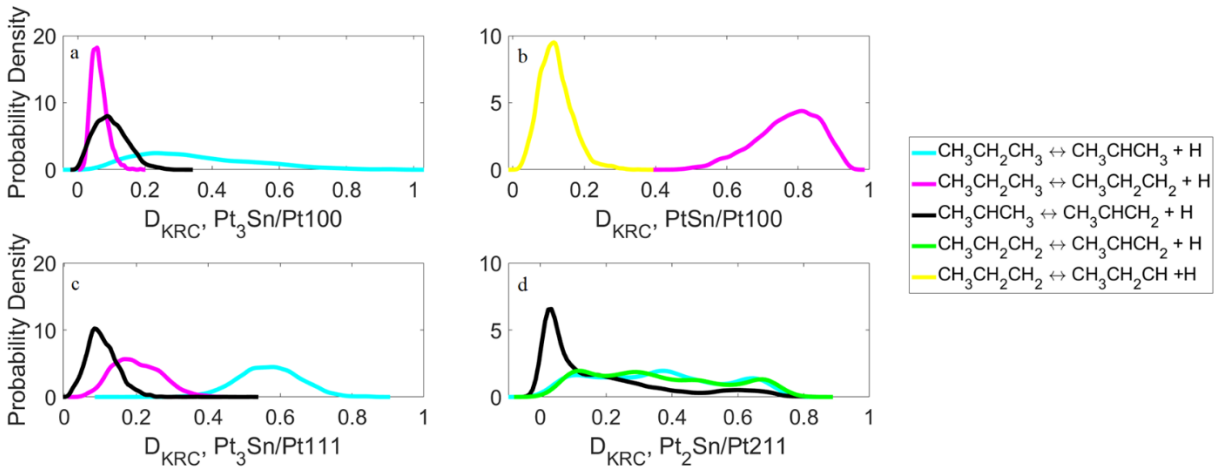

Figure B.7: Degree of kinetic rate control (D_{KRC}) calculated for $TOF_{Propylene}$ for the calibrated model.

B.6 Bibliography

1. Fricke, C; Rajbanshi, B.; Walker, E.; Terejanu, G.; Heyden, A.; Propane Dehydrogenation on Platinum Catalysts: Identifying the Active Sites through Bayesian Analysis, *ACS Catalysis*, 2022, Accepted

2. Waker, E.; Mitchell, D.; Terejanu, G. A.; Heyden, A. Identifying Active Sites of the Water-Gas Shift Reaction over Titania Supported Platinum Catalysts under Uncertainty. *ACS Catal.*, 2018, 8, 3990-3998

3. Bernardo, J.; Smith. A; Bayesian Theory. John Wiley, 1994

4. Barias, O. A.; Holmen, A.; Blekkan, E.A. Propane Dehydrogenation over Supported Pt and Pt–Sn Catalysts: Catalyst Preparation, Characterization, and Activity Measurements. *J. Catal.*, 1996, 158, 1–12

5. Zare, M.; Solomon, R. V; Yang, W.; Yonge, A.; Heyden, A.; "Theoretical Investigation of Solvent Effects on the Hydrodeoxygenation of Propionic Acid over a Ni(111) Catalyst Model. *J. Phys. Chem. C.* ,2020, 124 (30), 16488-16500

APPENDIX C

COPYRIGHTS AND PERMISSIONS

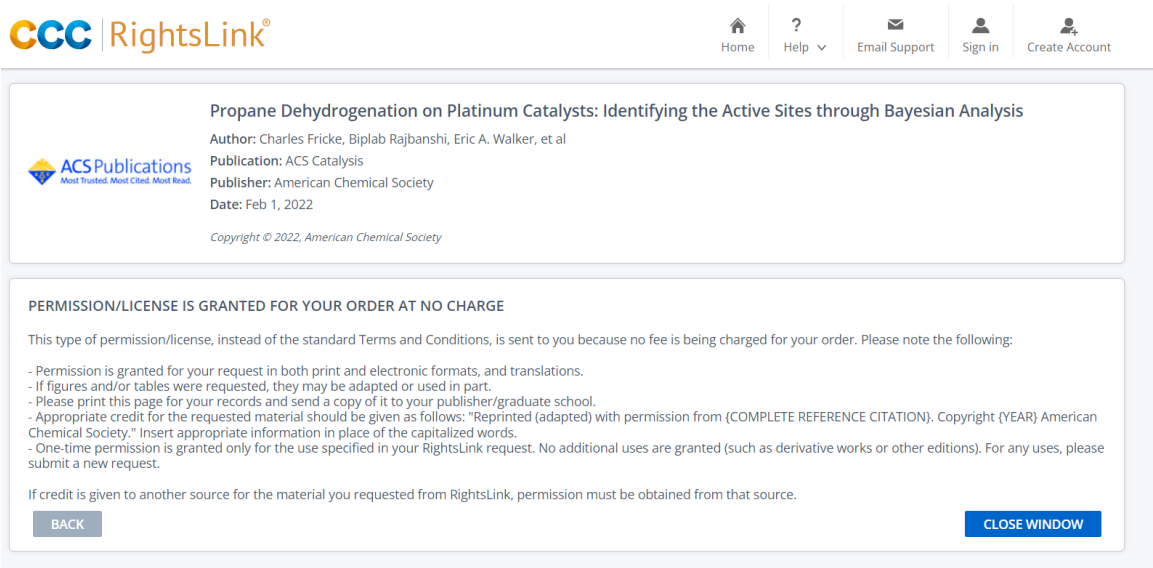

CCC RightsLink®

Home | Help | Email Support | Sign in | Create Account

ACS Publications
Most Trusted. Most Cited. Most Read.

Propane Dehydrogenation on Platinum Catalysts: Identifying the Active Sites through Bayesian Analysis

Author: Charles Fricke, Biplab Rajbanshi, Eric A. Walker, et al
Publication: ACS Catalysis
Publisher: American Chemical Society
Date: Feb 1, 2022

Copyright © 2022, American Chemical Society

PERMISSION/LICENSE IS GRANTED FOR YOUR ORDER AT NO CHARGE

This type of permission/license, instead of the standard Terms and Conditions, is sent to you because no fee is being charged for your order. Please note the following:

- Permission is granted for your request in both print and electronic formats, and translations.
- If figures and/or tables were requested, they may be adapted or used in part.
- Please print this page for your records and send a copy of it to your publisher/graduate school.
- Appropriate credit for the requested material should be given as follows: "Reprinted (adapted) with permission from {COMPLETE REFERENCE CITATION}. Copyright {YEAR} American Chemical Society." Insert appropriate information in place of the capitalized words.
- One-time permission is granted only for the use specified in your RightsLink request. No additional uses are granted (such as derivative works or other editions). For any uses, please submit a new request.

If credit is given to another source for the material you requested from RightsLink, permission must be obtained from that source.

BACK | CLOSE WINDOW